



THE EFFECT OF  
SYNTHETIC APERTURE RADAR IMAGE RESOLUTION  
ON TARGET DISCRIMINATION

THESIS

John E. McGowan, 2d Lt, USAF

AFIT/GE/ENG/10-18

DEPARTMENT OF THE AIR FORCE  
AIR UNIVERSITY

**AIR FORCE INSTITUTE OF TECHNOLOGY**

Wright-Patterson Air Force Base, Ohio

APPROVED FOR PUBLIC RELEASE; DISTRIBUTION UNLIMITED.

The views expressed in this thesis are those of the author and do not reflect the official policy or position of the United States Air Force, Department of Defense, or the United States Government.

AFIT/GE/ENG/10-18

THE EFFECT OF  
SYNTHETIC APERTURE RADAR IMAGE RESOLUTION  
ON TARGET DISCRIMINATION

THESIS

Presented to the Faculty  
Department of Electrical and Computer Engineering  
Graduate School of Engineering and Management  
Air Force Institute of Technology  
Air University  
Air Education and Training Command  
In Partial Fulfillment of the Requirements for the  
Degree of Master of Science in Electrical Engineering

John E. McGowan, B.S.E.E.

2d Lt, USAF

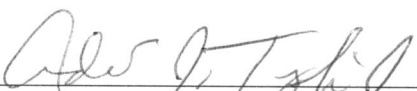
March 2010

APPROVED FOR PUBLIC RELEASE; DISTRIBUTION UNLIMITED.

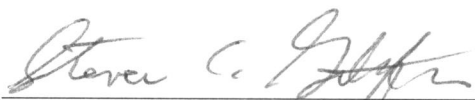
THE EFFECT OF  
SYNTHETIC APERTURE RADAR IMAGE RESOLUTION  
ON TARGET DISCRIMINATION

John E. McGowan, B.S.E.E.  
2d Lt, USAF

Approved:

  
\_\_\_\_\_  
Dr. Andrew J. Terzuoli, PhD (Chairman)

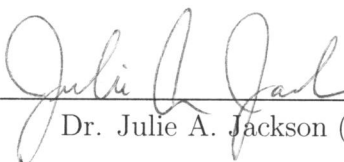
17 Mar 2010  
\_\_\_\_\_  
date

  
\_\_\_\_\_  
Dr. Steven C. Gustafson (Member)

17 Mar 10  
\_\_\_\_\_  
date

  
\_\_\_\_\_  
Dr. Richard K. Martin (Member)

10 Mar 2010  
\_\_\_\_\_  
date

  
\_\_\_\_\_  
Dr. Julie A. Jackson (Member)

17 Mar 2010  
\_\_\_\_\_  
date

*Abstract*

This research details the effect of spatial resolution on target discrimination in Synthetic Aperture Radar (SAR) images. Multiple SAR image chips containing targets and non-targets are used to test a baseline Automatic Target Recognition (ATR) system with reduced spatial resolution. Spatial resolution is reduced by lowering the pixel count or synthesizing a degraded image by filtering and reducing the pixel count. A two-parameter Constant False Alarm Rate (CFAR) detector is tested, and three feature sets, size, contrast, and texture, are used to train a linear classifier and to estimate probability density functions for the two classes. The results are scored using Area Under the Receiver Operating Characteristic (AUROC) curve. The CFAR detector is shown to perform better at a lower resolution. All three feature sets perform well together with degradation of resolution; separately the sets have different performances. The texture features perform the best because they do not depend on the number of pixels on the target; the size features perform the worst for the same reason. The contrast features yield improved performance when the resolution is slightly reduced.

## *Acknowledgements*

First and foremost, I am grateful to God for giving me the opportunity and strength to complete my Master's degree. I am thankful to be blessed with a very understanding and caring wife and three wonderful children, who have stood by me through all my struggles.

I would like to thank members of my committee: Dr. Terzuoli, Dr. Gustafson, Dr. Martin, and Dr. Jackson, for your support and direction that guided me through this process.

A special thank you to Ed Zelnio from AFRL/RYA for his time and intimate knowledge of this subject, as it was paramount to the successful completion of this research.

Lastly, I would like to thank AFRL/RYZT and NASIC/Data Analysis, for sponsoring this research.

John E. McGowan

## *Table of Contents*

	Page
Abstract . . . . .	iv
Acknowledgements . . . . .	v
List of Figures . . . . .	viii
List of Tables . . . . .	xii
List of Symbols . . . . .	xiii
List of Abbreviations . . . . .	xiv
I. Introduction . . . . .	1
1.1 Motivation . . . . .	1
1.2 Research Objectives . . . . .	2
1.3 Research Scope and Assumptions . . . . .	2
1.4 Organization . . . . .	2
II. Background . . . . .	3
2.1 Overview . . . . .	3
2.2 Radar Fundamentals . . . . .	3
2.3 Synthetic Aperture Radar (SAR) Principles . . . . .	4
2.3.1 System Properties . . . . .	5
2.3.2 Scene Properties . . . . .	10
2.4 Automatic Target Recognition (ATR) . . . . .	12
2.4.1 Prescreener . . . . .	12
2.4.2 Discriminator . . . . .	13
2.4.3 Classifier . . . . .	15
2.4.4 Measure of Performance . . . . .	19
III. Models and Data Generation . . . . .	24
3.1 Overview . . . . .	24
3.2 SAR Image Set . . . . .	24
3.3 Spatial Resolution Degradation . . . . .	24
3.3.1 Pixel Reduction . . . . .	25
3.3.2 Degraded Images . . . . .	26

	Page
IV. Experimental Method . . . . .	28
4.1 Overview . . . . .	28
4.2 Two-Parameter CFAR . . . . .	28
4.3 Discrimination . . . . .	29
4.3.1 Size Features . . . . .	30
4.3.2 Contrast Features . . . . .	30
4.3.3 Texture Features . . . . .	31
4.4 Classifier . . . . .	32
V. Results and Analysis . . . . .	33
5.1 Overview . . . . .	33
5.2 CFAR Detector . . . . .	33
5.3 Discriminating Features . . . . .	38
5.3.1 Size Features . . . . .	38
5.3.2 Contrast Features . . . . .	55
5.3.3 Texture Features . . . . .	66
5.3.4 All Nine Features . . . . .	77
5.4 Feature Comparison . . . . .	79
5.5 Summary . . . . .	85
VI. Conclusions . . . . .	86
6.1 Overview . . . . .	86
6.2 General Discussion . . . . .	86
6.3 Future Work . . . . .	87
Appendix A. Tables of AUROC . . . . .	88
Appendix B. App 2 . . . . .	93
B.1 Image Reduction . . . . .	93
B.2 Two-Paramter CFAR . . . . .	94
B.3 Feature Code . . . . .	97
B.4 Sub-Image . . . . .	104
B.5 Fisher Line . . . . .	107
B.6 ROC . . . . .	111
Bibliography . . . . .	113



## *List of Figures*

Figure		Page
2.1.	SAR collection geometry . . . . .	5
2.2.	SAR collection methods . . . . .	6
2.3.	One dimensional point target discrimination . . . . .	9
2.4.	Comparison between an optical image and a collection of SAR images taken at different azimuth angles . . . . .	11
2.5.	CFAR test window . . . . .	13
2.6.	The three dimensional feature space with the Fisher line and the projection onto the Fisher line . . . . .	16
2.7.	Example of Gaussian kernels applied to points in each classes .	17
2.8.	Example of feature projection onto the Fisher line . . . . .	18
2.9.	Threshold sweep to calculate ROC curve example . . . . .	20
2.10.	Gaussian distributions with varying mean to show the effect on ROC curves . . . . .	22
2.11.	Gaussian distributions with increasing variance to show the effect on ROC curves . . . . .	23
3.1.	Images from the MSTAR data set. . . . .	25
3.2.	Collection of the same SAR image with different pixel count. .	26
3.3.	Collection of the same SAR image with different levels of image degradation. . . . .	27
4.1.	ROC curves for two-parameter CFAR for different test box size.	29
4.2.	Collection of binary images of a T-72 with varying thresholds .	30
4.3.	Collection of binary images of clutter with varying thresholds .	31
5.1.	Plot of the two-parameter CFAR AUROC versus spatial resolu- tion in the x and y direction for image resolution reduction . .	35
5.2.	ROC curves for the original resolution, best performer, and worst performer for a CFAR detector with pixel count reduction. . .	36

Figure		Page
5.3.	ROC curves for the original resolution, best performer, and worst performer for a CFAR detector with image filtering degradation.	37
5.4.	The 3D size feature space for image chips with a resolution of 1 ft $\times$ 1 ft with Fisher line . . . . .	39
5.5.	The 3D size feature space for image chips with a resolution of 2 ft $\times$ 2 ft with Fisher line . . . . .	40
5.6.	The 3D size feature space for image chips with a resolution of 4 ft $\times$ 4 ft with Fisher line . . . . .	41
5.7.	The 3D size feature space for image chips with a resolution of 8 ft $\times$ 8 ft with Fisher line . . . . .	42
5.8.	The estimated pdfs of the two classes using Parzen windows with a Gaussian kernel . . . . .	43
5.9.	The estimated pdfs of the two classes using Gaussian pdfs . . .	44
5.10.	The estimate of the ROC curves for the size features . . . . .	45
5.11.	Plot of size features AUROC versus spatial resolution in the x and y directions for pixel reduction . . . . .	46
5.12.	Plot of mass features AUROC versus spatial resolution in the x and y directions for pixel reduction . . . . .	47
5.13.	Plot of Diameter feature AUROC versus spatial resolution in the x and y directions for pixel reduction . . . . .	48
5.14.	Plot of rotational inertia feature AUROC versus spatial resolution in the x and y directions for pixel reduction . . . . .	49
5.15.	Size features two classes pdfs . . . . .	50
5.16.	Plot of size features AUROC versus spatial resolution in the x and y directions for image filtering degradation . . . . .	51
5.17.	Plot of mass features AUROC versus spatial resolution in the x and y directions for image filtering degradation . . . . .	52
5.18.	Plot of Diameter feature AUROC versus spatial resolution in the x and y directions for image filtering degradation . . . . .	53
5.19.	Plot of rotational inertia feature AUROC versus spatial resolution in the x and y directions for image filtering degradation . .	54

Figure		Page
5.20.	Graph of the estimated pdfs of the Contrast features . . . . .	56
5.21.	Graph of the estimated pdfs of the Contrast features . . . . .	57
5.22.	Plot of contrast feature AUROC versus spatial resolution in the x and y directions for pixel reduction . . . . .	58
5.23.	Plot of peak CFAR feature AUROC versus spatial resolution in the x and y directions for image filtering degradation . . . . .	59
5.24.	Plot of mean CFAR feature AUROC versus spatial resolution in the x and y directions for pixel reduction . . . . .	60
5.25.	Plot of percent bright feature AUROC versus spatial resolution in the x and y directions for pixel reduction . . . . .	61
5.26.	Plot of contrast features AUROC versus spatial resolution in the x and y directions for image filtering degradation . . . . .	62
5.27.	Plot of peak CFAR feature AUROC versus spatial resolution in the x and y directions for image filtering degradation . . . . .	63
5.28.	Plot of mean CFAR feature AUROC versus spatial resolution in the x and y directions for image filtering degradation . . . . .	64
5.29.	Plot of percent bright feature AUROC versus spatial resolution in the x and y directions for image filtering degradation . . . . .	65
5.30.	Graph of the estimated pdfs of the Texture features . . . . .	67
5.31.	Graph of the estimated pdfs of the Texture features . . . . .	68
5.32.	Plot of texture features AUROC versus spatial resolution in the x and y directions for image filtering degradation . . . . .	69
5.33.	Plot of standard deviation feature AUROC versus spatial reso- lution in the x and y directions for image filtering degradation .	70
5.34.	Plot of rank filled ratio feature AUROC versus spatial resolution in the x and y directions for image filtering degradation . . . . .	71
5.35.	Plot of fractal dimension feature AUROC versus spatial resolu- tion in the x and y directions for image filtering degradation . .	72
5.36.	Plot of texture features AUROC versus spatial resolution in the x and y directions for image filtering degradation . . . . .	73

Figure		Page
5.37.	Plot of standard deviation feature AUROC versus spatial resolution in the x and y directions for image filtering degradation .	74
5.38.	Plot of rank filled ratio feature AUROC versus spatial resolution in the x and y directions for image filtering degradation . . . .	75
5.39.	Plot of fractal dimension feature AUROC versus spatial resolution in the x and y directions for image filtering degradation . .	76
5.40.	Plot of all nine features AUROC versus spatial resolution in the x and y direction for image resolution reduction . . . . .	78
5.41.	ROC curves for the original/best, and worst resolution for size features. . . . .	81
5.42.	ROC curves for the original, best, and worst resolution for contrast features. . . . .	82
5.43.	ROC curves for the original/best, and worst resolution for texture features. . . . .	83
5.44.	ROC curves for the original/best, and worst resolution for all nine features. . . . .	84

## *List of Tables*

Table		Page
2.1.	System properties that define spatial resolution . . . . .	6
2.2.	Best Set of discrimination features from the work conducted at Lincoln Laboratory [5] . . . . .	15
5.1.	Comparison of individual features from the work conducted at Lincoln Laboratory and this research [5] . . . . .	79
A.1.	AUROC for the Two-Parameter CFAR detector for reduced pixel count. . . . .	88
A.2.	AUROC for the Two-Parameter CFAR detector for image degra- dation by filtering. . . . .	89
A.3.	AUROC for individual Size Discriminating Features for reduced pixel count. . . . .	89
A.4.	AUROC for individual Size Discriminating Features for image degradation by filtering. . . . .	90
A.5.	AUROC for individual Contrast Discriminating Features for re- duced pixel count. . . . .	90
A.6.	AUROC for individual Contrast Discriminating Features for im- age degradation by filtering. . . . .	91
A.7.	AUROC for individual Texture Discriminating Features for re- duced pixel count. . . . .	91
A.8.	AUROC for individual Texture Discriminating Features for im- age degradation by filtering. . . . .	92

# *List of Symbols*

Symbol		Page
$T_r$	Round Trip Time . . . . .	3
$T_p$	Pulse Repetition Interval . . . . .	4
$f_p$	Pulse Repetition Frequency . . . . .	4
$\lambda$	Wavelength . . . . .	4
$v$	Velocity . . . . .	4
$\Delta y$	Azimuth Resolution . . . . .	6
B	BandWidth . . . . .	7
$\Delta x$	Range Resolution . . . . .	7
$\mu_c$	Mean Value of Clutter . . . . .	12
$\sigma_c$	Standard Deviation of Clutter . . . . .	12
$P_{fa}$	Probability of False Alarm . . . . .	19
$P_d$	Probability of Detection . . . . .	19

## *List of Abbreviations*

Abbreviation		Page
SAR	Synthetic Aperture Radar . . . . .	1
MSTAR	Moving and Stationary Target Acquisition and Recognition	2
Radar	RAdio Detection And Ranging . . . . .	3
EM	Electro-Magnetic . . . . .	3
PRI	Pulse Repetition Interval . . . . .	4
PRF	Pulse Repetition Frequency . . . . .	4
PSF	Point Spread Function . . . . .	5
LFM	Linear Frequency Modulated . . . . .	7
RCS	Radar Cross Section . . . . .	10
ROI	Region of Interest . . . . .	13
LDA	Linear Discriminant Analysis . . . . .	15
pdfs	probability density functions . . . . .	17
MOP	Measure of Performance . . . . .	19
ROC	Receiver Operating Characteristic . . . . .	19
AUROC	Area Under the ROC . . . . .	21

# THE EFFECT OF SYNTHETIC APERTURE RADAR IMAGE RESOLUTION ON TARGET DISCRIMINATION

## I. Introduction

Synthetic Aperture Radar (SAR) is an imaging technique that allows for operations in all weather conditions, day/night, and with great distance between the system and the scene to be imaged. SAR imaging has been utilized by both military and civilian sectors [4]. Uses include terrain mapping and surveillance operations, which both lead to a high volume of data. This high volume leads to problems in management of the system; for example in 2004 the Global Hawk was at 30% of usage because image analysts could not keep up with data being collected [8]. SAR has the ability to generate enormous amounts of data. Automatic screening of images to cue operators to zero in on areas of interest could reduce this burden.

Automated systems that screen images for targets are generally referred to as Automatic Target Recognition (ATR) systems. The study and development of ATR systems is a relatively young field that has roots in three fields: mathematics, pattern recognition, and computer science. Also, ATR is typically designed to take advantage of the unique physical traits of the physical system. Thus ATR that performs well on one type of system may not transfer to another. For example, an ATR system that performs facial recognition may not be able to distinguish different speech traits.

### ***1.1 Motivation***

The use of a SAR system to map large areas of the earth to detect possible objects of interest is a task that allows aircrew to have safe stand-off distance while monitoring the area. The images that are produced may not be sharp and clear, which makes it difficult for a human operator to find an object. Once an object is



located, the operator typically verifies the area with another sensor. This is a slow and ineffective way to operate, which motivates the need to understand how SAR image quality, as defined by its spatial resolution, affects ATR performance.

## ***1.2 Research Objectives***

The goal of this research is to show that an ATR can perform on lower resolution images and still maintain a high level of detection with minimal false alarms.

## ***1.3 Research Scope and Assumptions***

The scope of this research is limited to SAR images from the Moving and Stationary Target Acquisition and Recognition (MSTAR) data set collected by the Air Force Research Laboratory and publicly distributed through the Sensor Data Management System website. Testing is limited to the amplitude of the data because the MSTAR data set is distributed in a form that has an unknown weighting. Not knowing the weighting creates a problem in retrieving the original data. In order to reduce the resolution a spatial filter is used that works on the amplitude of the image only.

## ***1.4 Organization***

The remainder of this document is organized as follows. Chapter 2 provides background on SAR images and ATR process. Chapter 3 describes the SAR images used in this research and how they are manipulated to produce the desired image quality. Chapter 4 details the ATR process that is used to discriminate targets. Chapter 5 provides the results for ATR versus SAR image quality. Chapter 6 provides research conclusions and recommends future research.

## II. Background

### 2.1 Overview

This chapter provides a survey of radar systems properties and how they relate to Synthetic Aperture Radar (SAR) image quality, mainly the spatial resolution of the image. Spatial resolution is shown to depend on the PSF of the system, where a pixel in the image is an estimate of the Radar Cross Section (RCS) of the ground sample distance. An Automatic Target Recognition (ATR) that has been used to perform target discrimination is discussed. In order to assess the effectiveness of an ATR, a Measure of Performance (MOP) is introduced. MOP uses Probability of Detection ( $P_d$ ) and Probability of False Alarm ( $P_{fa}$ ), which can be graphically represented by a Receiver Operating Characteristic (ROC) curve. The ROC curve can be summarized in a single performance metric, known as the AUROC.

### 2.2 Radar Fundamentals

Radar is a detection system that exploits the use of the physical properties of Electro-magnetic (EM) fields. A known signal is generated and transmitted, through an antenna to propagate into the scene of interest. These fields interact with the objects in the scene and are scattered. A receiving antenna (which can be the same or different antenna than the transmitting antenna) is used to sense the scattered fields. These received signals are filtered and sampled to estimate the amplitude and distance of the reflecting object.

Basic radar systems use a pulsed signal to detect the distances of reflecting objects. The pulse signal is transmitted and when it interacts with an object the EM fields are scattered back to the radar. The returned signal is convolved with a time reversal of the transmitted signal; this is known as a matched filter. The expected measure of distance is

$$r_{dist} = \frac{cT_r}{2}, \quad (2.1)$$

where  $T_r$  is the round trip time and  $c$  is the speed of light in the medium.

After the radar system transmits a signal, it has a pre-determined time in which to transmit another pulse. This waiting period is called Pulse Repetition Interval (PRI),  $T_p$ , and the reciprocal is called Pulse Repetition Frequency (PRF),  $f_p$ . The PRF is used to detect the unambiguous range of targets, expressed as

$$R_{un} = \frac{T_p c}{2} = \frac{c}{2f_p}. \quad (2.2)$$

Radars use an antenna to transmit the signal giving the signal directivity and gain, which can be expressed by the antenna pattern. The azimuth resolution for a single transmission is

$$r_{az} = \frac{\lambda D}{l}, \quad (2.3)$$

where  $D$  is the distance from the antenna,  $l$  is the length of the aperture, and  $\lambda$  is the wavelength of the signal.

### ***2.3 Synthetic Aperture Radar (SAR) Principles***

The use of radar to form an image dates back to 1951 when Carl Wiley developed a method known as Doppler beam sharpening [14]. SAR images are produced from the relative motion between a scene and the radar. This motion allows for the radar antenna to sample the scene, thus synthesizing a larger aperture. Figure 2.1 illustrates a simple collection path. The radar platform moves in the  $y$  direction (azimuth) with a velocity  $v$  and transmits pulses in the  $x$  direction (range) at different points. The return pulses are combined in phase to produce a larger synthetic aperture, thus allowing for greater resolution than that of the original antenna.

SAR image properties can be separated into two different categories; system and scene [7]. The system properties are under the control of the system designer, and have predictable functionality. The scene properties are generated from the scene being imaged.

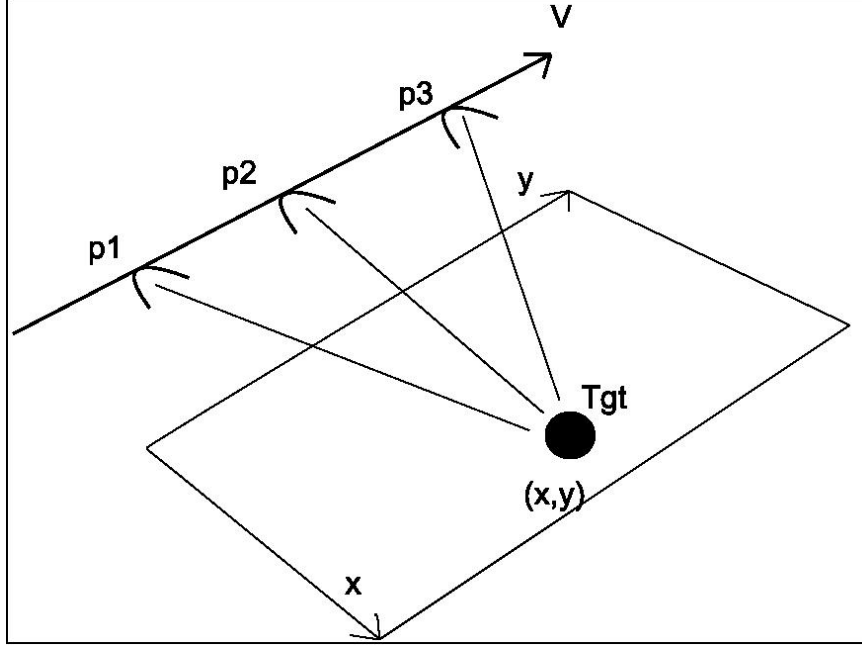
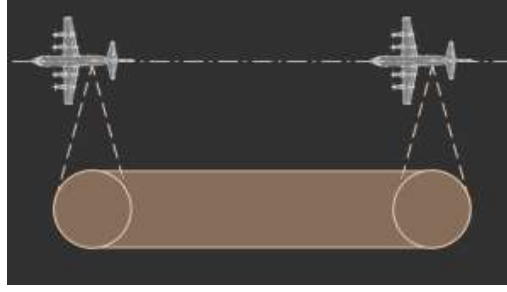
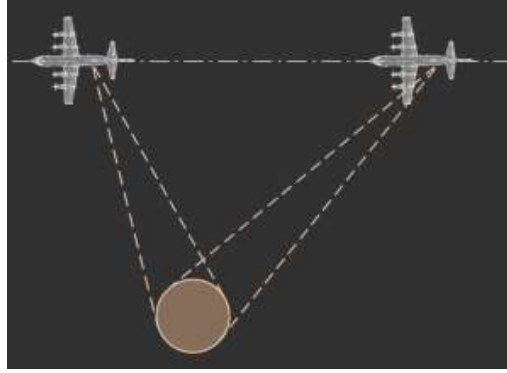


Figure 2.1: The radar platform moves with a velocity  $v$  in the  $y$ -direction while the antenna points in  $x$ -direction. At each point  $p1$ ,  $p2$ , and  $p3$  the system samples the scene.

*2.3.1 System Properties.* SAR system performance is described by its Point Spread Function (PSF), which depends on the bandwidth,  $B$ , of the radar signal and the collection length. Table 2.1 shows how range and azimuth spatial resolutions are calculated based on the collection mode. The two collection modes are stripmap and spotlight. The data used for this research was collected in the spotlight mode, but both modes are discussed for completeness. In stripmap, the aircraft flies in a straight path and the signal is transmitted perpendicular to the direction of flight. In spotlight, the aircraft steers the beam to stare at the same swath of ground. Figure 2.2 depicts the two modes. Carrara [1] notes that differences in the modes are limiting factors on azimuth resolution and scene coverage. In stripmap mode the beamwidth of the antenna limits the azimuth resolution, and the data collection limits the azimuth scene coverage. The spotlight mode limits the azimuth resolution by its data collection length, and the antenna beam width limits the maximum azimuth scene coverage.



(a) Stripmap



(b) Spotlight

Figure 2.2: [a] and [b] images show the collection method for the stripmap mode and spotlight mode, respectively.

Table 2.1: System properties that define spatial resolution

	Stripmap	Spotlight
Range Resolution( $\Delta x$ )	$\frac{c}{2B}$	$\frac{c}{2B}$
Azimuth Resolution( $\Delta y$ )	$\frac{\lambda}{2}$	$\frac{\lambda}{2\Delta\theta}$

The PSF, which is the impulse response or response to a point target, is used as a measure of image quality of the system by defining the spatial resolution by the -3dB cutoff of the main lobe [11]. The PSF depends on the range resolution  $\Delta x$  and azimuth resolution  $\Delta y$  [11]. The expected PSF is

$$\text{PSF} = \text{sinc}(\Delta x)\text{sinc}(\Delta y). \quad (2.4)$$

SAR has an impulse response with sidelobes which cause blurring/smearing of the image. Different types of windowing techniques can be used to suppress the sidelobes.

Range is the distance perpendicular to the path of flight, and depends on the bandwidth of the radar signal [4]. The signal model used most often for SAR is the Linear Frequency Modulated (LFM) chirp model, because it allows for increased range resolution through pulse compression [11]. The range resolution of a radar system is determined by the ability to separate two closely spaced targets, and is shown to depend on the inverse of the bandwidth  $B$  of the pulse [11] as

$$\Delta x = \frac{c}{2B}, \quad (2.5)$$

which shows the predicted range resolution,  $\Delta x$ , versus  $B$ . This result is from the output of the matched filter, which maximizes the output signal to noise ratio [10]. Figure 2.3 shows the effect of bandwidth on range resolution for a simulation of three point targets with 1.5 m spacing. A transmitted signal with a  $B$  of 100 MHz corresponds to a  $\Delta x$  of 1.5 m, which cannot resolve the point targets (see Figure 2.3 [a]). A transmitted signal with a  $B$  of 200 MHz corresponds to a  $\Delta x$  of 7.5 m, which is sufficient to resolve the three point targets (see Figure 2.3 [b]). Even though the signal with a  $B$  of 100 MHz has a resolution equal to the spacing of the point targets, it still could not resolve them because the response from each target is still wide enough to corrupt the next target.

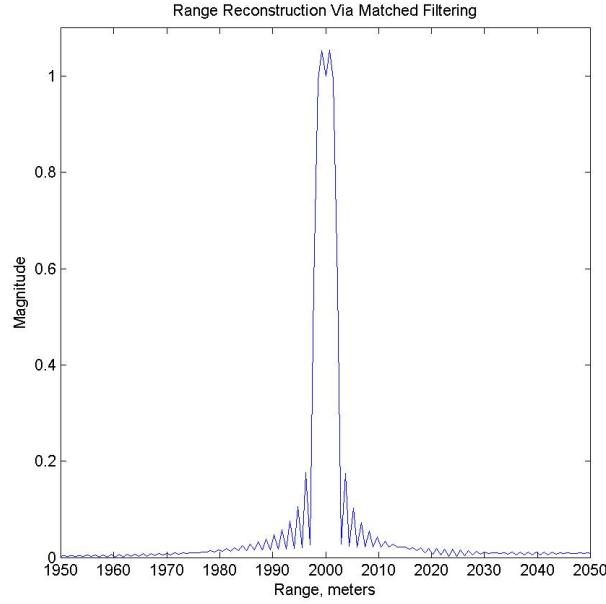
While the resolution in the range direction is determined by a single transmission, the azimuth resolution is more complicated, making SAR unique and allowing for imaging capabilities. The azimuth resolution is also defined by its ability to separate two objects. This resolution depends on the length of the aperture, wavelength, and distance from the radar. However, it can be shown that with SAR, the azimuth resolution only depends on half the length of the aperture [15], i.e.

$$\Delta y = \frac{l}{2}. \quad (2.6)$$

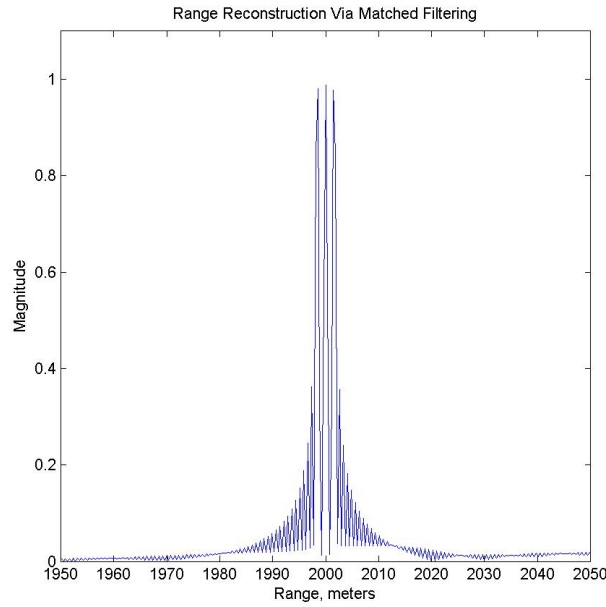
This is the case for an aircraft moving in a straight path with the antenna looking perpendicular, but if the antenna is steered to stare at an area, as is the case for

spotlight, the azimuth resolution is determined by

$$\Delta y = \frac{\lambda}{2\Delta\theta}. \quad (2.7)$$



(a) 100 MHz



(b) 200 MHz

Figure 2.3: The effect of bandwidth on discriminating point targets can be seen in the [a] and [b]. Three point targets are located at 1998.5m, 2000m, and 2001.5m [a] shows the output of the matched filter for a radar signal with a bandwidth of 100 MHz and the three point targets cannot be seen separated. [b] shows the output of the matched filter for a radar signal with a bandwidth of 200 MHz and the three individual point targets can be seen.



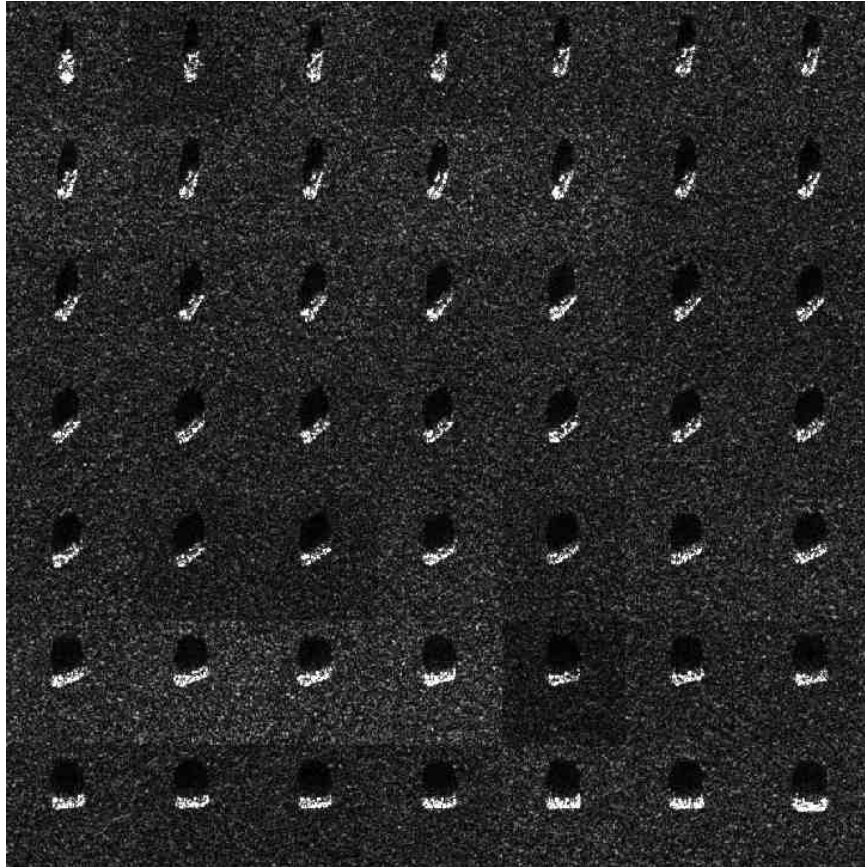
*2.3.2 Scene Properties.* The system properties control spatial resolution, but the scene makes up the content. The scene has three categories: noise, target, and clutter. Noise and clutter can then be separated into sub categories to better classify their effects. Noise in the image can be described as additive or multiplicative, but these effects are not a part of this research and will not be discussed further.

*2.3.2.1 Target.* To detect a target, prior knowledge of its return signal is needed. The target Radar Cross Section (RCS) describes the return echo from the object, but any small changes in the look angle between the object and the radar can greatly change the RCS. For SAR imagery this angle and wavelength dependence can cause images of the same scene to look very different. Figure 2.4 illustrates this with the BTR-60 imaged over varying azimuth angles. The brighter sides are on the side of the radar, while a shadow is cast because of the lack of returned energy. An optical photograph of a BTR-60 is shown for reference.

*2.3.2.2 Clutter.* The return from clutter is the largest competing factor in the natural environment for target detection, by human operator or ATR. To model clutter, everything in the desired environment is considered to affect the system, with probability density functions used to model their effects. Much research has gone into trying to measure, model, and predict the radar returns from natural clutter [15]. According to [10] the four most common distributions used are Rayleigh, log-normal, Weibull, and K-distribution; the Rayleigh distribution is the most popular [10]. For this research clutter is separated into two classes: natural and man-made. Natural clutter is more dispersive and is easier to separate than man-made objects. Man-made objects provide greater confusion for detecting targets of interest.



(a) BTR-60 optical image



(b) BTR-60 collection of SAR images

Figure 2.4: [a] an optical image of a BTR 60. [b] a collection of SAR images of a BTR60 as the angle between the radar and the vehicle is varied.

## 2.4 Automatic Target Recognition (ATR)

The ATR method used in this thesis is based on the method developed at Lincoln Laboratory [6]. It consists of three parts: prescreener, discriminator, and classifier. The prescreener identifies image chips with objects of interest from full scene imagery. The discriminator rejects image chips that do not contain targets of interest. The classifier then puts the targets into different classes. Separating the process into sections reduces the complexity and computational cost of the system.

*2.4.1 Prescreener.* Detection algorithms can use two different thresholding techniques, global and adaptive. Global thresholding selects a threshold, and anything greater than that value is flagged as a detection. This technique is very simple to implement, but can cause numerous false alarms. Adaptive thresholding adjusts the threshold by the local statistics around the test pixel.

A popular technique for prescreening SAR images for targets uses the belief that returns from man-made objects are stronger than those from the surrounding natural clutter. A likelihood test is used, referred to as a two-parameter CFAR test [6]:

$$\frac{x - \mu_c}{\sigma_c} \underset{<}{\overset{>}{\gtrless}} \gamma, \quad (2.8)$$

where  $x$  is the pixel under test,  $\mu_c$  and  $\sigma_c$  are the mean and standard deviation of the clutter, and  $\gamma$  is an adjustable threshold. The pixel is considered to be a target if it is greater than the threshold and a non-target otherwise. This type of test assumes that the clutter distribution is known and that the amplitude of the target pixel to clutter statistic ratio is greater than some threshold. To determine the clutter, a square annular region surrounding the test pixel is used to window the scene to determine  $\mu_c$  and  $\sigma_c$ . To ensure that the background clutter is not corrupted by the target, a guard window is constructed around the test pixel as shown in Figure 2.5. It has been noted [6] that this stage can be conducted at a lower resolution than the original

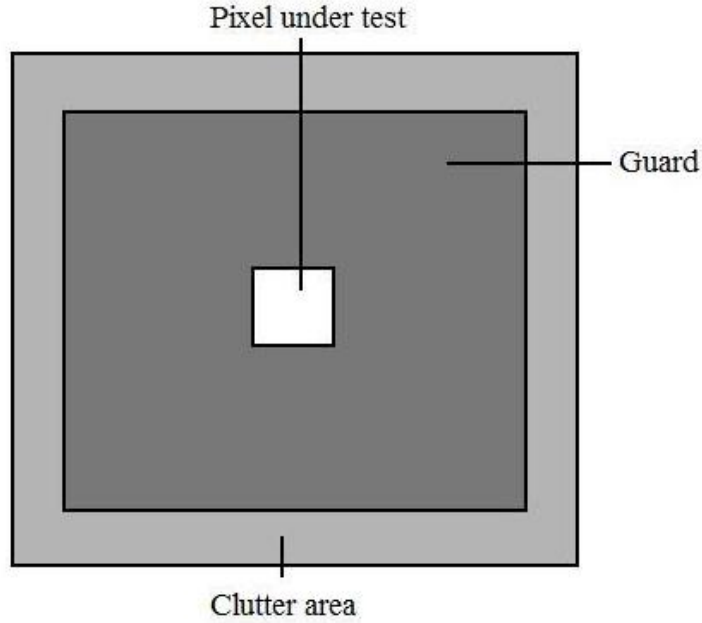


Figure 2.5: CFAR test window depicting the test pixel area, guard area, and the clutter area. This image illustrates the method to screen out the effects of a target corrupting the clutter statistics.

image. Once a pixel is declared a target, then a section around the pixel is considered a Region of Interest (ROI), and is sent to the discrimination stage.

*2.4.2 Discriminator.* Once the prescener identifies a ROI where a potential target is located, the discrimination stage rejects regions containing clutter that pass the detector. The properties of the target then need to be considered in order to differentiate between objects. Three types of features are considered: size, contrast, and texture. Properties of the target in the image are referred to as a feature. Different types of discriminating features that can be used to separate targets from clutter are covered in [3]. Following is a list of the three feature sets and a description of individual features:

## Size Features

*Mass* is the sum of pixels in a binary image;

*Diameter* is the length of the smallest box that encloses all the bright scatters in a binary image;

*Rotational Inertia (normalized)* is the second mechanical moment about the center of the binary image;

## Contrast Features

*Peak CFAR* is the maximum value in the CFAR image;

*Mean CFAR* is the mean value of the CFAR image;

*Percent Bright* is the percentage of pixels that exceed a predetermined value;

## Texture Features

*Standard Deviation* is the standard deviation of the image;

*Fractal Dimension* is the log difference of all one pixel size boxes and two pixel size boxes that encompass all the bright scatters in the binary image;

*Rank Filled Ratio* is the ratio of the power in the brightest 5% scatters versus the total power of the image;

These features have been shown to successfully separate image chips between man-made and natural clutter [12]. The binary image is constructed from a threshold test to select the brightest scatterers and set those pixel values to one in the image, then zero out all others. The CFAR image is the output of the image chip where the two-parameter CFAR detector is conducted on each pixel in the image.

Table 2.2 is from research done on the resolution and polarization of SAR images and how ATR performance is affected [5]. The study only used two spatial resolutions, 1 ft and 1 m. Discriminating features that perform the best per resolution are indicated. The study shows that three features perform well for both resolutions: ranked

filled ratio, mass, and mean CFAR. This indicates that ATR can be conducted at lower resolutions; the Lincoln Laboratory study stops at 1 m, but this research looks at lower resolutions.

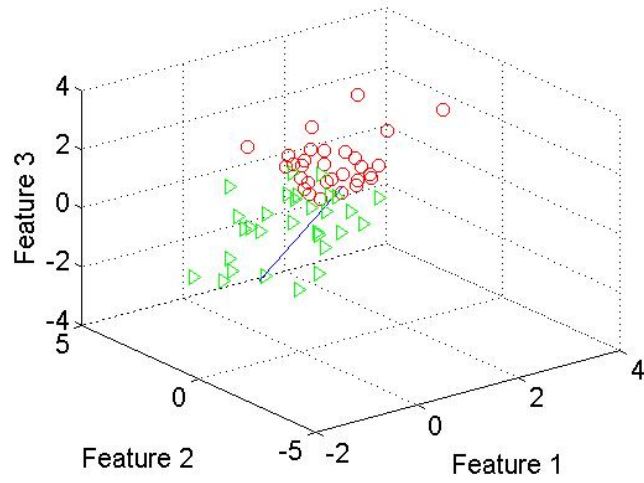
Table 2.2: Best Set of discrimination features from the work conducted at Lincoln Laboratory [5]

Feature	1 ft $\times$ 1 ft	1 m $\times$ 1 m
Standard Deviation	✓	
Rank Filled Ratio	✓	✓
Fractal Dimension		✓
Mass	✓	✓
Diameter		
Normalized Rotational Interia		
Peak CFAR		✓
Mean CFAR	✓	✓
Percent Bright		

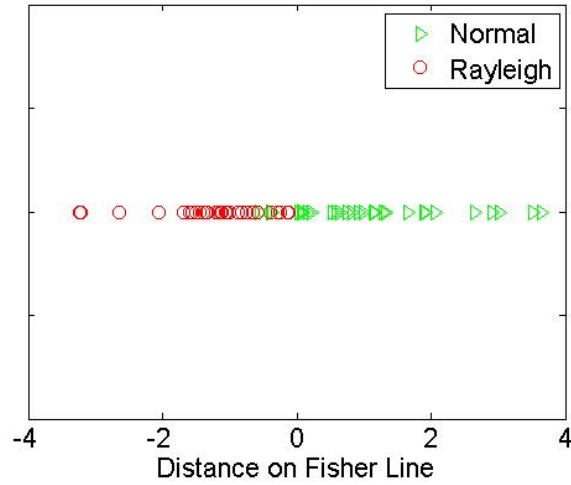
*2.4.3 Classifier.* Different techniques can be used to reduce the dimensionality of the data by mapping the data to a lower dimension. Linear Discriminant Analysis (LDA), also referred to as Fisher’s LDA, is a commonly used technique [8]. LDA performs dimension reduction, while preserving the class discrimination information as much as possible. LDA fails when the discriminatory information is in the variance of the data and not the mean [13]. LDA projects  $n$  dimensional feature spaces onto a line, known as the Fisher line, allowing for multi-dimensional problems to be reduced to one dimension. The Fisher line maximizes the separation of the between-class means while minimizing the in-class variance of the projected points, or expressed as

$$J = \frac{\mu_1 - \mu_2}{\sigma_1^2 + \sigma_2^2}, \quad (2.9)$$

where  $\mu_1$  and  $\mu_2$  are the mean for the two classes, and  $\sigma_1^2$  and  $\sigma_2^2$  are the variance for the two classes [13]. Figure 2.6 [a] shows a three dimensional feature space of two classes, generated by the normal (circles) and Rayleigh (triangles) distributions, and the Fisher line. Figure 2.6 [b] shows the projection of the points onto the Fisher line.



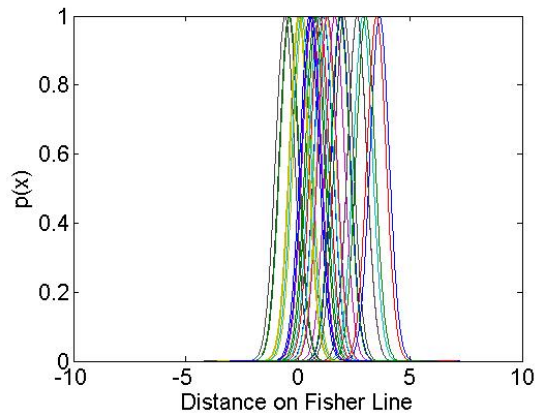
(a) Feature Space



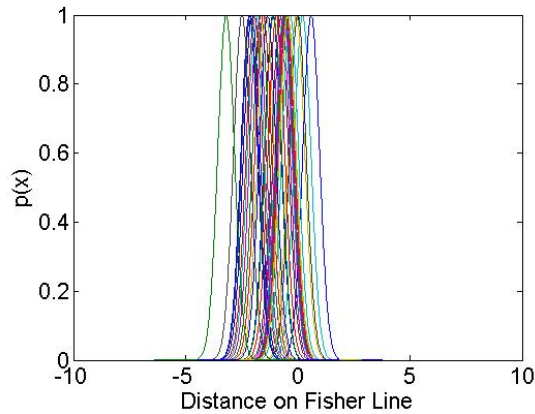
(b) Project onto Fisher Line

Figure 2.6: [a] is the three dimensional feature space for the two classes (circles and triangles) with the Fisher line, and [b] is the projection of the two classes onto the Fisher line.

The points for the classes on the Fisher line allow probability density functions (pdfs) of each class to be estimated. Parzen windows can be used to estimate the pdf of each class. A kernel function, such as a Gaussian, is located over each point to estimate the pdf of each class, as seen in Figure 2.7. The variance of the Gaussian kernel is adjusted until the sum of all in-class Gaussians is unimodal. Figure 2.8 shows the estimated pdfs for the two classes. A threshold test on the Fisher line can be used to determine the class of an image.



(a) Normal (triangles) class



(b) Rayleigh (circles) class

Figure 2.7: Example of Gaussian kernels applied to points in each classes.



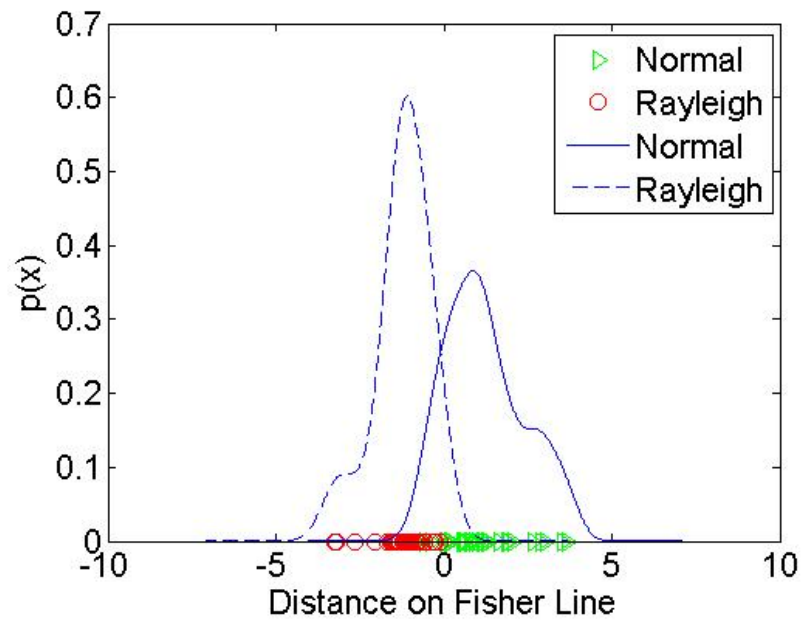


Figure 2.8: The projection of three feature points in each of the two classes (circles and triangles) onto the Fisher line. Parzen windows are used to estimate the pdf of each class. Here Parzen windows uses a Gaussian kernel over each point, then for each class the variance of the Gaussian is varied until the sum produces a unimodal function.

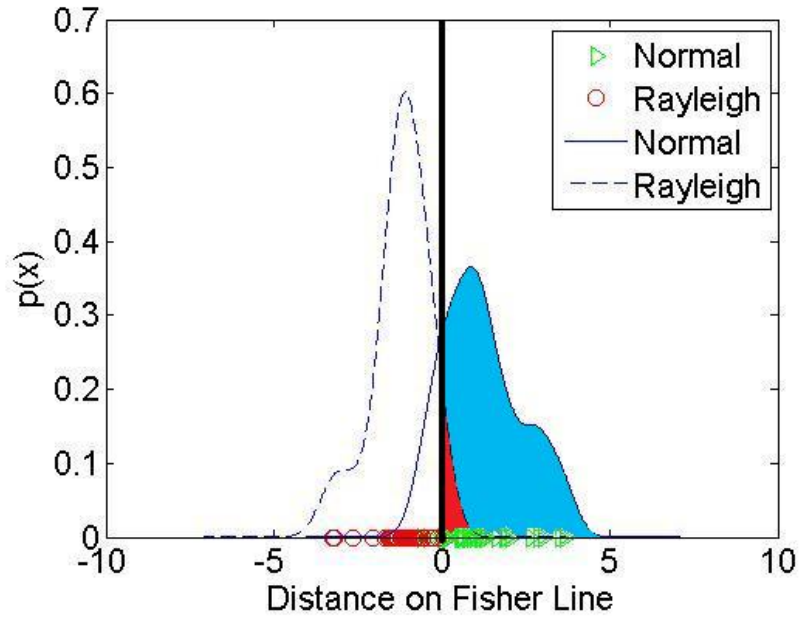
2.4.4 *Measure of Performance.* To compare different ATR performances a measure is needed. Probability of False Alarm ( $P_{fa}$ ) and Probability of Detection ( $P_d$ ) are two of the most common Measures of Performance (MOP) that can be used to describe the performance of an ATR.  $P_{fa}$  is the ratio of the number of non-targets declared as targets to the number of non-targets tested. The  $P_d$  is the ratio of the number of detected targets to the total number of targets:

$$P_{fa} = \frac{\text{Number of Non-Targets declared a Target}}{\text{Total number of Non-Targets}} \quad (2.10)$$

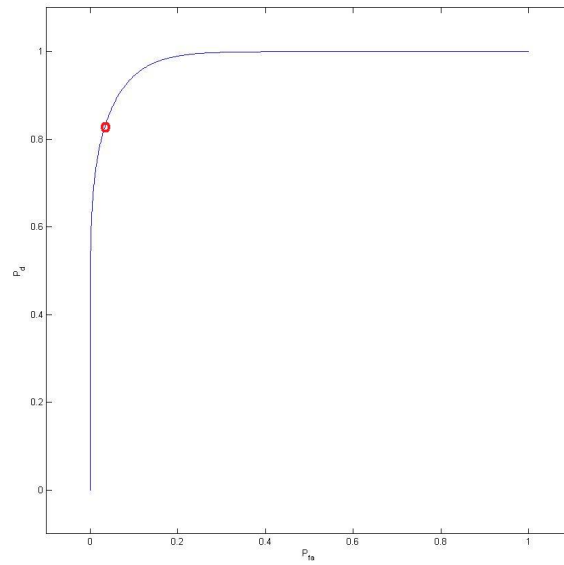
$$P_d = \frac{\text{Number of Targets declared a Target}}{\text{Total number of Targets}}. \quad (2.11)$$

The Receiver Operating Characteristic (ROC) is a graphical representation of  $P_d$  versus  $P_{fa}$ . In [9] it is shown that the curve does not decrease and that each point on the curve is from the threshold required to get that  $P_{fa}$  and  $P_d$  performance.

A ROC can be generated by testing a decision rule for varying thresholds, and comparing results to truth to calculate  $P_d$  and  $P_{fa}$  for each threshold. To produce a complete ROC curve the threshold must be varied so that  $P_d$  and  $P_{fa}$  have values from 0 to 1. Another method to produce a ROC curve is by sweeping a threshold across two pdfs. Each pdf represents a different class, target class and non-target, as the threshold is moved across the line the area of each of the pdfs is summed to calculate  $P_{fa}$  and  $P_d$ . Figure 2.9 illustrates this technique. In Figure 2.9 [a] the threshold line is indicated by the vertical black line,  $P_d$  is represented by the blue area and  $P_{fa}$  by the red area. These values are shown in Figure 2.9 [b] where  $P_{fa}$  and  $P_d$  for that threshold are indicated by a red circle. As this threshold line is moved the red circle traces out the ROC curve.



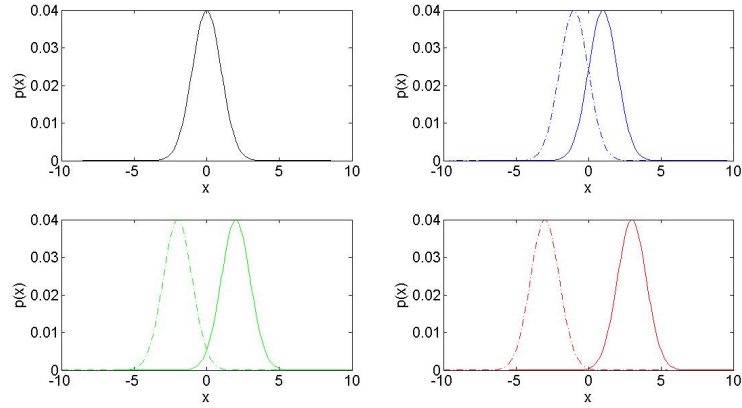
(a) Threshold test



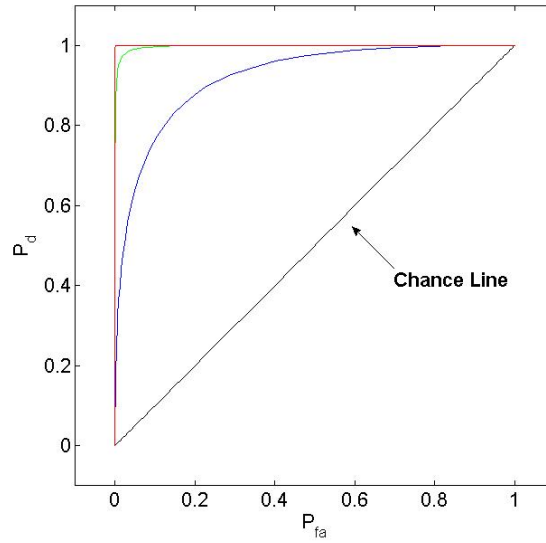
(b) ROC

Figure 2.9: [a] shows two pdfs with a threshold line. The shade areas represent  $P_{fa}$  (red) and  $P_d$  (blue) for the given threshold on the Fisher line. [b] is the corresponding ROC curve with the threshold point, indicated by a red circle, showing the  $P_{fa}$  and  $P_d$  point from [a].

Figures 2.10 and 2.11 show two scenarios; varying the mean to increase the separation of the two pdfs, and increasing the variance of one pdf, respectively. Figure 2.10 [a] shows four different cases of class separation, with each class represented by a Gaussian distribution. For each of these cases the separation of the between-class mean is different. This separation can be visually depicted by the ROC curves in Figure 2.10 [b]. The two overlapping pdfs produce the chance line, but as they separate the line is pulled towards the upper left corner. When the pdfs are non-overlapping the ROC curve forms a right angle signifying good class separation. In Figure 2.11 [a] four Gaussian distributions are shown with the same mean, but with the variance of one class increasing. This causes the ROC in Figure 2.11 [b] to cross the chance line, illustrating an ineffective test. Area Under the ROC (AUROC) is used to describe the performance as a single value. An AUROC of 1.0 shows good separation of the two classes, while a score of 0.5 indicates that the two classes have a complete overlap and the test is useless. In Chapter 5 we use the AUROC to compare the effectiveness of size, contrast, and texture features to separate target and non-target classes in SAR imagery as we image resolution is reduced.

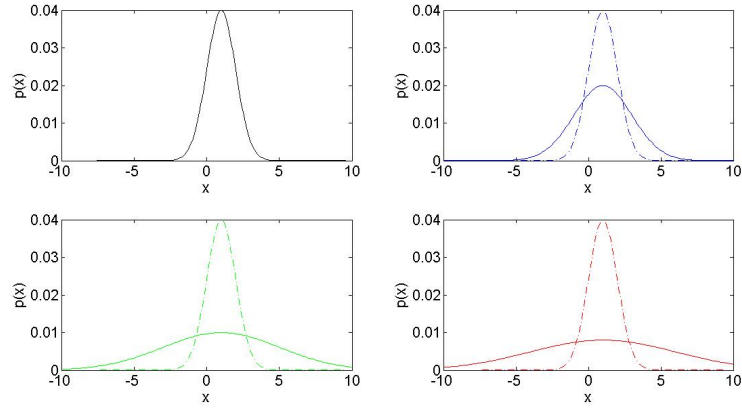


(a) Gaussian distribution

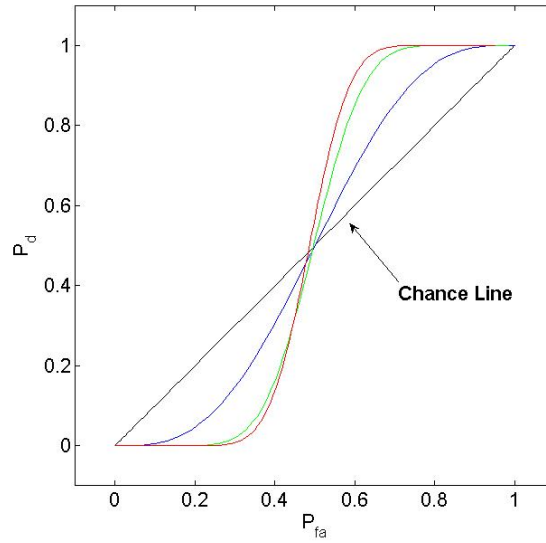


(b) ROC curves

Figure 2.10: [a] Gaussian distributions that have unit variance with different means. [b] ROC curves, illustrating the separation of the distributions in [a]. [c] Gaussian distributions with one having zero mean and unit variance and the other with zero mean and increasing variance.



(a) Gaussian distribution



(b) ROC curves

Figure 2.11: [a] Gaussian distributions with one having zero mean and unit variance and the other with zero mean and increasing variance. [b] ROC curves, illustrating the effect of increasing variance in [c]. Notice that as the variance increases the ROC curve becomes more vertical, indicating a lack of class separation.

### III. Models and Data Generation

#### 3.1 Overview

This chapter presents the SAR data set used for this research. The images are distributed in fixed  $1 \text{ ft} \times 1 \text{ ft}$  resolution, and the spatial resolution of the images is reduced in two different manners, pixel count reduction and filtering followed by downsampling.

#### 3.2 SAR Image Set

The MSTAR public data set is used for this research [8]. It is taken from a single channel X-band collection with a resolution of  $1 \text{ ft} \times 1 \text{ ft}$  in the spotlight mode. It contains a large set of target and non-target (clutter) image chips. Figure 3.1 shows four image chips; [a], [b], and [c] are a T-72, ZSU-23-4, and BTR-60, respectively, and [d] is a clutter image chip. The data is distributed in complex-value form with unknown weighting. Weighting is normally applied to suppress the sidelobes of the PSF. Unknown weighting impedes resolution reduction. Normally, the best way to reduce the resolution of complex imagery is to:

1. Compute 2D FFT;
2. Remove weighting;
3. Sub-divide aperture (frequency domain);
4. Re-apply weighting to sub-aperture;
5. Compute 2D inverse FFT.

Since the weighting is unknown, this technique cannot be used. Instead, we consider only the image amplitude and study two alternative approaches—pixel reduction and filtering degradation—to reduce image resolution.

#### 3.3 Spatial Resolution Degradation

Spatial resolution is varied in two manners; reduction of pixel count and spatial filtering followed by downsampling. Only three variations of spatial resolutions are

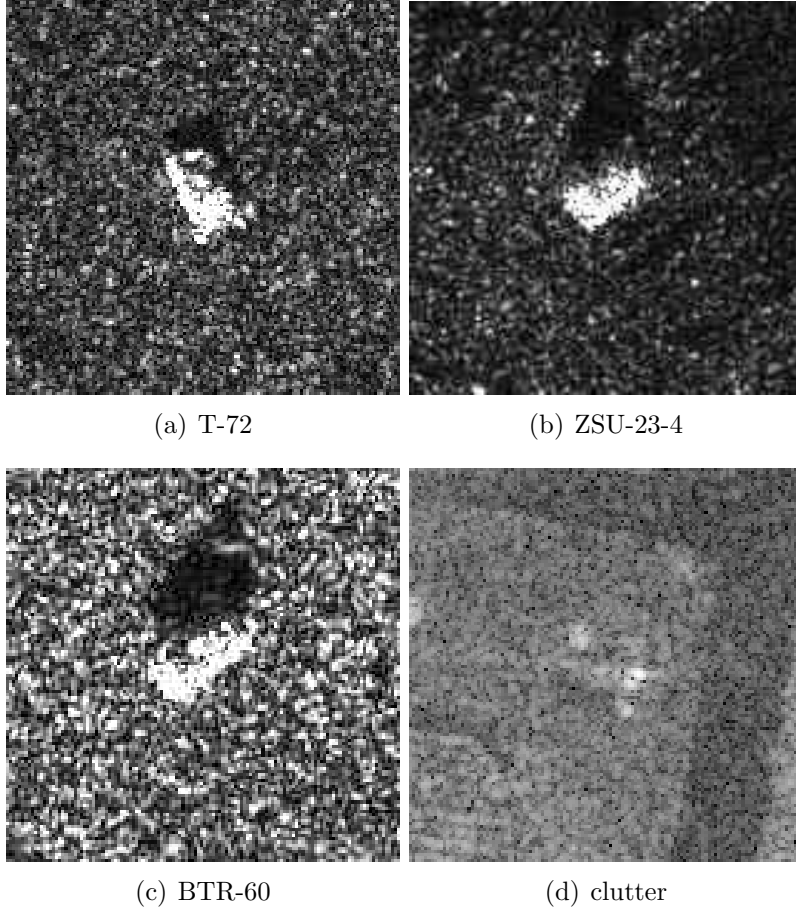


Figure 3.1: Examples of MSTAR image chips with 1 foot resolution.

produced; 2 ft, 4 ft, and 8 ft for both the x and y directions. The lowest spatial resolution considered is equal to the minimum target width. Resolution in the x and y direction is varied independently, resulting in sixteen combinations of x-y pixel resolution.

*3.3.1 Pixel Reduction.* Reduction in pixel count represents a reduced resolution, allowing for the same image to be processed with less pixels. The pixel count is reduced by averaging adjoining pixels to match the desired resolution; i.e. averaging a  $2 \times 2$  pixel block into 1 pixel for 2 ft resolution. Figure 3.2 shows the same image with different pixel counts. Figure 3.2 [a] is a zoomed in image of a T-72, Figure 3.2 [b] the pixel count reduced by 2 in both directions, representing a spatial resolution



of  $2 \text{ ft} \times 2 \text{ ft}$ , Figure 3.2 [c] and Figure 3.2 [d] are reductions of 4 and 8, respectively, of the original image.

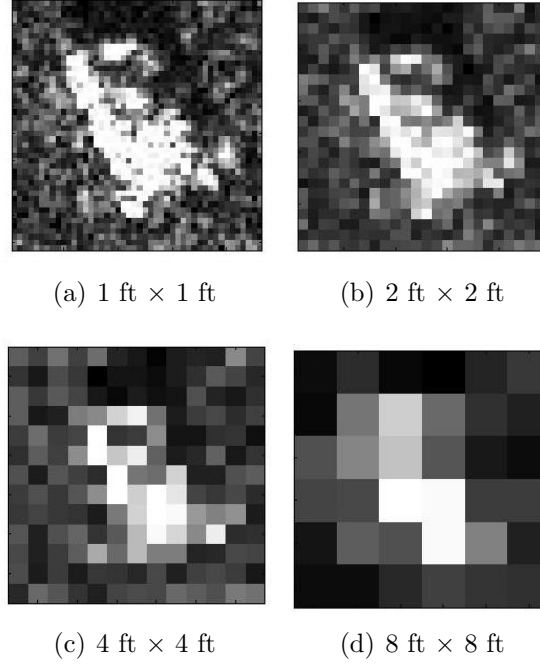


Figure 3.2: Effect of pixel averaging to reduce image resolution for a MSTAR image of a T-72 main battle tank that is centered in an open field.

*3.3.2 Degraded Images.* Pixel count reduction degrades the image, but it does not accurately model a collection where the PSF of the system has a wider mainlobe, corresponding to a decrease in spatial resolution. To simulate a coarser resolution than the original, the image is filtered with the following modified Hamming window:

$$H[p] = 0.54 + 0.46 \cos \frac{2\pi p}{2^{-m}X}, \quad (3.1)$$

and then reduced in pixel count as described in [2]. Here  $X$  is the length of the  $x$  dimension of the original image,  $p$  is defined from 0 to  $X-1$ , and  $m$  is the reduction factor, which is the  $\log_2$  value of the desired coarser resolution. The 2-D modified

Hamming window is defined by:

$$H[p, q] = H[p]H[q], \quad (3.2)$$

where  $q$  is defined from 0 to  $Y-1$ , and  $Y$  is the length of the  $y$  dimension. The steps to degrade the image are as follows: take the Fourier transform of the image, multiply it with the filter  $H[p, q]$ , take the Fourier transform of the product, and then downsample pixel count to match the simulated resolution. Figure 3.3 [a] shows the original image of a T-72, top left, and the output of this process for the 2 ft (Figure 3.3 [b]), 4 ft (Figure 3.3 [c]), and 8 ft (Figure 3.3 [d]) image degradation. When these images are compared to Figure 3.2, a noticeable blurring of the image is observable.

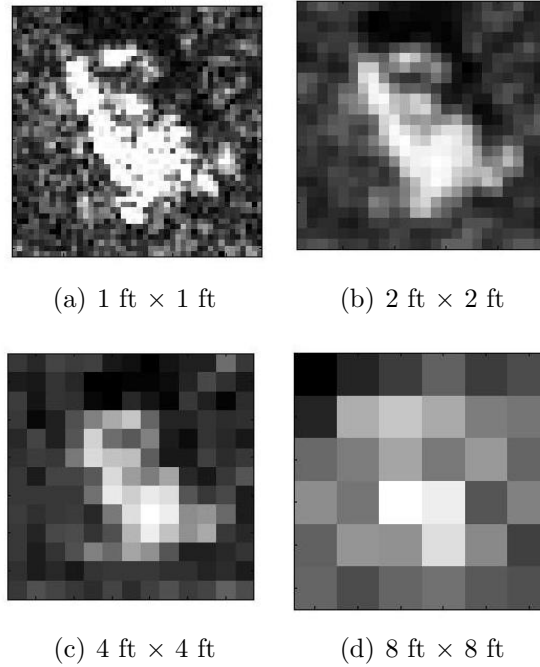


Figure 3.3: Effect of image degradation to reduce image resolution for a MSTAR image of a T-72 main battle tank that is centered in an open field.

## IV. Experimental Method

### 4.1 Overview

This chapter details the techniques used to classify SAR images into two classes: target and non-target. The two-parameter CFAR test pixel is resized to allow for consistent performance. Feature sets—size, contrast, and texture—used to separate target and non-target classes are described. Then a linear classifier is constructed to use the features for classification. Only the image pixel gray values are used for these tests. Each image is normalized before testing to ensure the dynamic range is the same.

### 4.2 Two-Parameter CFAR

To test the performance of the two-parameter CFAR detector the center pixel is tested against a threshold; the results are then compared to truth to score  $P_d$  and  $P_{fa}$ , as described in Equations (2.11) and (2.10). ROC curves are constructed by recording  $P_d$  and  $P_{fa}$  for each threshold. To ensure an unbiased test for the two-parameter CFAR detector, the test pixel size is optimized. Otherwise, reducing the resolution causes the test pixel to be larger, corrupting the results. The test pixel now can be considered a test box, and the ratio test from chapter 2 can be modified to

$$\frac{E[x] - \mu_c}{\sigma_c} \gtrless \gamma, \quad (4.1)$$

where  $x$  can be more than a single pixel, and the expected value of the test box is used. To find the test box size with the best performance 180 original image chips, with resolution of 1 ft  $\times$  1 ft, are tested with different test box sizes: 1 pixel  $\times$  1 pixel (1 pixel), 2 pixels  $\times$  2 pixels (4 pixels), 4 pixels  $\times$  4 pixels (16 pixels), and 8 pixels  $\times$  8 pixels (64 pixels). Figure 4.1 shows ROC curves for the different test box sizes. Figure 4.1 [c], 16 pixels, can be visually verified as the best performer, and will be used as the test box size. Figure 4.1 [a], 1 pixel, is the worst performer. The larger test boxes contain more information, causing the increase in performance. When resolution is reduced the test box will be modified to match the new spatial

resolution, i.e. an image with resolution of  $2 \text{ ft} \times 2 \text{ ft}$  would have a test box size of  $2 \text{ pixels} \times 2 \text{ pixels}$ .

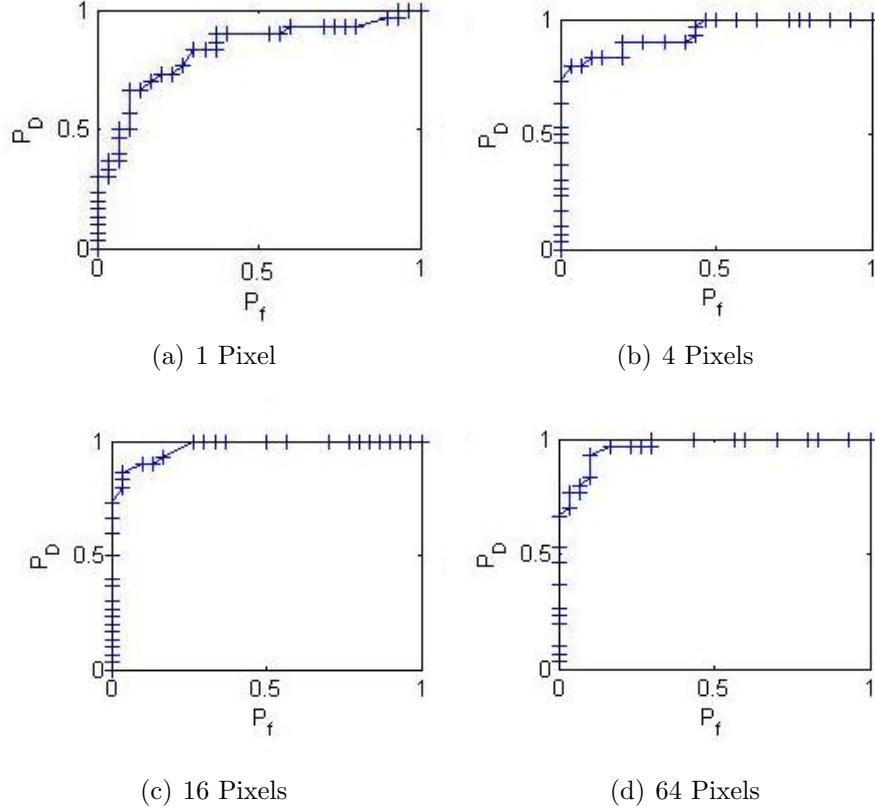


Figure 4.1: ROC curves for different test box sizes.

### 4.3 Discrimination

Different feature spaces—size, contrast, and texture—have been shown to effectively discriminate targets in SAR images [3]. Two sub-images used in this research are the CFAR image and the binary image. The CFAR image is the output of the two-parameter CFAR detector on every pixel. The binary image is generated from a threshold test. The threshold is chosen to pass maximum pixels from the target and to minimize bright spots from background clutter in the image. Figures 4.2 and 4.3 show binary images of various thresholds for a target and non-target. A threshold of 0.90 is selected to create binary images based.

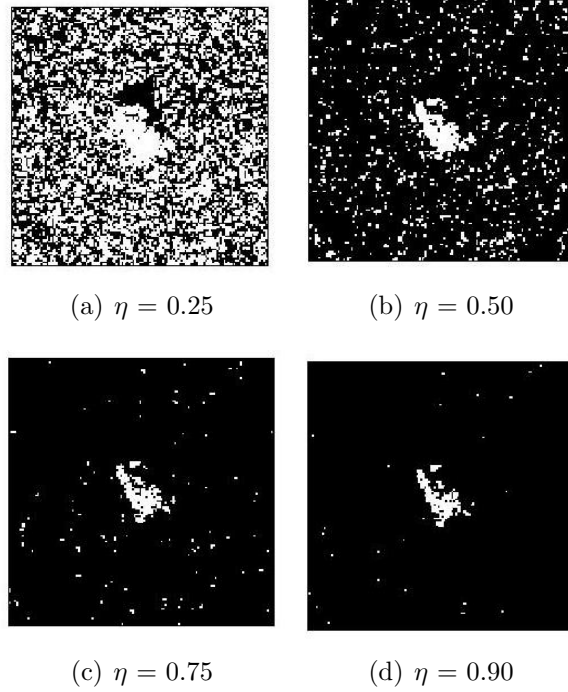


Figure 4.2: Binary image of test of target as threshold  $\eta$  varies.

*4.3.1 Size Features.* Size features use the physical size of the target to differentiate between classes. Features in the size set are: mass, diameter, and normalized rotational inertia. Mass is calculated by summing the binary image pixels. Each pixel is either a 1 or 0, making this feature highly dependent on the threshold of the binary image. Diameter of the image chip is determined by the smallest dimension of a box that encloses the bright pixels in the binary image. Rotational inertia is defined as

$$v_{rot} = \frac{1}{XY} \sum_x^X \sum_y^Y (B[x, y])r[x, y], \quad (4.2)$$

where  $B(x, y)$  is the binary image,  $r[x, y]$  of pixel  $[x, y]$  is the distance from the center of mass, and  $X$  and  $Y$  are the length of each image dimension.

*4.3.2 Contrast Features.* To compute contrast features, a CFAR image is constructed. This image is created using a CFAR pixel test on each pixel in the original image being tested. Peak CFAR is the maximum pixel value in the CFAR

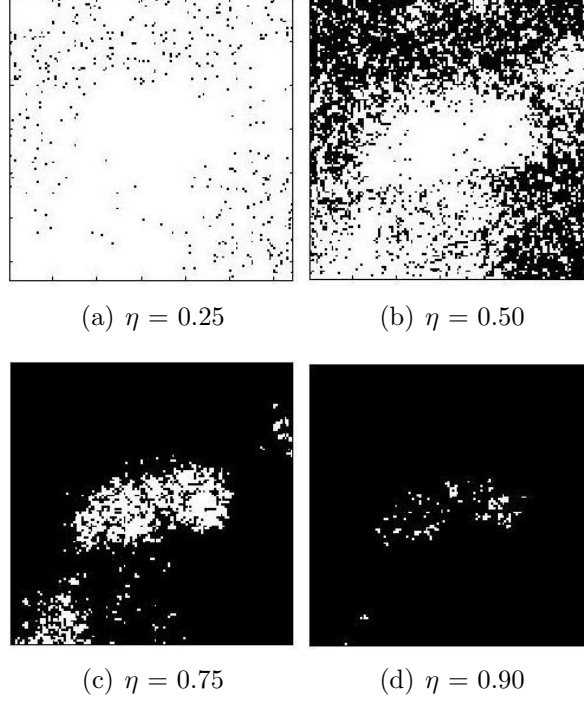


Figure 4.3: Binary image of clutter as threshold  $\eta$  varies.

image. Mean CFAR is the average value of the pixels in the CFAR image. Percent bright CFAR is calculated by summing the pixel values of the image derived from the multiplication of the binary and CFAR image. This value is normalized by the total number of pixels in the image.

*4.3.3 Texture Features.* Texture features are standard deviation, fractal dimension, and rank filled ratio. The standard deviation is generated by taking the standard deviation of pixel gray values of the image. The fractal dimension feature calculates the spatial distribution of the image chip. This feature is based on the knowledge that targets have closely spaced bright pixels while clutter is more dispersive. The fractal dimension of an image chip is:

$$dim = \frac{\log M_1 - \log M_2}{\log 2}, \quad (4.3)$$

where  $M_1$  is the number of bright pixels in the binary image and  $M_2$  is the number of  $2 \times 2$  pixel boxes needed to encase all the bright pixels [3]. The rank filled ratio

is computed from the top  $N$  scatters of the image. A percentage threshold is chosen to select the top  $N$  bright scatters of the image; these scatters are summed up and divided by the total value of the image.

#### 4.4 *Classifier*

This research is not concerned with the identification of individual vehicles but the ability to distinguish between target and non-target images. The features from the discrimination stage are used to create a  $n$  dimensional feature space; where  $n$  is the number of features extracted from an image. The feature space is projected onto the Fisher line, reducing the problem from  $n$  dimensions to one. The fisher line is in the feature space such that the Fisher ratio is maximized. The Fisher ratio is the squared difference of the means of the projected points in the two classes divided by the sum of their variances. The slope of the Fisher line may be found from their proportionality to the elements of the largest eigenvector of the product of a between-class matrix and the inverse of the within-class matrix. The slopes may also be found by numerically maximizing the Fisher ratio, or projected may be found directly using elementary least squares [13].

Each of the feature points that are projected onto the Fisher line can be used to estimate the pdfs of each class by using Parzen windows with Gaussian kernels [13], expressed as

$$p = \frac{1}{n} \sum_{i=1}^x \frac{1}{\sqrt{2\pi}\sigma} e^{-\frac{(x-x_i)^2}{2\sigma^2}}, \quad (4.4)$$

where  $n$  is the number of samples in the class,  $x_i$  is the location of each point on the Fisher line that the individual Gaussians are projected onto, and  $\sigma^2$  is the variance of the Gaussian. Here  $\sigma^2$  is the smoothing factor and is varied until the pdf is unimodal. Sweeping a threshold across the pdfs generates a ROC curve, providing a measure on how well the features separate the two classes. The AUROC is used as the performance metric for each given feature set per resolution, allowing for visual inspection of performance across all resolutions.

## V. Results and Analysis

### 5.1 Overview

This section presents the results for the performance of target discrimination in SAR images for various resolutions. First the two-parameter CFAR detector and discriminating features results are presented using plots of the AUROC versus the resolution. The individual features from each feature set are presented to evaluate the top performers. Then ROC curves for the original resolution, best performer, and worst performer for the two-parameter CFAR detector, discriminating features, and statistical classifier are presented. Appendix 1 lists all of the AUROC values for the combinations of spatial resolutions for all feature sets.

Top performers are shown to be the texture and all nine feature sets for both resolution reduction techniques, with AUROC staying above 0.90. Both contain the rank filled ratio feature, which in itself has AUROC staying above 0.90. In this research the rank filled ratio is the most robust feature across spatial resolutions.

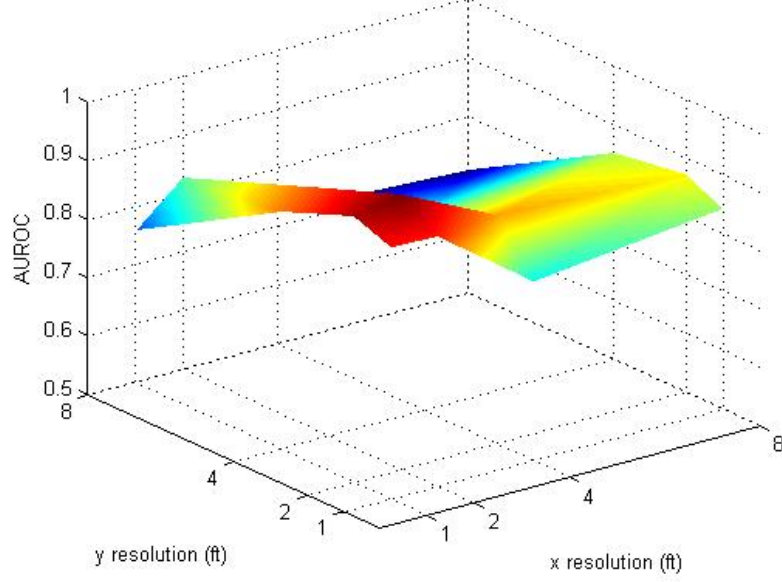
### 5.2 CFAR Detector

The two-parameter detector tests the center pixels of 90 images from each class, target and non-target, where the results are compared to truth to score  $P_d$  and  $P_{fa}$  for each threshold. In Figure 5.1 the AUROC is plotted against the x and y resolutions, providing overall shapes for performance. Figure 5.1 [a] shows AUROC results for resolution degradation by pixel reduction and Figure 5.1 [b] shows AUROC results for resolution degradation by filtering degradation. In Figure 5.1 [a] the performance can be seen to increase with a slight reduction in resolution and then taper off. Also, the  $x$  direction can be seen to be more dominant than the  $y$  direction, because the  $y$  direction has a steeper slope. Figure 5.1 [b] shows that the overall target detection performance of the filtering degradation is greater than the pixel reduction and that neither direction is dominant.

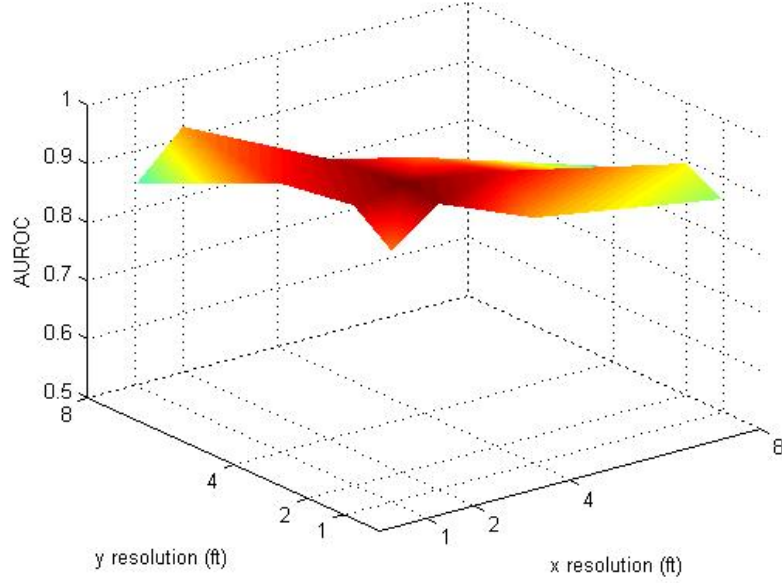
Figures 5.2 and 5.3 shows ROC curves for the original resolution, best performer, and worst performer. The AUROC for the original image is 0.85. The  $2\text{ft} \times 2\text{ft}$



resolution is the best performer for both pixel count reduction and image degradation with an AUROC of 0.90 and 0.95. The worst performer for both is the  $8\text{ft} \times 8\text{ft}$  resolution with an AUROC of 0.72 and 0.80.



(a) Pixel Reduction Case



(b) Filtering Degradation Case

Figure 5.1: Graphs [a] and [b] show AUROC versus the resolution in the x and y direction. Here [a] is for reduction in pixel count, which shows an increase in performance with a slight reduction in resolution and then a reduction in performance, and [b] is for filtering degradation, which shows an increase in performance with a slight reduction in resolution.

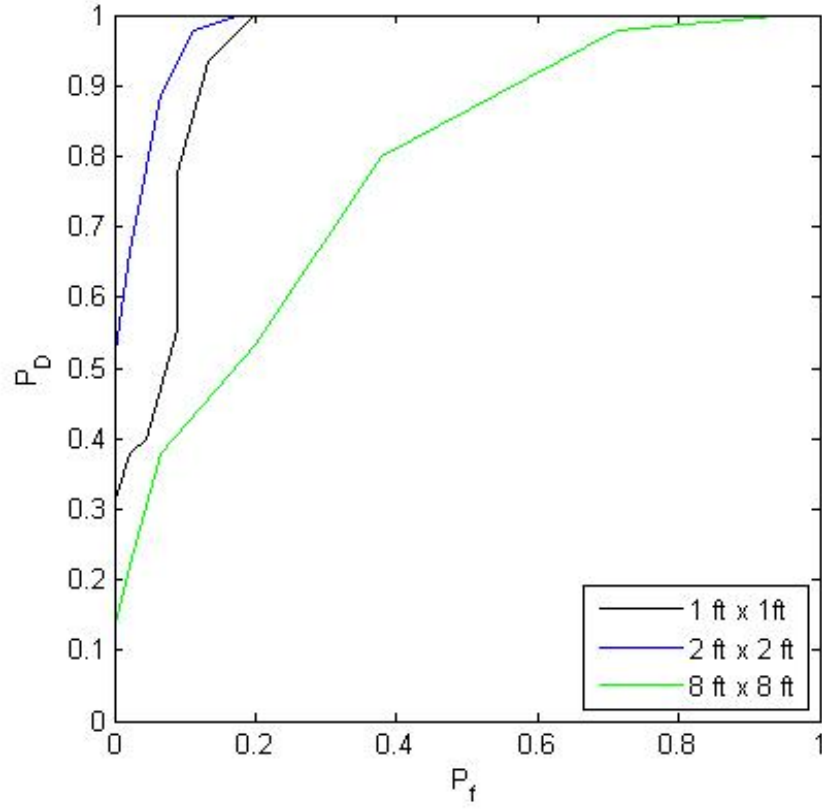


Figure 5.2: ROC curves for the two parameter CFAR detector for pixel count reduction. The graph shows ROC curves for the original resolution, best resolution and worst resolution performance. The AUROC for the original is 0.93. The best performer is  $2 \text{ ft} \times 2 \text{ ft}$  resolution with AUROC of 0.97, and the worst performer is  $8 \text{ ft} \times 8 \text{ ft}$  resolution with an AUROC of 0.71.

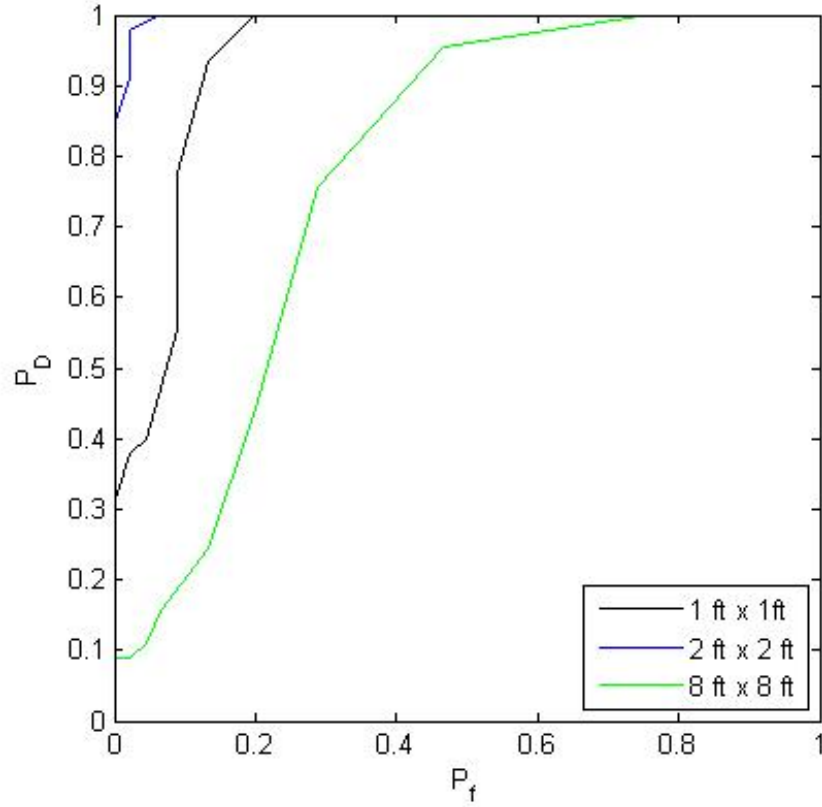


Figure 5.3: ROC curves for the two parameter CFAR detector for filtering degradation. The graph shows ROC curves for the original resolution, best resolution and worst resolution performance. The AUROC for the original is 0.93. The best performer is  $2 \text{ ft} \times 2 \text{ ft}$  resolution with an AUROC of 0.99, and the worst performer is  $8 \text{ ft} \times 8 \text{ ft}$  resolution with an AUROC of 0.72.

### 5.3 Discriminating Features

This section shows results from tests of the three feature sets—size, contrast, and texture—for the different resolution combinations. All nine features that make up the three feature sets are combined into a nine feature set, and individual features of each set are evaluated to assess if one is dominant. These sets are used to create a multi-dimensional feature space that is projected onto the Fisher line to separate the points into two classes: target and non-target. The size feature set uses pixel reduction steps through this process and shows the results at each step, but all other sets have only the results presented. The results are shown by graphing AUROC versus the spatial resolution of the image pixel size.

*5.3.1 Size Features.* The three size features—mass, diameter, and rotational inertia—are extracted from 180 image chips. Figures 5.4, 5.5, 5.6, and 5.7 show plots of the feature space with the Fisher line for four different spatial resolutions: original 1 ft  $\times$  1 ft resolution, 2 ft  $\times$  2 ft resolution, 4 ft  $\times$  4 ft resolution, and 8 ft  $\times$  8 ft resolution, respectively. All combinations of resolution are tested, but these four are used to illustrate the process. The target class is indicated by ‘+’ and the non-target class by ‘o’. From these plots it is apparent that the separation of the two classes worsens as resolution is degraded. Figure 5.7 shows the two classes almost completely overlapping, but to clarify the separation of the two classes these points are projected onto the Fisher line.

Figures 5.8 and 5.9 show the results of projecting the feature points for each image chip onto the Fisher line and estimating the pdfs of the two classes. The two different estimation techniques are Parzen windows with a Gaussian kernel and using the mean and standard deviation of the projected points of the two classes to estimate a Gaussian pdf. From the estimated pdfs ROC curves are derived by varying the threshold to estimate  $P_d$  and  $P_{fa}$ . Figure 5.10 shows the ROC curves for four different resolutions: 1 ft, 2 ft, 4 ft, and 8 ft. The AUROC can be derived from these results as a single value to grade the feature sets. Figure 5.10 shows the

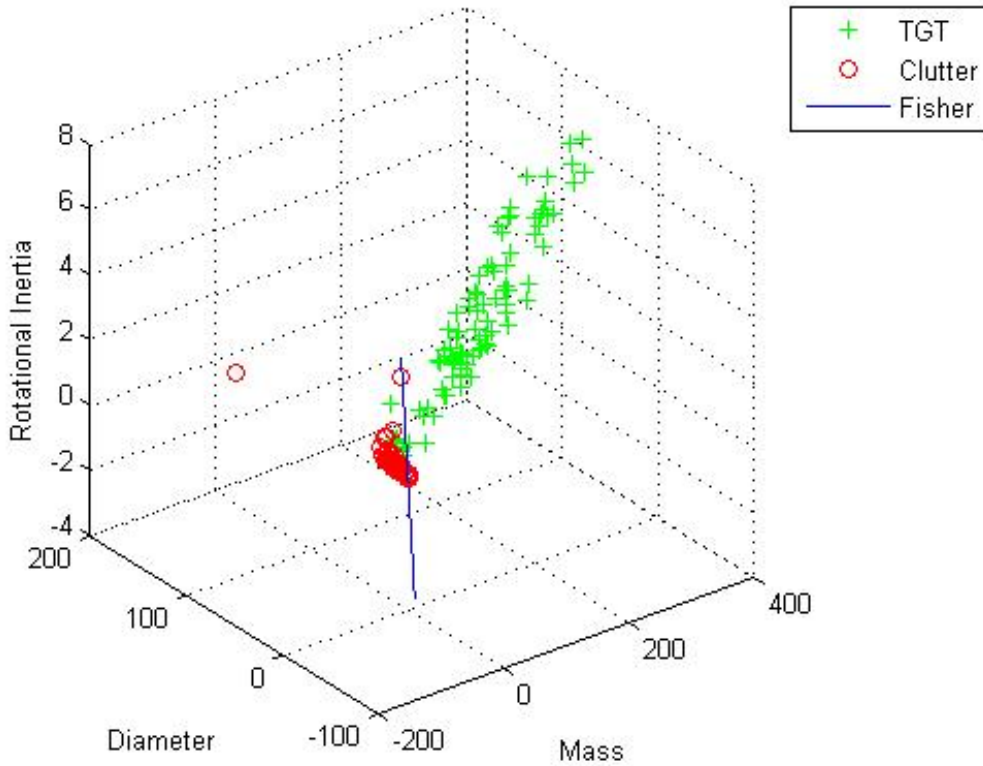


Figure 5.4: The 3D size feature space for image chips with a resolution of  $1 \text{ ft} \times 1 \text{ ft}$ . The two class are targets, '+', and non-targets, 'o'. The Fisher line is drawn in the space for each of the graphs.

resulting ROC curves for the two estimating techniques. Since the Parzen window and Gaussian pdf estimates produce similar AUROC values, only the Parzen window technique is used for the rest of the research.

Figure 5.15 shows the plots for the estimated pdfs for the filtering degradation. The pdfs overlap as the resolution is lowered, indicating that these features do not perform well at lower resolutions

Figures 5.11 and 5.16 show that the features are sensitive to resolution, which is expected since these features are based on the number of pixels on a target. As the pixel count is reduced, more of the information for this feature space is lost, and the two classes become less separable. Figure 5.11 shows the AUROC staying about the

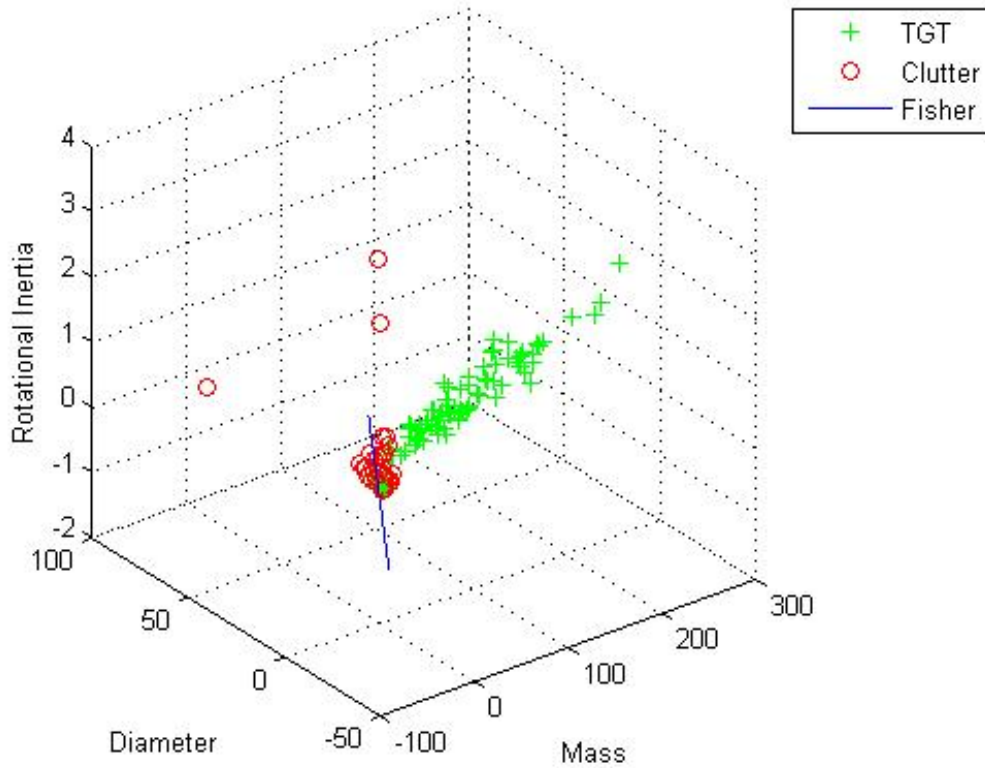


Figure 5.5: The 3D size feature space for image chips with a resolution of  $2 \text{ ft} \times 2 \text{ ft}$ . The two class are targets, '+', and non-targets, 'o'. The Fisher line is drawn in the space for each of the graphs.

same as long as either the  $x$  or  $y$  resolution is at the highest. Figure 5.16 shows the AUROC dropping off with any reduction in resolution.

AUROC performance is shown for the individual size features. Figures 5.12, 5.13, and 5.14 show the results for mass, diameter, and rotational inertia features, respectively, for pixel reduction. Figures 5.17, 5.18, and 5.19 show the results for mass, diameter, and rotational inertia features, respectively, for the image degradation. The mass feature is seen as the most robust of all the size features since the AUROC stays above 0.70. The diameter feature is the worst performer, and has a maximum AUROC of 0.62. For the filtering degradation, the AUROC curves for all three features quickly degrade. The results suggest that these features are best when used with higher resolution.

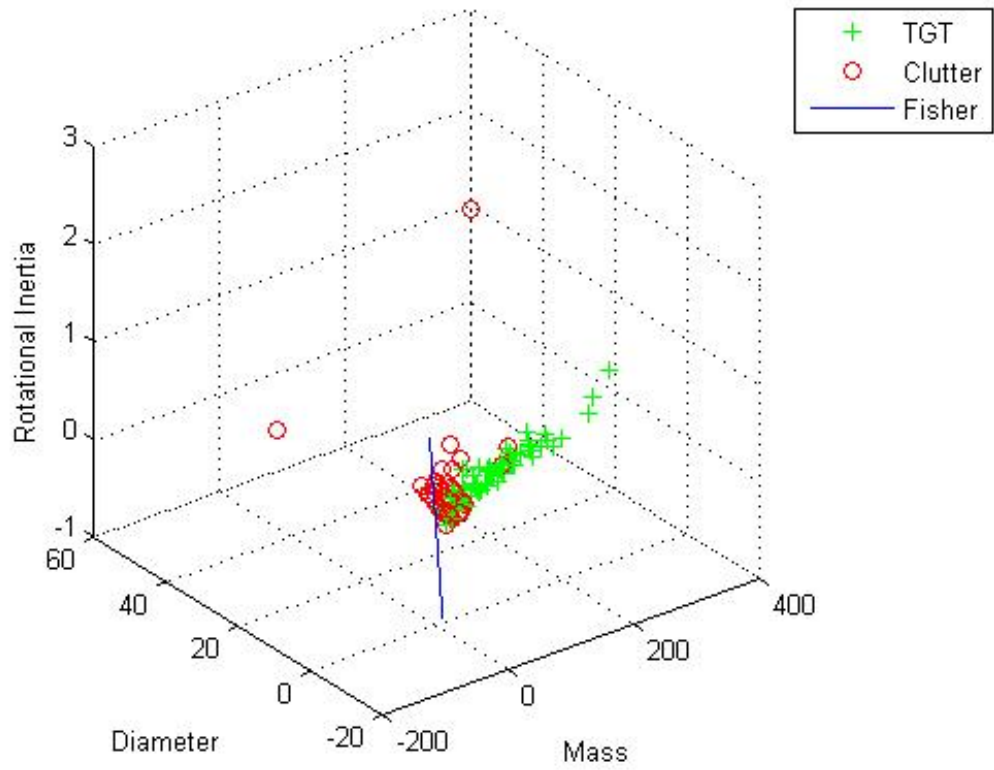


Figure 5.6: The 3D size feature space for image chips with a resolution of  $4 \text{ ft} \times 4 \text{ ft}$ . The two class are targets, '+', and non-targets, 'o'. The Fisher line is drawn in the space for each of the graphs.



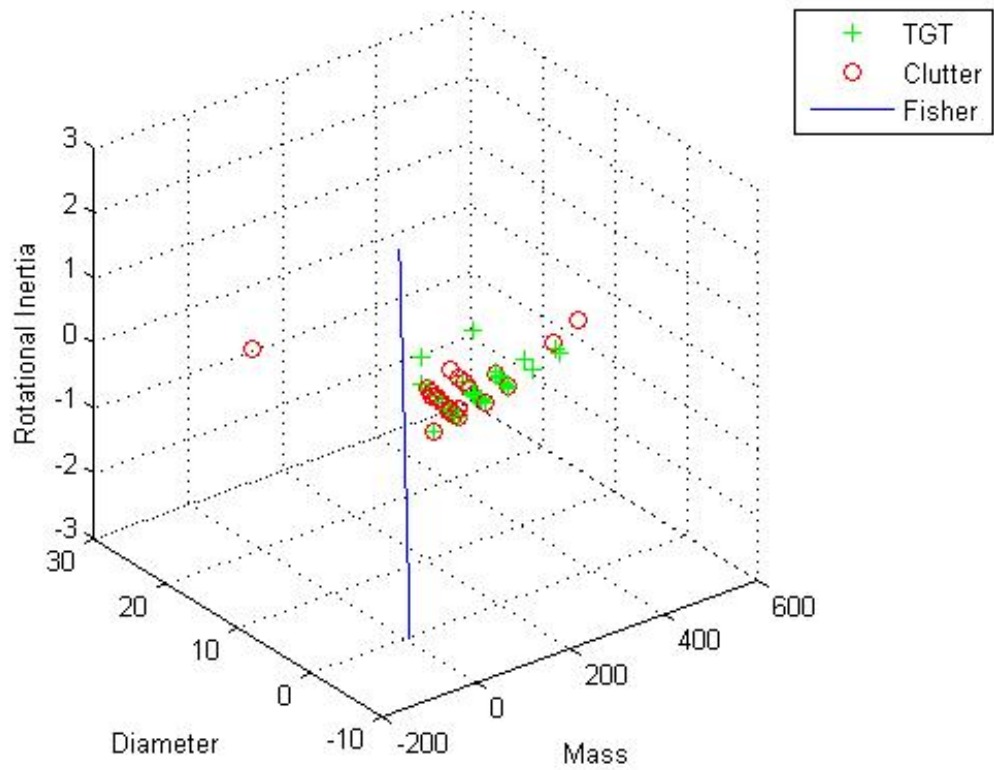
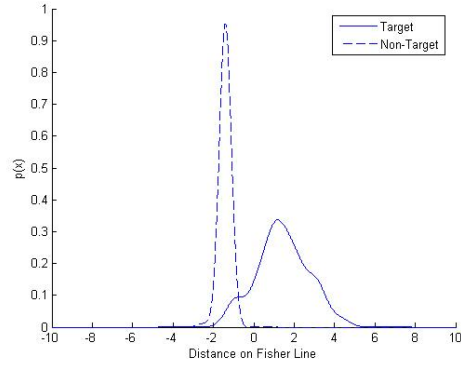
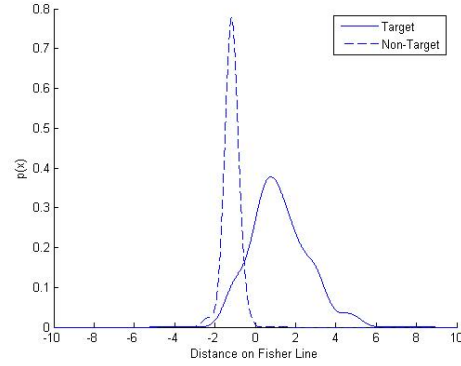


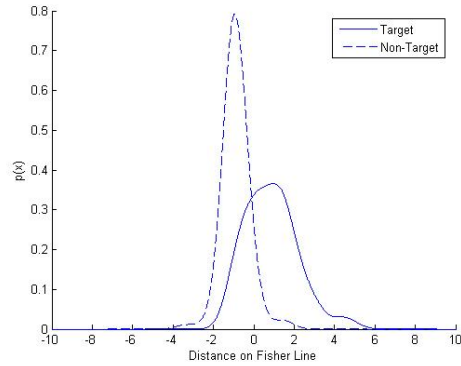
Figure 5.7: The 3D size feature space for image chips with a resolution of  $8 \text{ ft} \times 8 \text{ ft}$ . The two class are targets, '+', and non-targets, 'o'. The 8 ft resolution shows the two classes completely overlapping. The Fisher line is drawn in the space for each of the graphs.



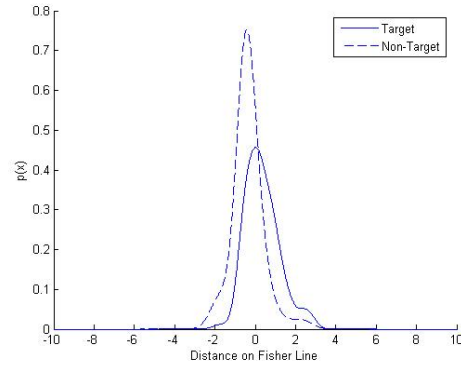
(a) 1 ft  $\times$  1 ft



(b) 2 ft  $\times$  2 ft

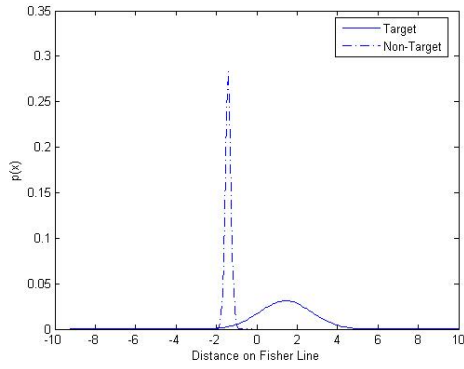


(c) 4 ft  $\times$  4 ft

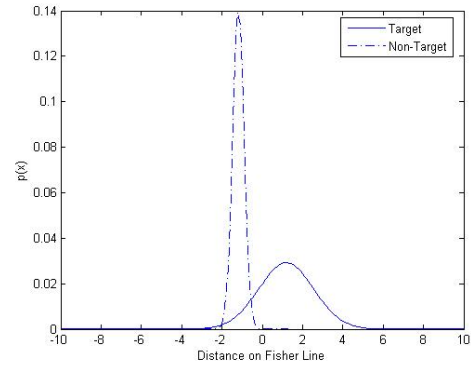


(d) 8 ft  $\times$  8 ft

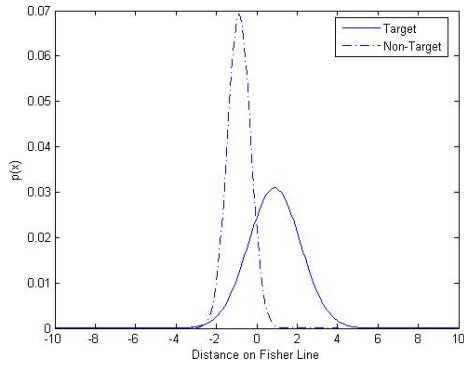
Figure 5.8: The estimated pdfs of the two classes after the size features are projected onto the Fisher line for the pdfs that are estimated using Parzen windows with a Gaussian kernel. Each of the four plots are for different spatial resolutions of the image chips. [a] is for 1 ft  $\times$  1 ft, [b] is for 2 ft  $\times$  2 ft, [c] is for 4 ft  $\times$  4 ft, and [d] is for 8 ft  $\times$  8 ft.



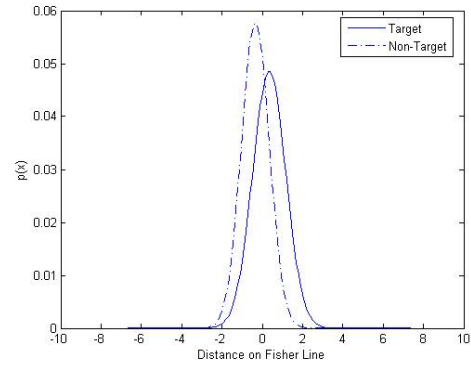
(a)  $1 \text{ ft} \times 1 \text{ ft}$



(b)  $2 \text{ ft} \times 2 \text{ ft}$

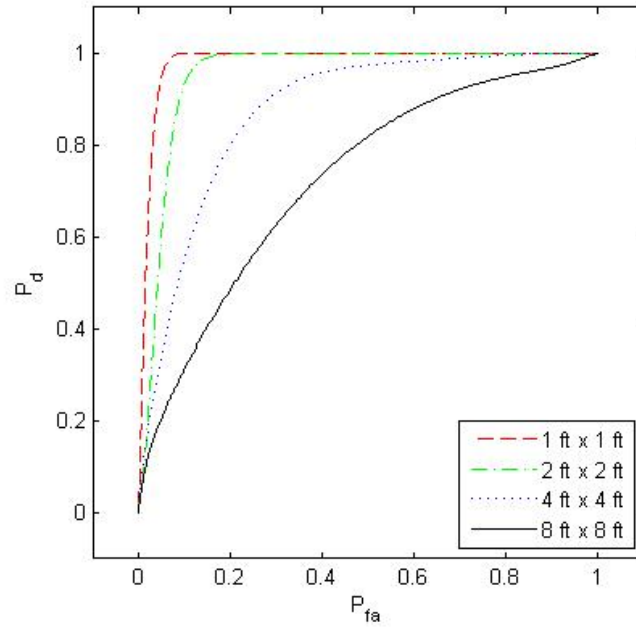


(c)  $4 \text{ ft} \times 4 \text{ ft}$

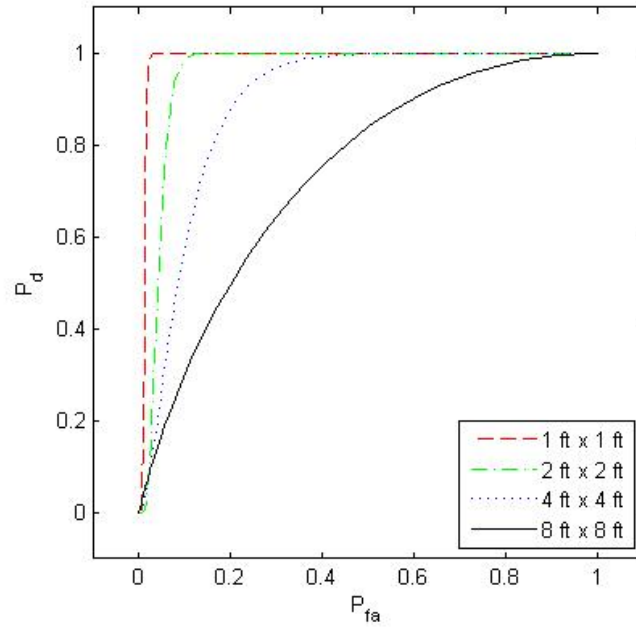


(d)  $8 \text{ ft} \times 8 \text{ ft}$

Figure 5.9: The estimated pdfs of the two classes after the size features are projected onto the Fisher line for the Gaussian pdfs. Each of the four plots are for different spatial resolutions of the image chips. [a] is for  $1 \text{ ft} \times 1 \text{ ft}$ , [b] is for  $2 \text{ ft} \times 2 \text{ ft}$ , [c] is for  $4 \text{ ft} \times 4 \text{ ft}$ , and [d] is for  $8 \text{ ft} \times 8 \text{ ft}$ .



(a) ROC from Parzen windows



(b) ROC from Gaussian

Figure 5.10: The two graphs are estimated ROC curves for a two class test using pdfs estimated from the size features of SAR image chips. [a] is from pdfs created using Parzen windows with Gaussian kernels. [b] is from pdfs created with Gaussian pdfs using the mean and standard deviation of the two classes. The AUROCs are 0.985 for 1 ft  $\times$  1 ft resolution, 0.952 for 2 ft  $\times$  2 ft resolution, 0.887 for 4 ft  $\times$  4 ft resolution, and 0.724 for 8 ft  $\times$  8 ft resolution.

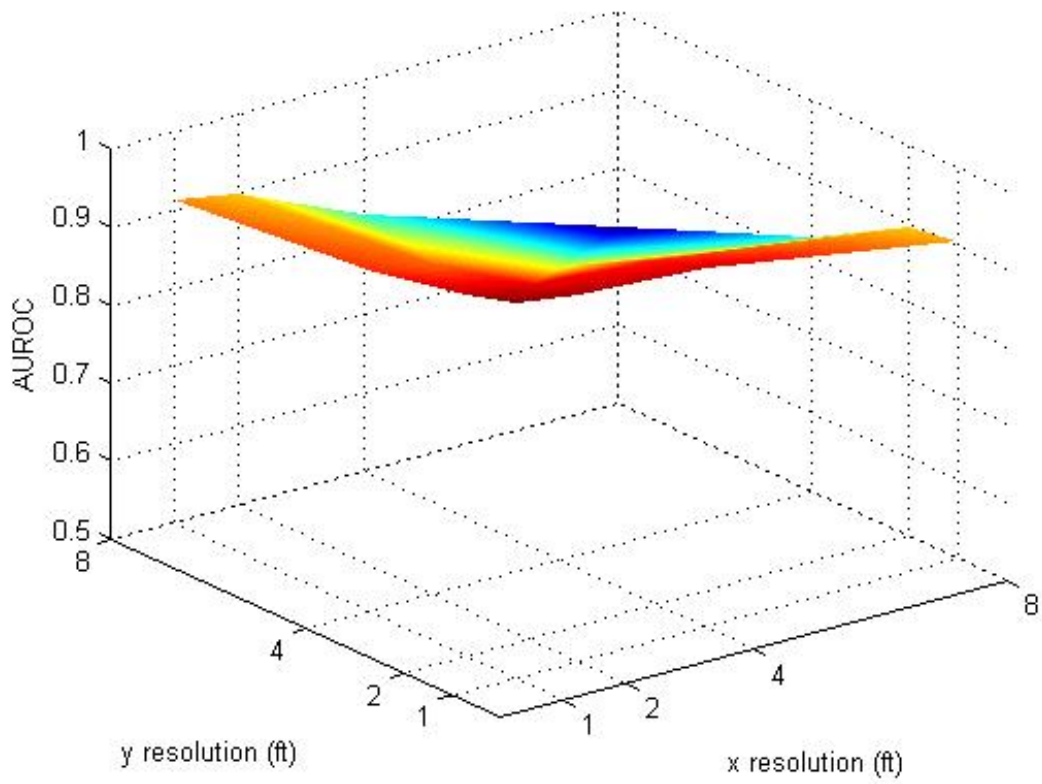


Figure 5.11: AUROC versus resolution in the x and y directions for the size features for pixel reduction.

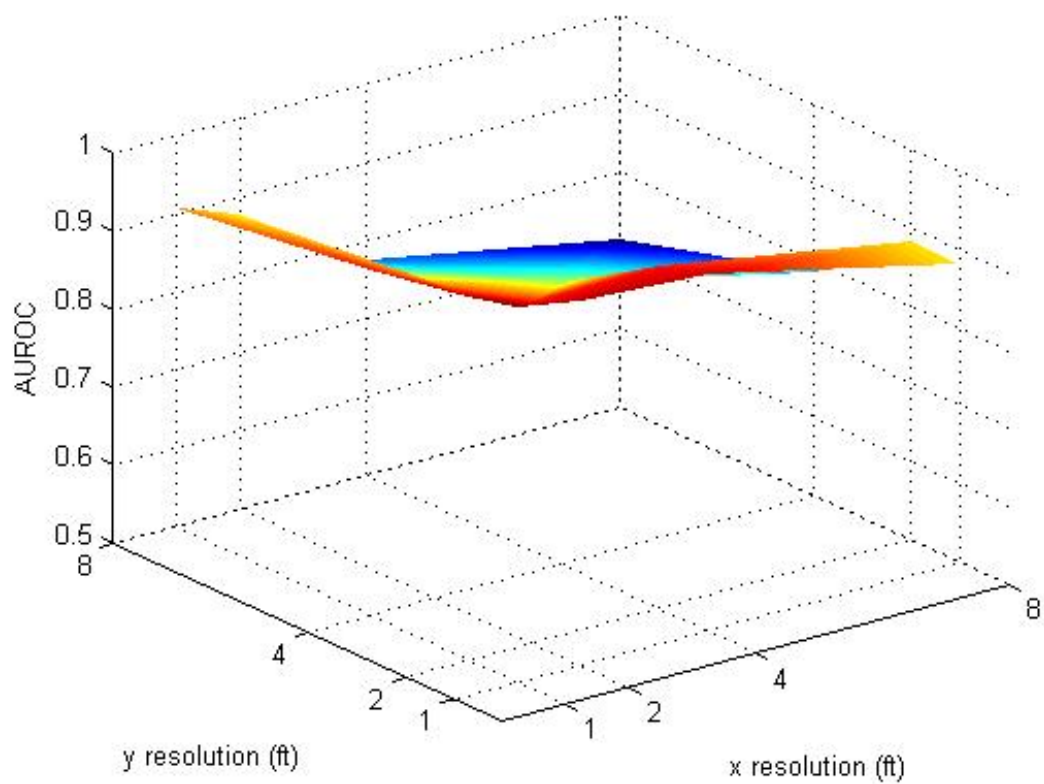


Figure 5.12: AUROC versus resolution in the x and y directions for the peak CFAR feature for pixel reduction.

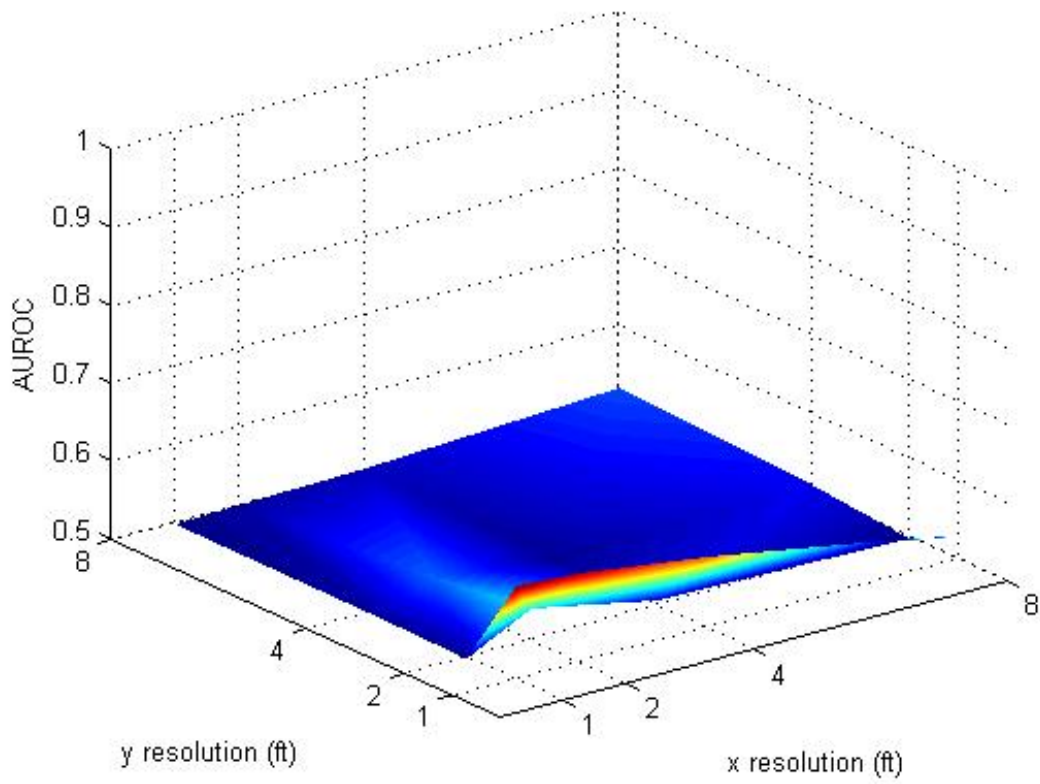


Figure 5.13: AUROC versus resolution in the x and y directions for the diameter feature for pixel reduction.

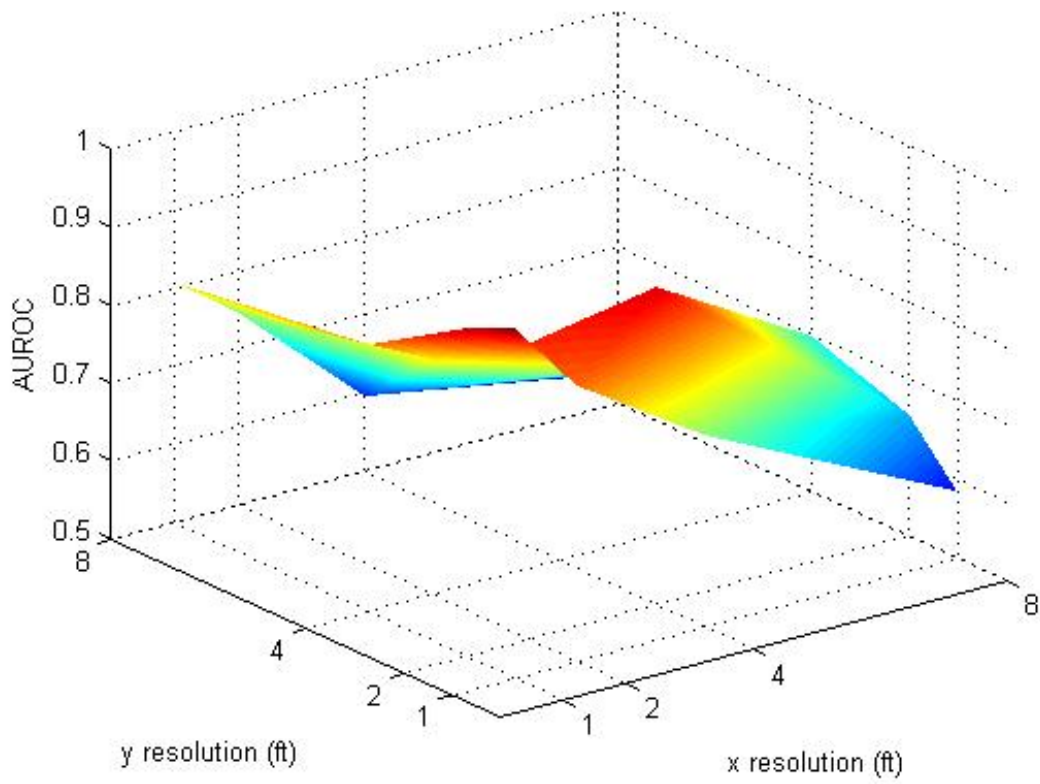
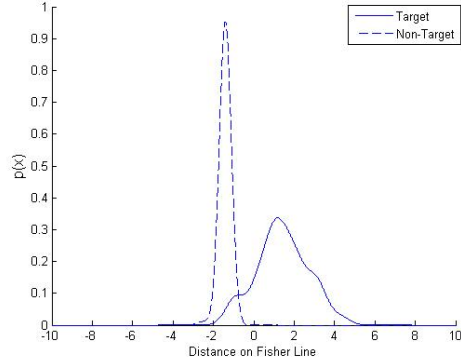
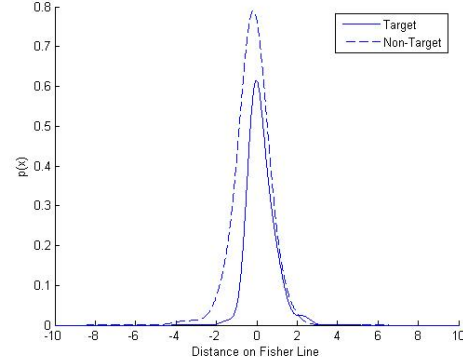


Figure 5.14: AUROC versus resolution in the x and y directions for the rotational inertia feature for pixel reduction.

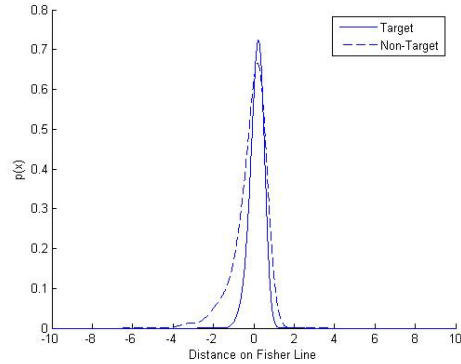




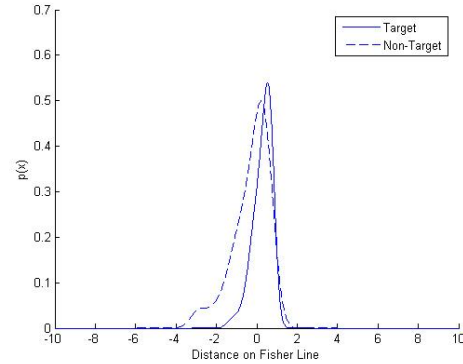
(a) 1 ft  $\times$  1 ft



(b) 2 ft  $\times$  2 ft



(c) 4 ft  $\times$  4 ft



(d) 8 ft  $\times$  8 ft

Figure 5.15: The estimated pdfs of the two classes after the size features are projected onto the Fisher line and estimated using Parzen windows with a Gaussian kernel. Resolution is reduced by filtering degradation. Each of the four plots are for different spatial resolutions of the image chips. [a] plot is for 1 ft  $\times$  1 ft, [b] is for 2 ft  $\times$  2 ft, [c] is for 4 ft  $\times$  4 ft, and [d] is for 8 ft  $\times$  8 ft. The pdfs overlap as the resolution is lowered, indicating that these features do not perform well at lower resolutions.

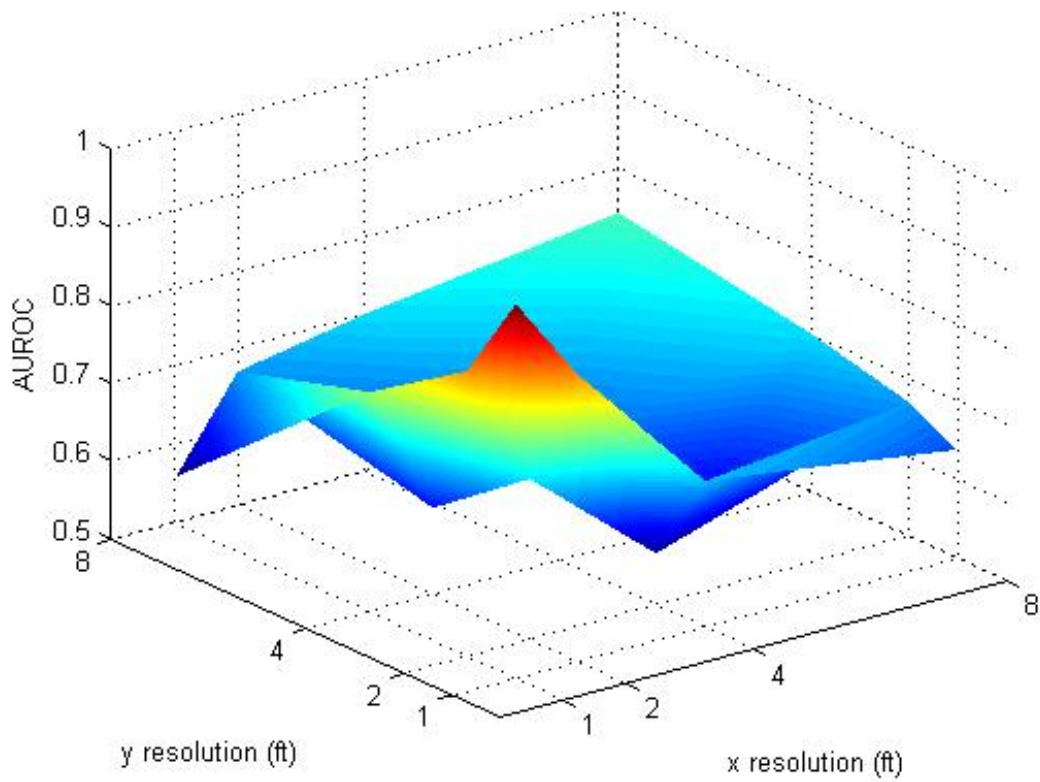


Figure 5.16: AUROC versus resolution in the x and y directions for the size features for image filter degradation.

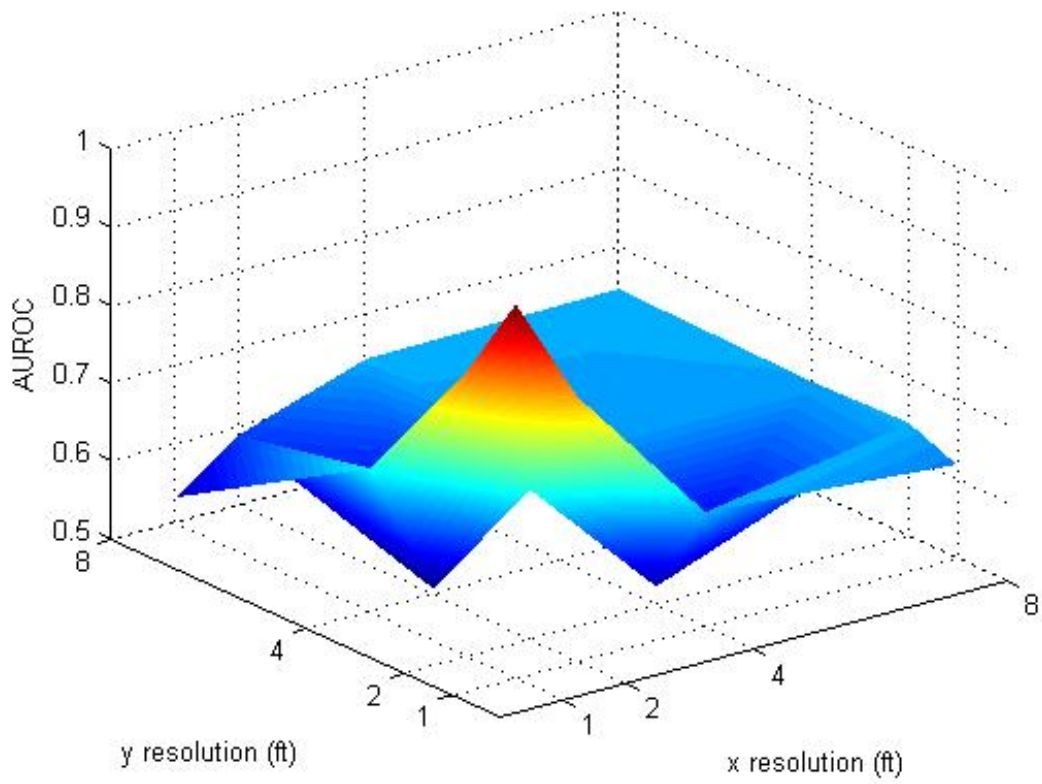


Figure 5.17: AUROC versus resolution in the x and y directions for the mass feature for image filter degradation.

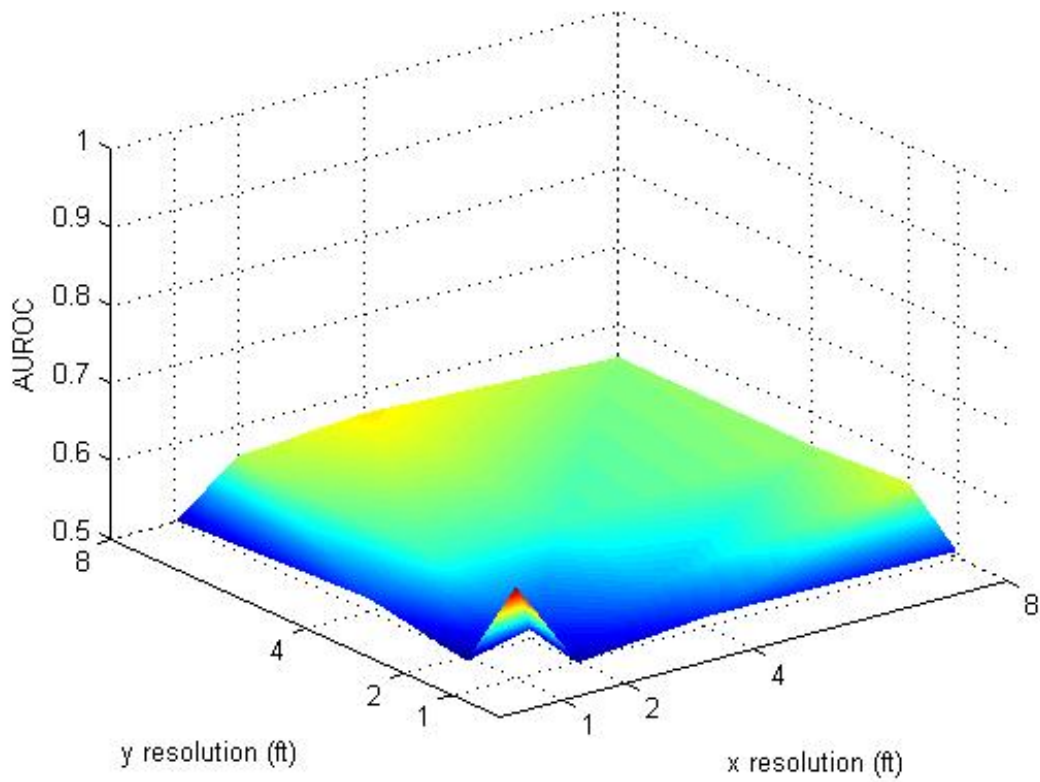


Figure 5.18: AUROC versus resolution in the x and y directions for the diameter feature for image filter degradation.

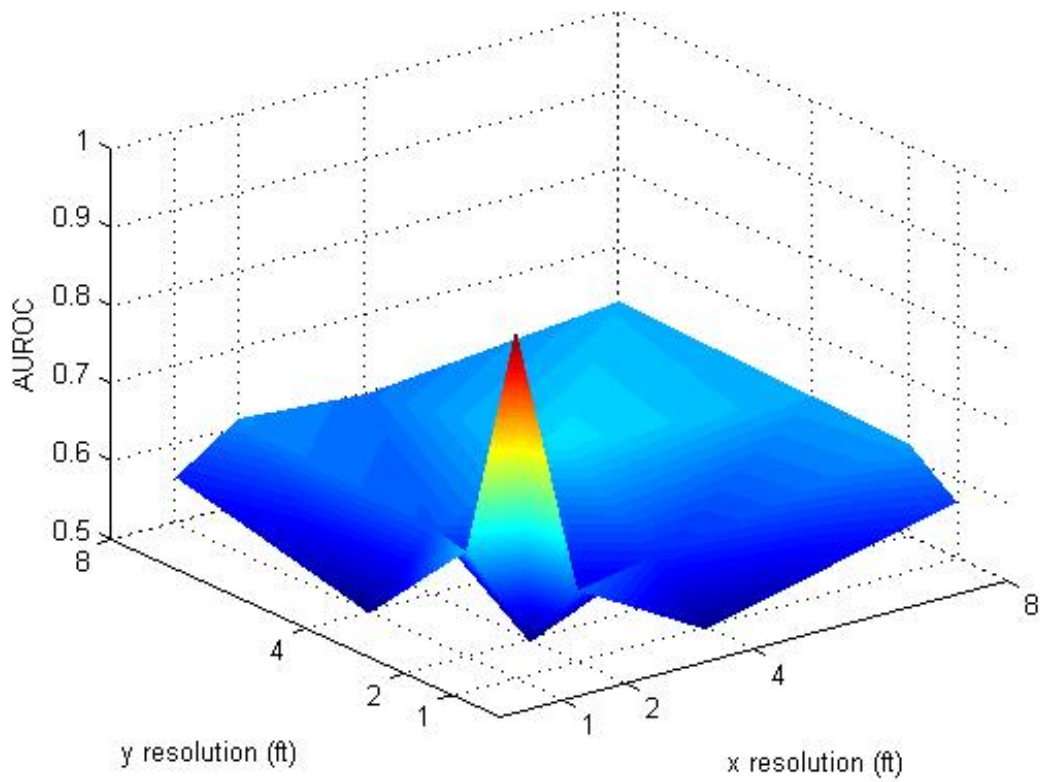
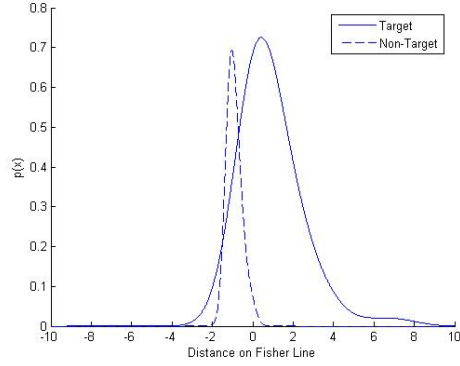


Figure 5.19: AUROC versus resolution in the x and y directions for the rotational inertia feature for image filter degradation.

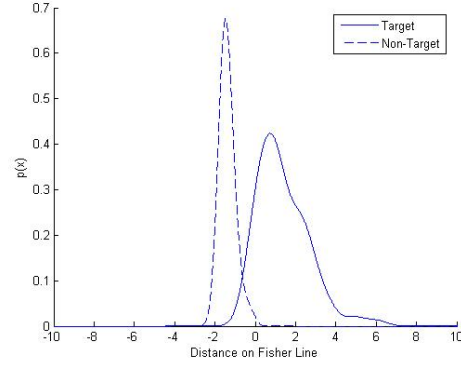
*5.3.2 Contrast Features.* Figure 5.20 and Figure 5.21 show the estimated pdfs for the  $1\text{ ft} \times 1\text{ ft}$ ,  $2\text{ ft} \times 2\text{ ft}$ ,  $4\text{ ft} \times 4\text{ ft}$ , and  $8\text{ ft} \times 8\text{ ft}$  resolutions for pixel count reduction and filtering degradation, respectively. Figure 5.20 shows that the two classes stay relatively separated. Figure 5.21 shows that as the resolution is decreased the target pdf variation increases until it almost covers the non-target class.

Figures 5.22 and 5.26 show variations in AUROC for the contrast features as a function of image resolution. Figure 5.22 shows that in the case of resolution degradation via pixel reduction, the AUROC for contrast features improves at  $2\text{ ft} \times 2\text{ ft}$  resolution, but then declines for further resolution degradation. This performance mirrors the CFAR detector and is not unexpected because the contrast features are derived from images created by the two-parameter CFAR test.

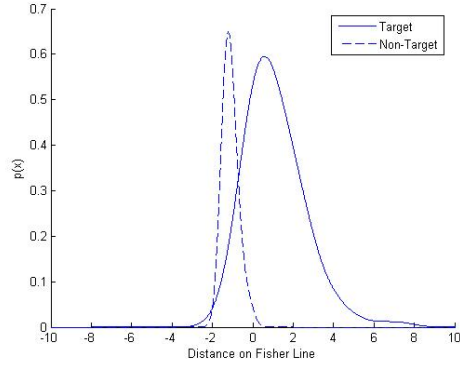
AUROC performance is shown for the individual contrast features. Figures 5.23, 5.24, and 5.25 show the results for the peak CFAR, mean CFAR, and percent bright features, respectively, for pixel reduction. Figures 5.27, 5.28, and 5.29 show the results for peak CFAR, mean CFAR, and percent bright features, respectively, for the image degradation. The percent bright feature is the best performer and the mean CFAR is the worst performer.



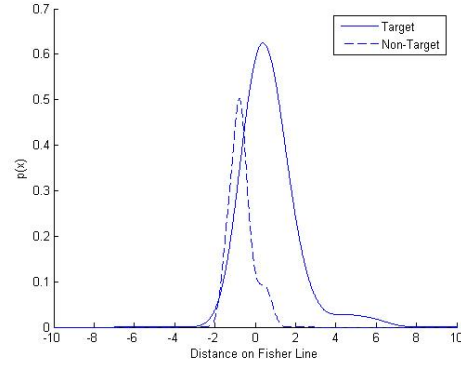
(a) 1 ft  $\times$  1 ft



(b) 2 ft  $\times$  2 ft

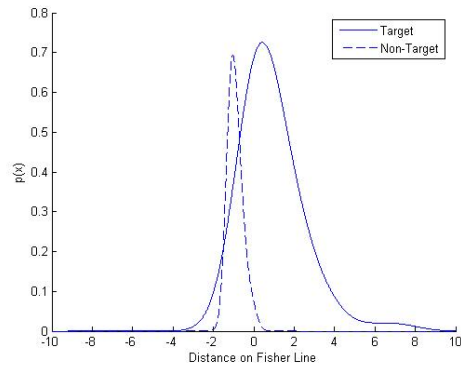


(c) 4 ft  $\times$  4 ft

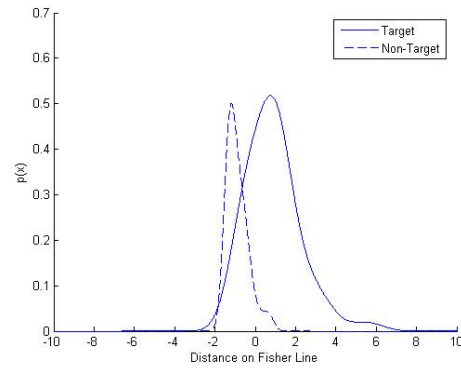


(d) 8 ft  $\times$  8 ft

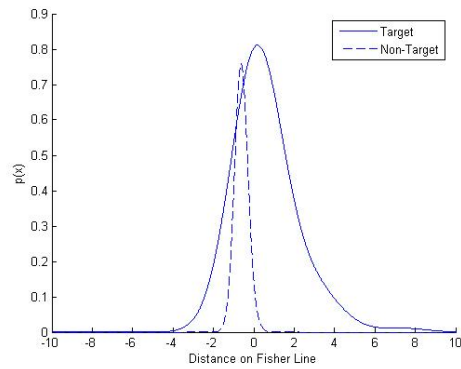
Figure 5.20: These graphs show the estimated pdfs for the contrast features for resolutions of 1 ft, 2 ft, 4, ft, and 8 ft in both the x and y directions. The resolution is reduced by pixel reduction. The dotted pdf represent non-target class and the solid pdf represent the target class. [a] is 1 ft  $\times$  1 ft, [b] is 2 ft  $\times$  2 ft, [c] is 4 ft  $\times$  4 ft, and [d] is 8 ft  $\times$  8 ft.



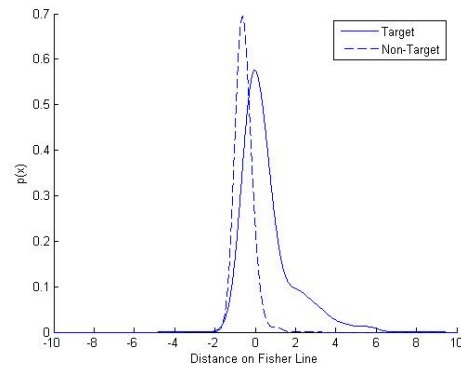
(a) 1 ft  $\times$  1 ft



(b) 2 ft  $\times$  2 ft



(c) 4 ft  $\times$  4 ft



(d) 8 ft  $\times$  8 ft

Figure 5.21: These graphs show the estimated pdfs for the contrast features for resolutions of 1 ft, 2 ft, 4, ft, and 8 ft in both the x and y directions. The resolution is reduced by filtering degradation. The dotted pdf represent non-target class and the solid pdf represent the target class. [a] is 1 ft  $\times$  1 ft, [b] is 2 ft  $\times$  2 ft, [c] is 4 ft  $\times$  4 ft, and [d] is 8 ft  $\times$  8 ft.



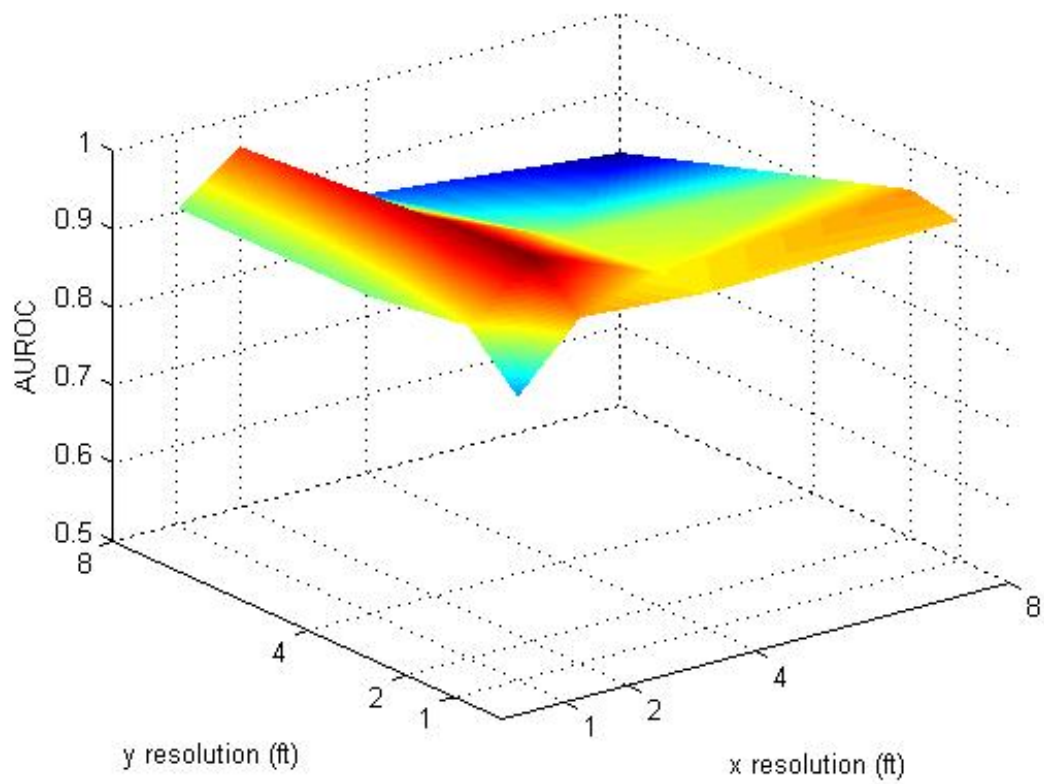


Figure 5.22: AUROC versus resolution in the x and y directions for the contrast features for pixel reduction.

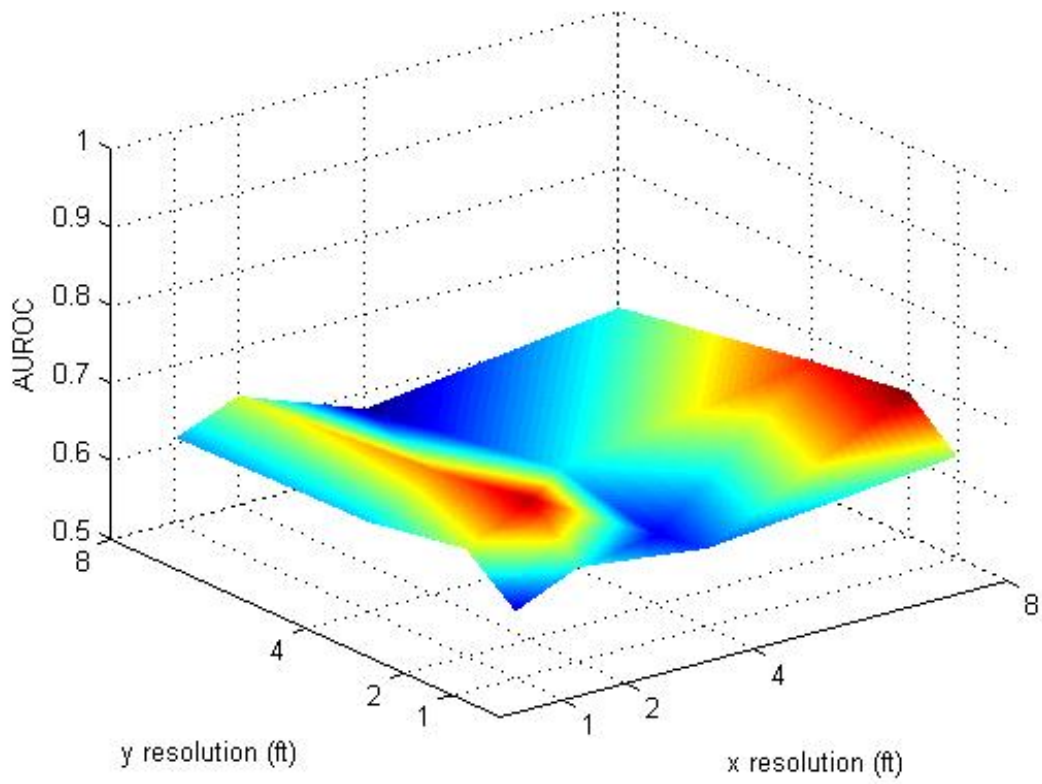


Figure 5.23: AUROC versus resolution in the x and y directions for the peak CFAR feature for pixel reduction.

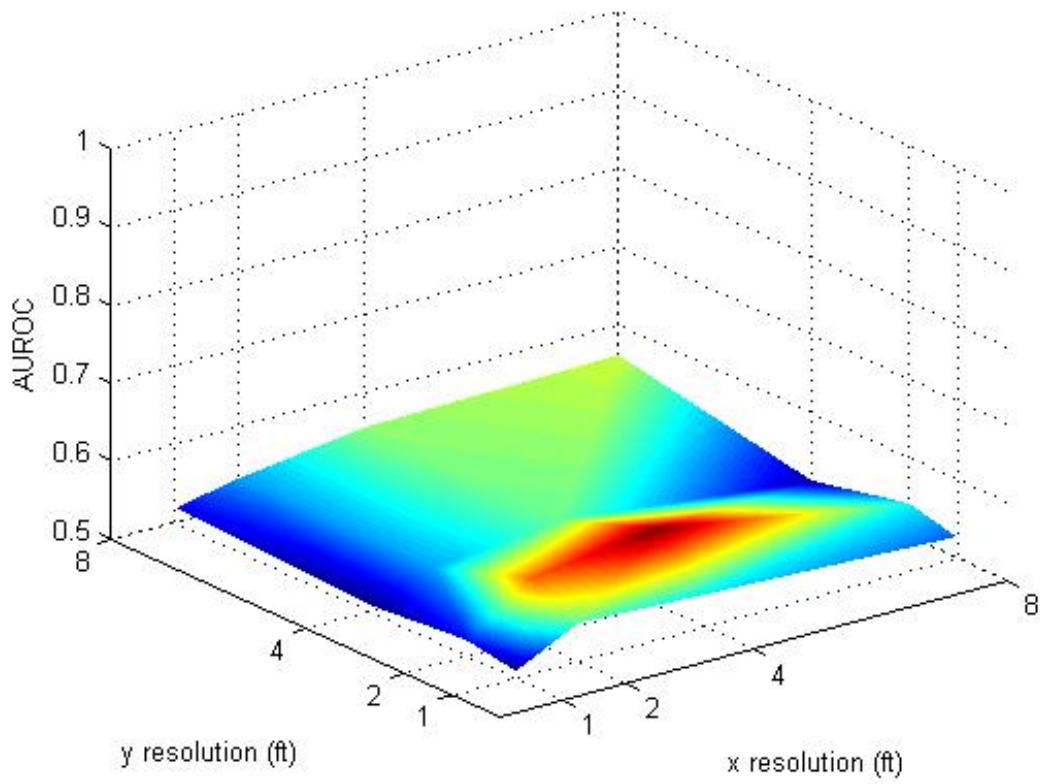


Figure 5.24: AUROC versus resolution in the x and y directions for the mean CFAR feature for pixel reduction.

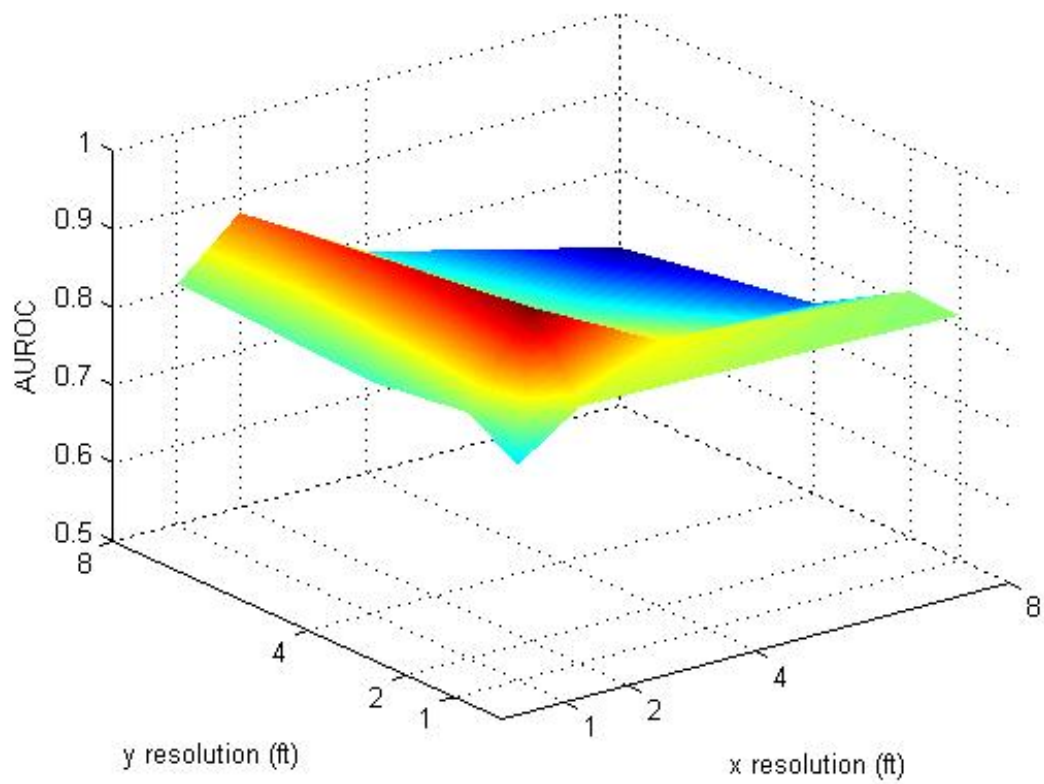


Figure 5.25: AUROC versus resolution in the x and y directions for the percent bright feature for pixel reduction.

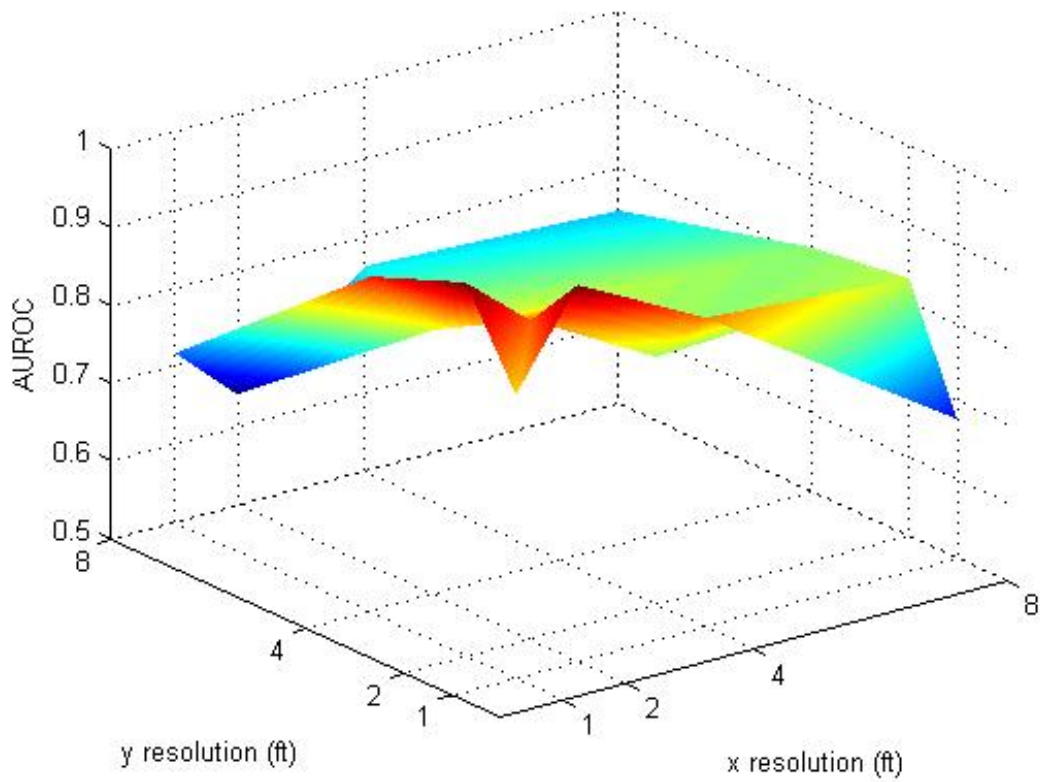


Figure 5.26: AUROC versus resolution in the x and y directions for the contrast features for image filter degradation.

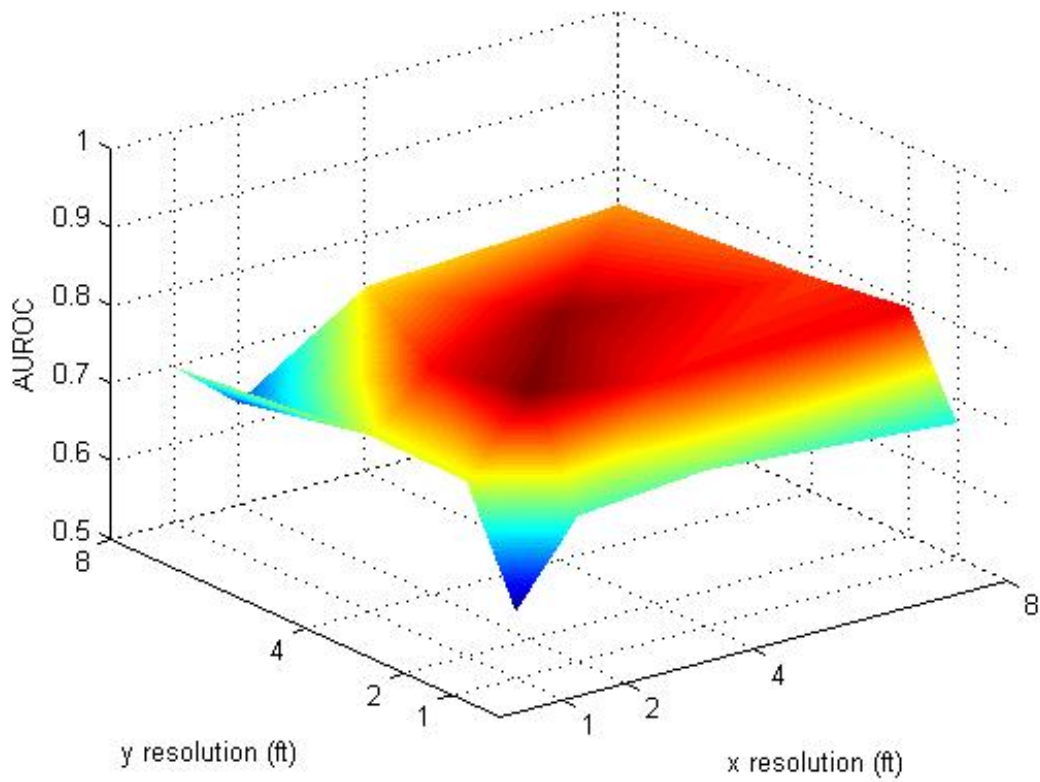


Figure 5.27: AUROC versus resolution in the x and y directions for the peak CFAR feature for image filter degradation.

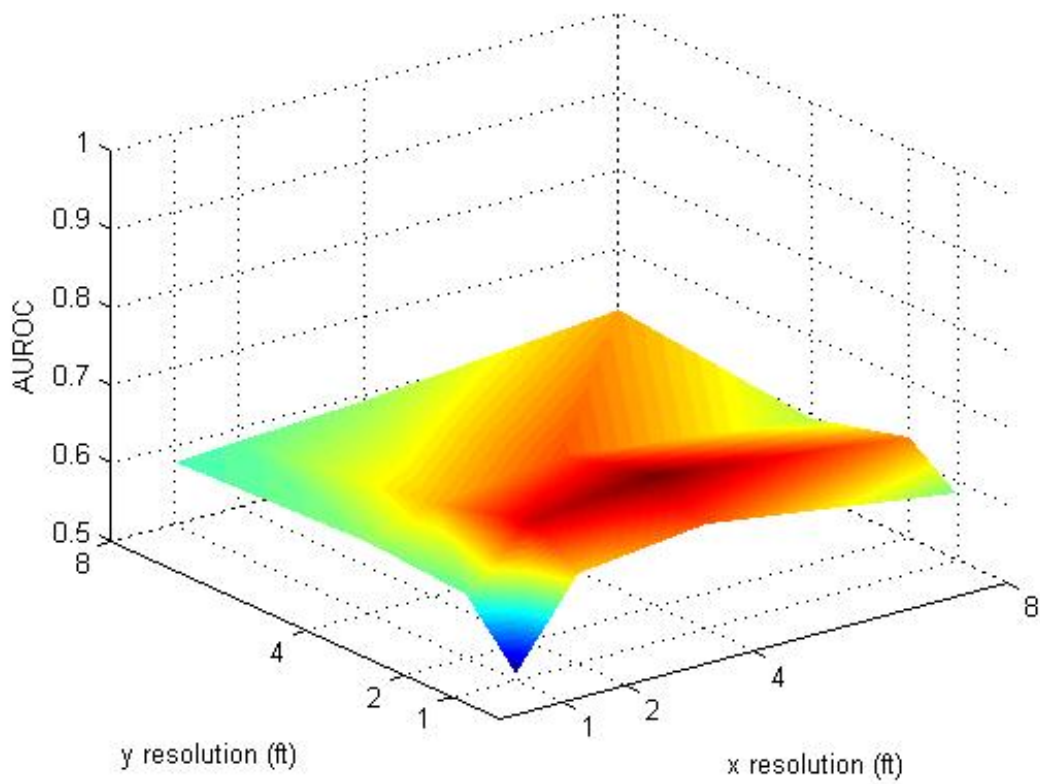


Figure 5.28: AUROC versus resolution in the x and y directions for the mean CFAR feature for image filter degradation.

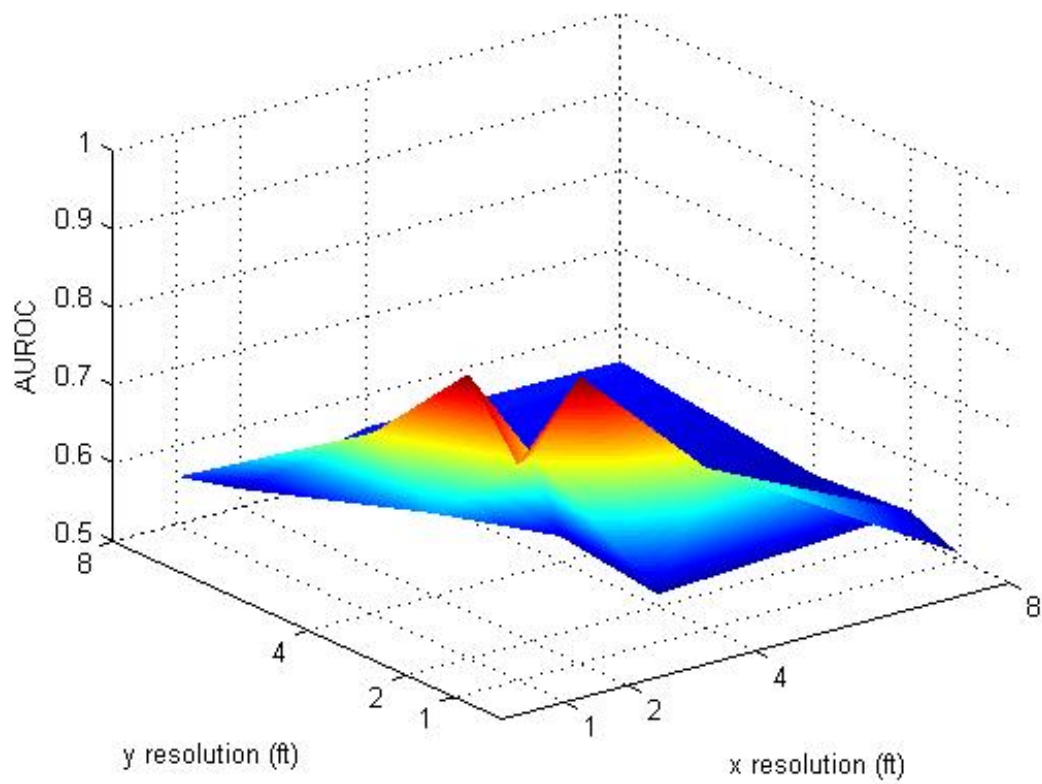


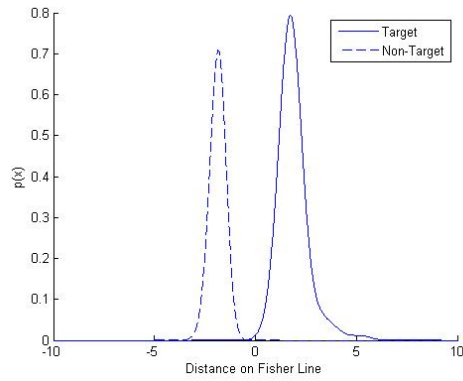
Figure 5.29: AUROC versus resolution in the x and y directions for the percent bright feature for image filter degradation.



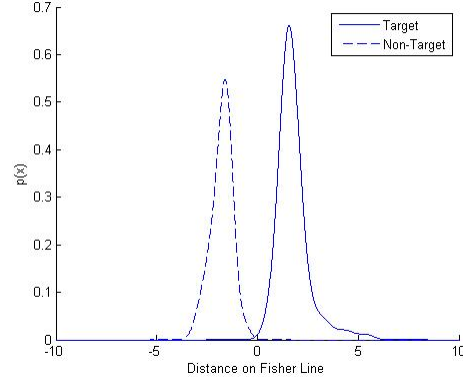
*5.3.3 Texture Features.* Figure 5.30 [a] and 5.31 [b] show the estimated pdfs for pixel reduction and filtering degradation, respectively. Each figure has 1 ft  $\times$  1 ft, 2 ft  $\times$  2 ft, 4 ft  $\times$  4 ft, and 8 ft  $\times$  8 ft resolutions. The target class is indicated by the solid line and the non-target class by the dotted lines. In the pixel reduction case the pdfs for each class remain relatively the same for each resolution. For filtering degradation the overall shape of the classes start to change and the pdfs overlap each other.

Figure 5.32 and 5.36 show AUROC versus the spatial resolution for the texture feature set and the individual features for pixel count reduction and filtering degradation. The texture features performed the best of all the feature sets. This is because the texture feature set is not as dependent on the number of pixels but on their spatial distribution. Of the three features in the texture feature set the rank filled ratio is the top performer, and the worst performer is the fractal dimension, although many references reviewed it highly [5]. The reason for its degraded performance may be due to the clutter chips that are used for the non-target class containing man-made objects and fractal dimension separates out natural clutter.

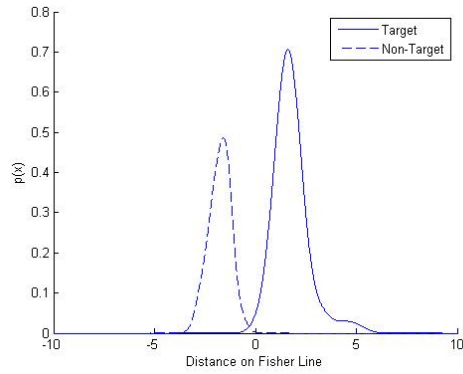
AUROC performance is shown for the individual texture features. Figures 5.33, 5.34, and 5.35 show the results for the standard deviation, fractal dimension, and rank filled ratio features, respectively, for pixel reduction. Figures 5.37, 5.38, and 5.39 show the results for standard deviation, fractal dimension, and rank filled ratio features, respectively, for the image degradation.



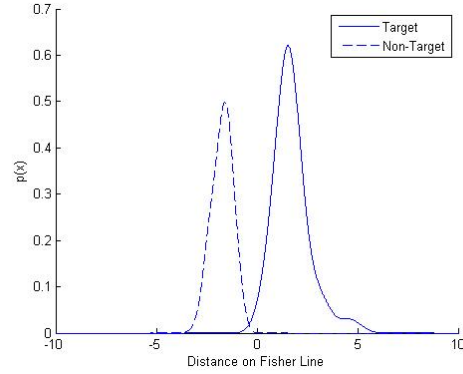
(a) 1 ft  $\times$  1 ft



(b) 2 ft  $\times$  2 ft

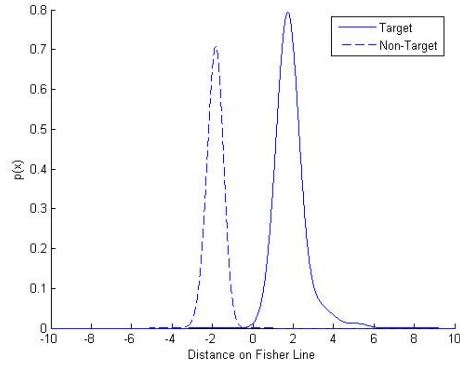


(c) 4 ft  $\times$  4 ft

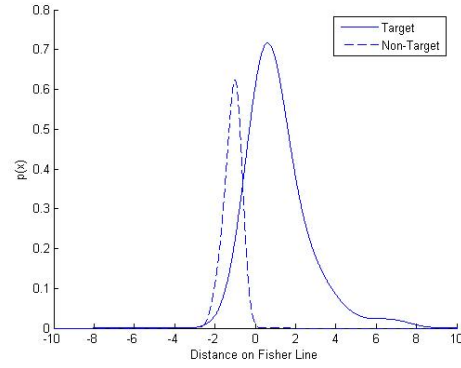


(d) 8 ft  $\times$  8 ft

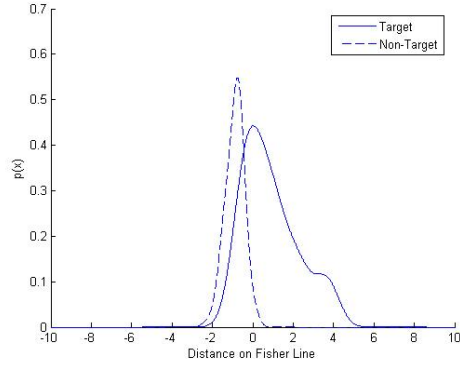
Figure 5.30: These graphs show the estimated pdfs for the texture features for resolutions of 1 ft, 2 ft, 4, ft, and 8 ft in both the x and y directions. The resolution is reduced by pixel reduction. The dotted pdf represents non-target class and the solid pdf represents the target class. [a] is 1 ft  $\times$  1 ft, [b] is 2 ft  $\times$  2 ft, [c] is 4 ft  $\times$  4 ft, and [d] is 8 ft  $\times$  8 ft.



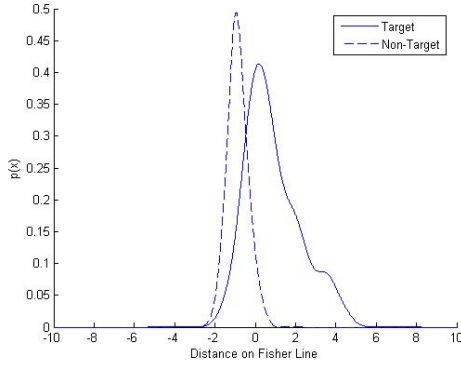
(a) 1 ft  $\times$  1 ft



(b) 2 ft  $\times$  2 ft



(c) 4 ft  $\times$  4 ft



(d) 8 ft  $\times$  8 ft

Figure 5.31: These graphs show the estimated pdfs for the texture features for resolutions of 1 ft, 2 ft, 4, ft, and 8 ft in both the x and y directions. The resolution is reduced by filtering degradation. The dotted pdf represents non-target class and the solid pdf represents the target class. [a] is 1 ft  $\times$  1 ft, [b] is 2 ft  $\times$  2 ft, [c] is 4 ft  $\times$  4 ft, and [d] is 8 ft  $\times$  8 ft.

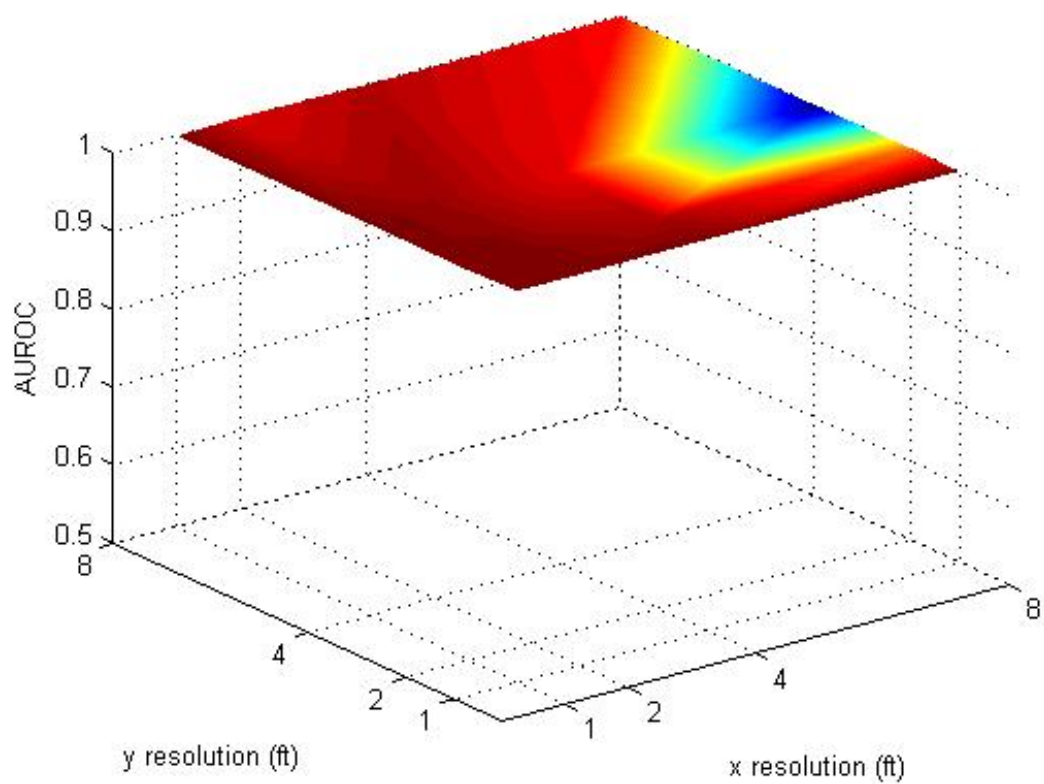


Figure 5.32: AUROC versus resolution in the x and y directions for the texture features for image filter degradation.

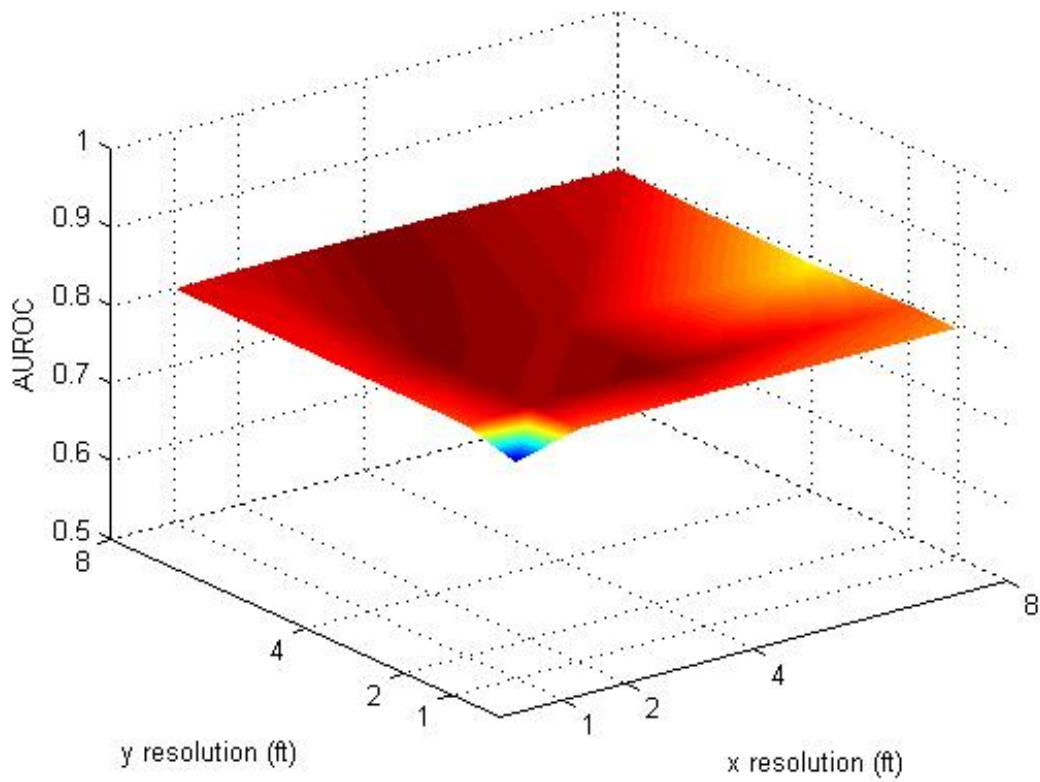


Figure 5.33: AUROC versus resolution in the x and y directions for the standard deviation feature for image filter degradation.

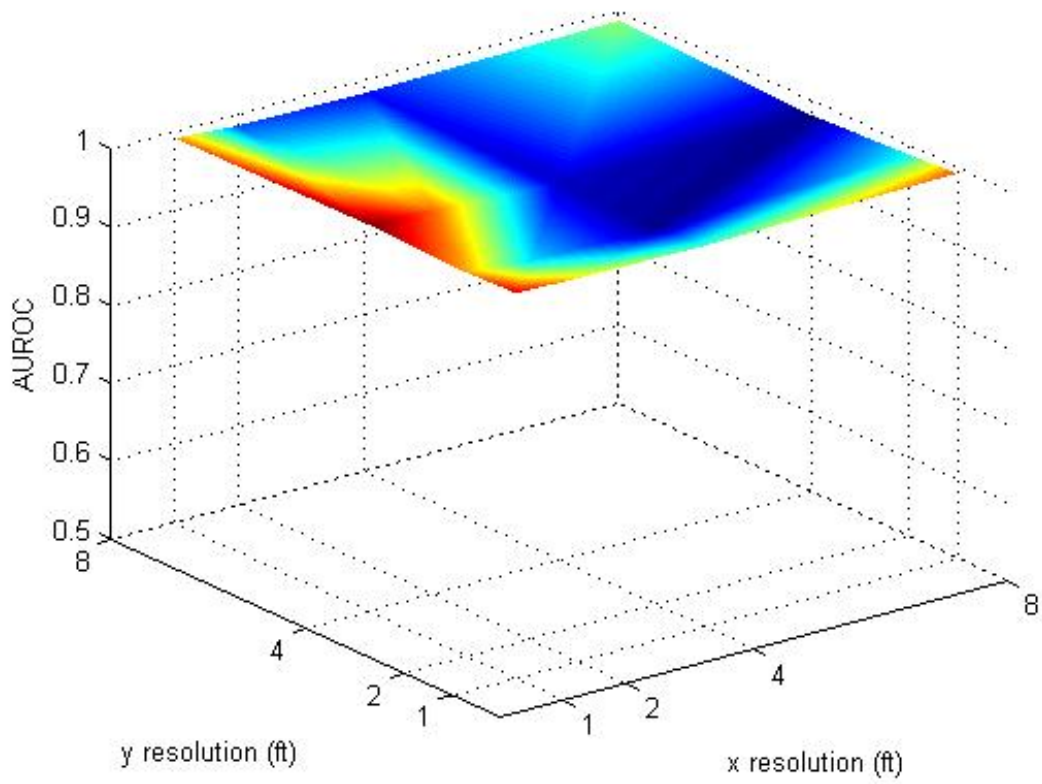


Figure 5.34: AUROC versus resolution in the x and y directions for the rank filled ratio feature for image filter degradation.

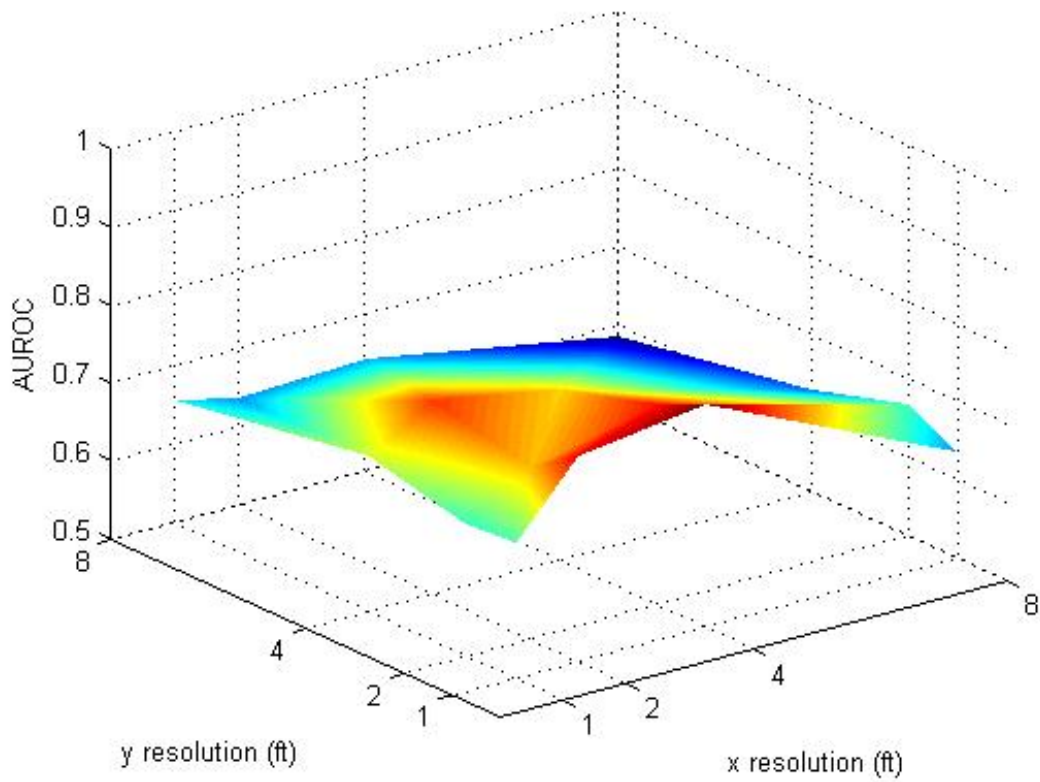


Figure 5.35: AUROC versus resolution in the x and y directions for the fractal dimension feature for image filter degradation.

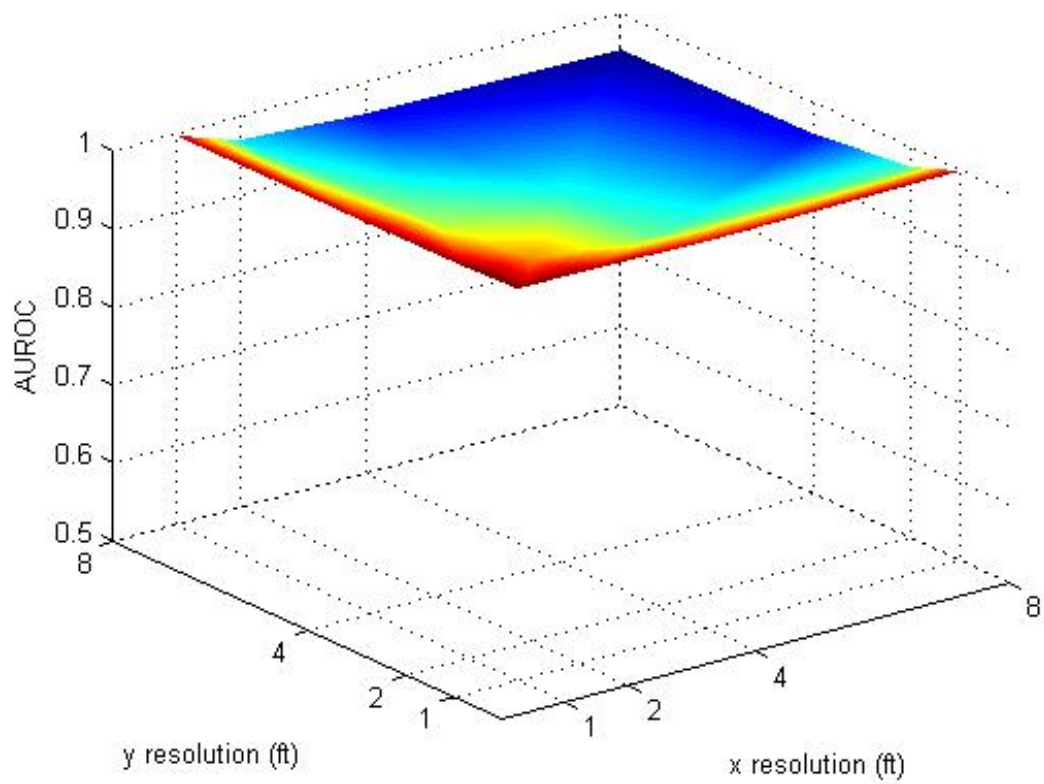


Figure 5.36: AUROC versus resolution in the x and y directions for the texture features for image filter degradation.



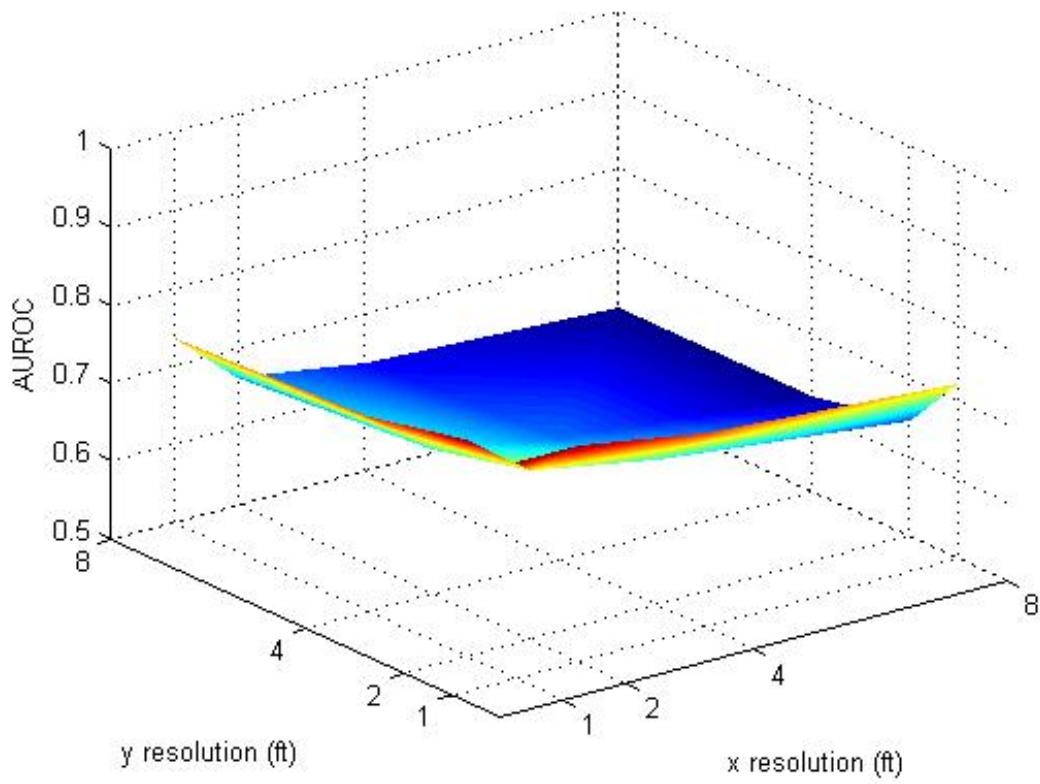


Figure 5.37: AUROC versus resolution in the x and y directions for the standard deviation feature for image filter degradation.

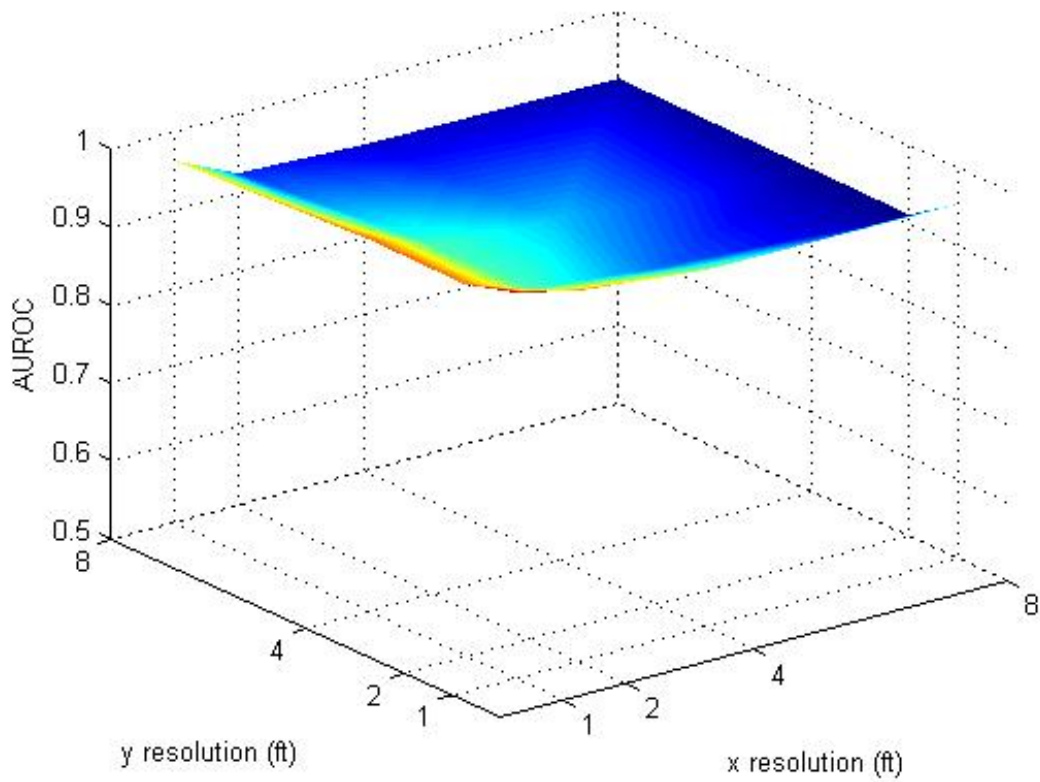


Figure 5.38: AUROC versus resolution in the x and y directions for the rank filled ratio feature for image filter degradation.

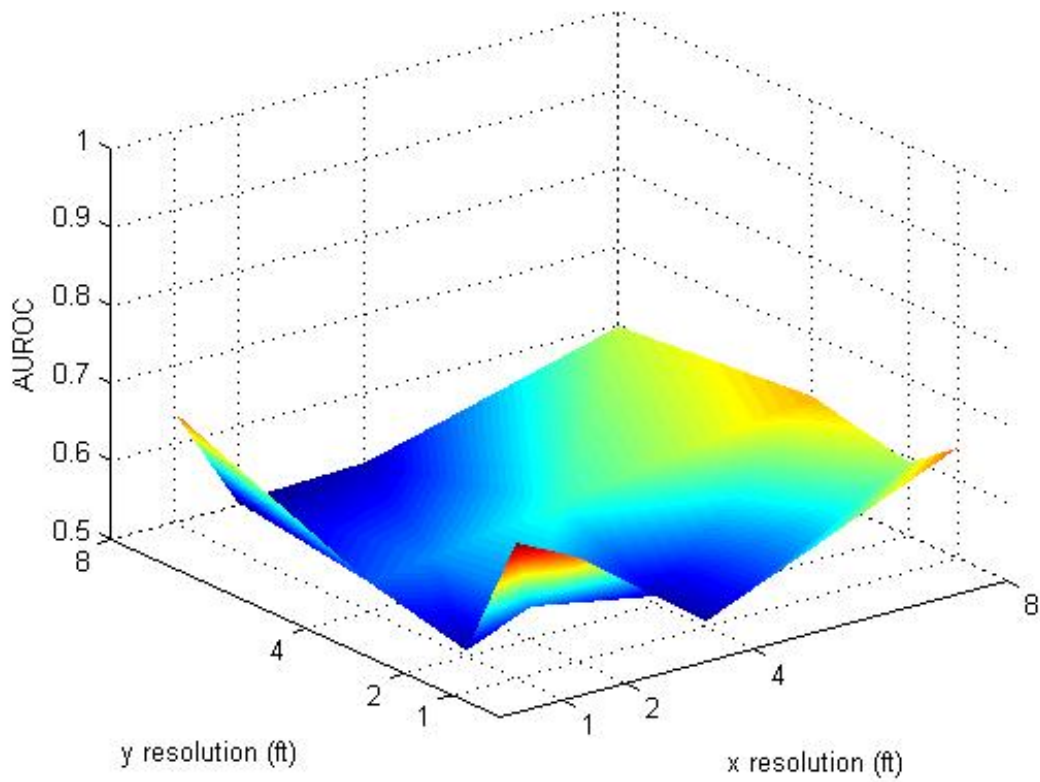
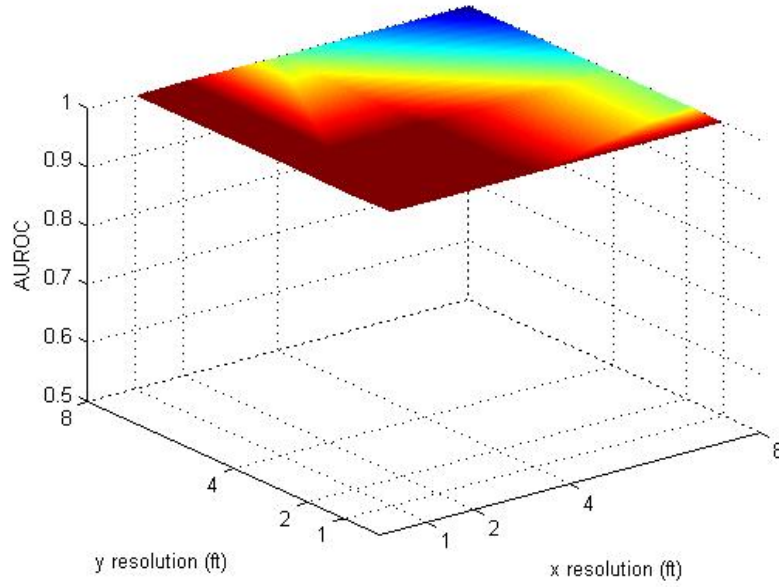
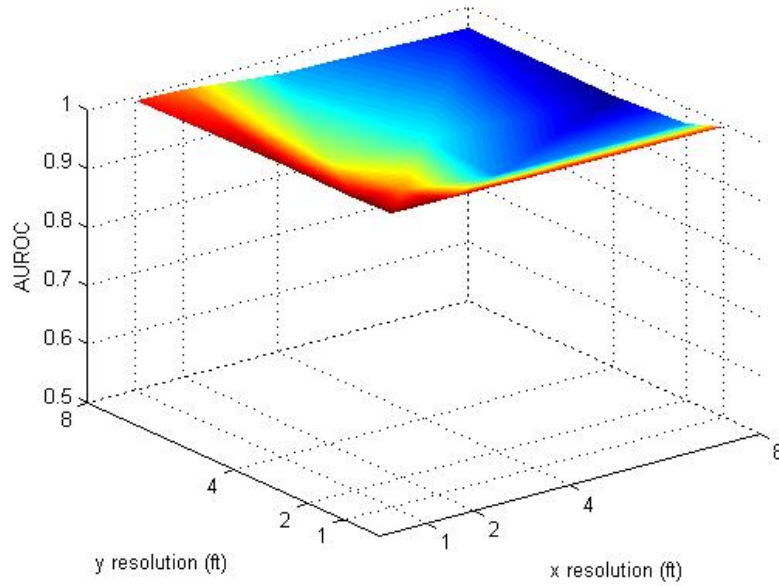


Figure 5.39: AUROC versus resolution in the x and y directions for the fractal dimension feature for image filter degradation.

*5.3.4 All Nine Features.* The all nine feature set is the combination of all size, texture, and contrast features. Figures 5.40 [a] and 5.40 [b] show AUROC versus the x and y spatial resolution for pixel reduction and filtering degradation, respectively. The nine features provide good class separability between the target and non-target classes. The pixel reduction AUROC stays within 0.01% of 1.0 and the image filtering degradation AUROC stays above 0.90, indicating good performance for all combinations of resolution. Overall performance does not improve significantly over the texture feature set by combining all nine features.



(a) Pixel Reduction Case



(b) Filtering Degradation Case

Figure 5.40: AUROC versus resolution in the x and y direction for all nine features for pixel count reduction and filtering degradation. [a] is for the pixel count reduction, showing that for all resolutions the performance is within .01%. [b] is for the image filtering degradation, where the performance stays above 0.90.

## 5.4 Feature Comparison

Table 2.2 shows the results of the same features for research done on 1 ft and 1 m resolution SAR images and which of the individual features performed best for each of the resolutions [5]. Table 5.1 repeats Table 2.2, except the 1 m  $\times$  1 m is replaced with 4 ft  $\times$  4 ft. An *X* indicates good performance, from either resolution reduction technique, for a feature from this research; a checkmark is from the original study. AUROC of 0.90 or greater constitutes a good feature. Three features did well at both 1 ft and 1 m: rank filled ratio, mass, and mean CFAR, from the original study. Results of this research did not agree, except for the rank filled ratio.

Table 5.1: Comparison of individual features from the work conducted at Lincoln Laboratory and this research [5]

Feature	1 ft $\times$ 1 ft	4 ft $\times$ 4 ft
Standard Deviation	✓	
Rank Filled Ratio	✓ <i>X</i>	✓ <i>X</i>
Fractal Dimension		✓
Mass	✓ <i>X</i>	✓
Diameter		
Normalized Rotational Interia		
Peak CFAR		✓
Mean CFAR	✓	✓
Percent Bright		

The rank filled ratio feature performs the best for all resolutions as seen in Figure 5.32 [d] and Figure 5.36 [d]. The overall shape of the rank filled ratio AUROC versus spatial resolution is the dominant shape in the texture features plots and with all nine features, which leads to the conclusion of these experiments that it is the dominant performer.

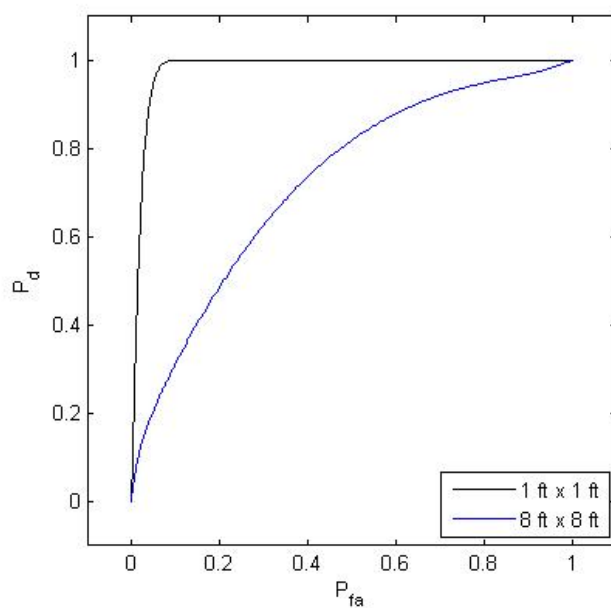
Size feature performance worsens with reduction in resolution; this is expected because these features are dependent on the bright returns from the targets. The AUROC of the original image is 0.98. For pixel reduction the 1 ft  $\times$  1 ft is the best performer, while the worst performer is for 8 ft  $\times$  8ft resolution with an AUROC of 0.72. For filtering degradation the best performer is also 1 ft  $\times$  1ft, and the worst

performance is for  $1 \text{ ft} \times 8 \text{ ft}$  with a AUROC of 0.56. Filtering degradation performs worse than pixel reduction because of the smearing effect of a larger PSF. Figure 5.41 shows the ROC curve results of the original, top, and worst performers.

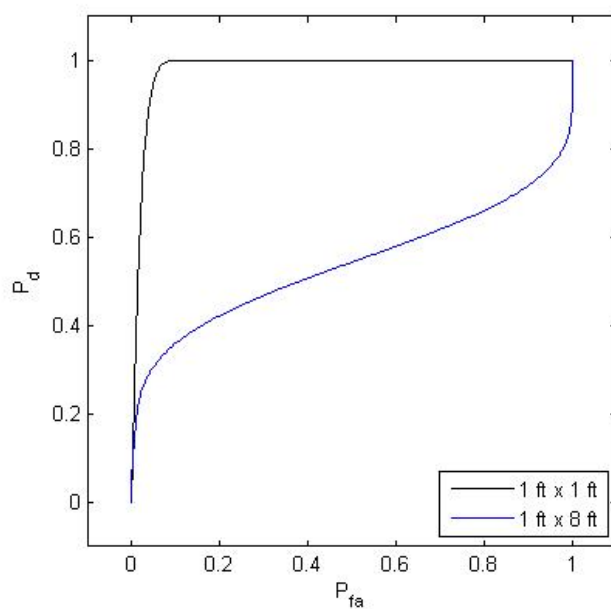
Contrast feature performance closely matches the CFAR detector performance, with a slight reduction in resolution the performance increased, then worsened. This is reasonable since all the features are based on the CFAR generated image. The AUROC for the  $1 \text{ ft} \times 1 \text{ ft}$  is 0.86. For pixel reduction, the best performance is for  $2 \text{ ft} \times 2 \text{ ft}$  resolution with a AUROC of 0.99. The worst performance is for  $8 \text{ ft} \times 8 \text{ ft}$  resolution with a AUROC of 0.82. For filtering degradation the best performer is for  $1 \text{ ft} \times 2 \text{ ft}$  resolution with a AUROC of 0.98. The worst performer is for  $8 \text{ ft} \times 8 \text{ ft}$  resolution for a AUROC of 0.64. Figure 5.42 shows the ROC curve results of the original, best, and worst performers for both reduction techniques. The tails on the ROC curves show that the estimated pdfs have high overlap and that a non-linear classification could allow for more class separation.

The texture features perform extremely well for both cases. This is because these features rely more on the statistics of the ROI and the spatial distribution of the scatters rather than pixel count. The  $1 \text{ ft} \times 1 \text{ ft}$  resolution AUROC is 1.0. For pixel reduction almost every resolution produces an AUROC of 1.0 to within 0.02%. Filtering degradation has good performance also; the worst performance is for  $1 \text{ ft} \times 8 \text{ ft}$  resolution with a AUROC of 0.89. Figure 5.43 shows the ROC curves results for the original, best, and worst performers of each reduction technique.

The all nine features perform well in separating the two classes. The lower pixel count shows almost perfect separation for all sixteen combinations, where every AUROC is 1.0 to within 0.02%. The filtering degradation performs well with the worst performance at a AUROC of 0.96. Figure 5.44 [a] and 5.44 [b] shows ROC curves for pixel reduction and filtering degradation, respectively.



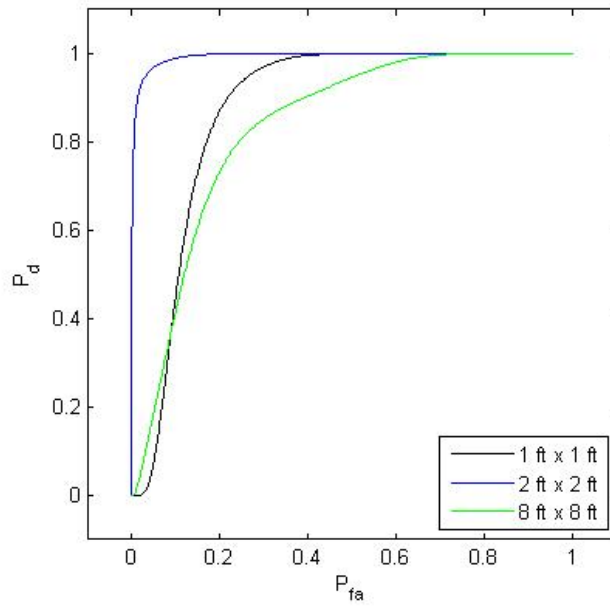
(a) Pixel Reduction



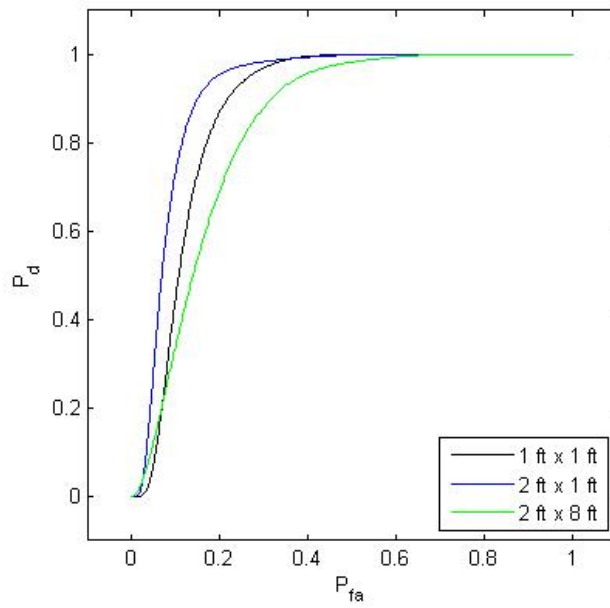
(b) Image Degradation

Figure 5.41: ROC curves for the original/best (1 ft  $\times$  1 ft for [a] and [b]), and worst resolution (8 ft  $\times$  8 ft for [a] and 1 ft  $\times$  8 ft for [b]) for the size features.



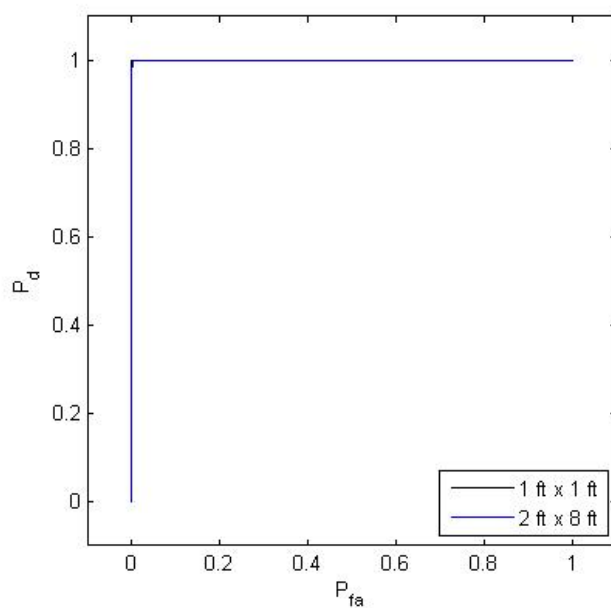


(a) Pixel Reduction

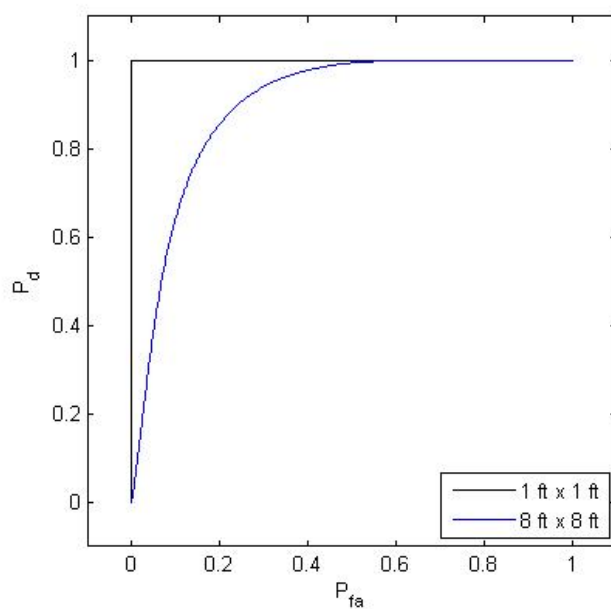


(b) Image Degradation

Figure 5.42: ROC curves for the original (1 ft  $\times$  1 ft for [a] and [b]), best (2 ft  $\times$  2 ft for [a] and 2 ft  $\times$  1 ft for [b]), and worst resolution (8 ft  $\times$  8 ft for [a] and 2 ft  $\times$  8 ft for [b]) for the contrast features.

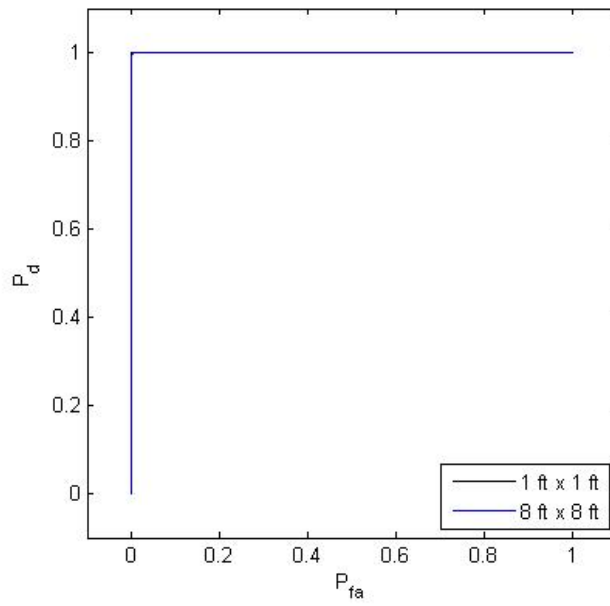


(a) Pixel Reduction

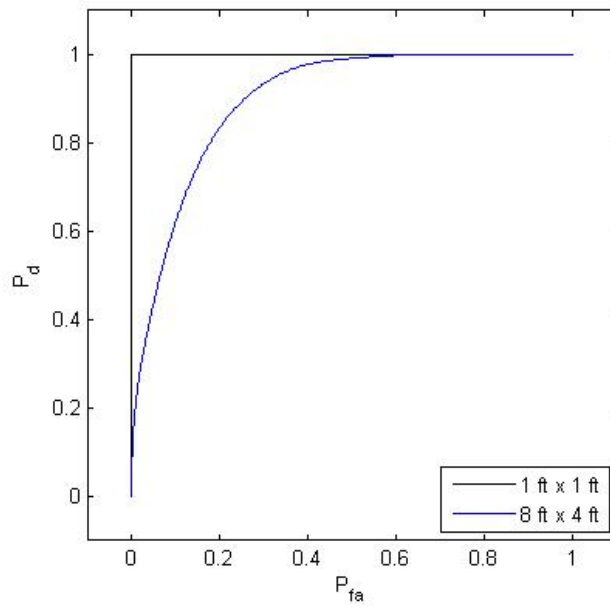


(b) Image Degradation

Figure 5.43: ROC curves for the original/best (1 ft  $\times$  1 ft for [a] and [b]), and worst resolution (2 ft  $\times$  8 ft for [a] and 8 ft  $\times$  8 ft for [b]) for the texture features.



(a) Pixel Reduction



(b) Image Degradation

Figure 5.44: ROC curves for the original/best (1 ft  $\times$  1 ft for [a] and [b]), and worst resolution (8 ft  $\times$  8 ft for [a] and 8 ft  $\times$  4 ft for [b]) for all nine features.

## 5.5 *Summary*

This chapter shows the results of detection and discrimination of targets as the spatial resolution of the SAR image is degraded. The performance for the two-parameter CFAR peaked at  $2\text{ ft} \times 2\text{ ft}$  resolution for both resolution variation techniques. All nine feature and texture feature sets performed the best; while the size features performed worst with reduction in resolution. The contrast features were shown to be ineffective, due to the ROC curves crossing the chance line. The performance of each of the sets was dominated by one feature of each set with the other two features only adding minor improvements to performance. Overall the rank filled ratio was the top individual feature with AUROC staying above 0.90.

## VI. Conclusions

### 6.1 Overview

This thesis shows how different discriminating features perform for different levels of spatial resolution. All nine features and texture features are shown to be the most robust of the feature sets, while the size features are the worst performers. The contrast features yield improved performance when the resolution is slightly reduced. The rank filled ratio was seen to be the top performer of all the individual features.

### 6.2 General Discussion

This research looks at the performance of ATR to discriminate between targets and non-targets for various levels of resolution. The test is designed to provide the maximum performance from ATR, where changes in the performance could only be attributed to differences in resolution. The resolution is lowered in two different ways. In the first the higher resolution image is averaged to yield a lower pixel count. This is a simulation of a system processing less information from a scene, allowing for an increase in speed. In many of the results it is seen that if either direction is maintained at 1 ft, the performance level is relatively the same. The other scenario simulates the same scene imaged for coarser resolutions. The two-parameter CFAR detector had a better performance with this technique than with pixel reduction. The increase in performance is due to the smearing of the energy, where smaller groups of bright scatters are smeared into the other dim pixels, and larger groups of bright scatters (targets) are still smeared but the area stays bright.

The best overall performer is the texture feature set for both reduction techniques, but this can be attributed to the rank filled ratio feature. This feature's AUROC versus resolution shape dominated the overall shape of the texture feature set shape. This research shows that the rank filled ratio is the essential feature to be used in ATR.

### ***6.3 Future Work***

Though this research shows how resolution affects the performance of ATR, there are a multitude of factors that need to be investigated, such as the contrast in the image, noise effects, phase history of the scene, and how clutter in the scene affects performance. For example, the phase history is like color to an optical picture, it adds more information on how to make a decision. How that phase changes with varying resolution has a large impact on an ATR. The target chips used in this research are all located in an open field and not obscured, but in real scenes targets can be close to trees, buildings, roads, and other targets. Factors such as these that affect ATR performance can be minimized if the right feature set is selected for the correct image quality. Knowledge of these factors can lead to an adaptive algorithm that analyzes the image and selects the optimum feature set.

## *Appendix A. Tables of AUROC*

Table A.1: AUROC for the Two-Parameter CFAR detector for reduced pixel count.

Two-Parameter CFAR	$\Delta x$	$\Delta y$
0.93	1	1
0.93	2	1
0.80	4	1
0.84	8	1
0.95	1	2
0.97	2	2
0.89	4	2
0.87	8	2
0.90	1	4
0.92	2	4
0.83	4	4
0.85	8	4
0.76	1	8
0.82	2	8
0.72	4	8
0.71	8	8

Table A.2: AUROC for the Two-Parameter CFAR detector for image degradation by filtering.

Two-Parameter CFAR	$\Delta x$	$\Delta y$
0.93	1	1
0.98	2	1
0.91	4	1
0.86	8	1
0.98	1	2
0.99	2	2
0.97	4	2
0.89	8	2
0.96	1	4
0.98	2	4
0.94	4	4
0.83	8	4
0.84	1	8
0.92	2	8
0.80	4	8
0.72	8	8

Table A.3: AUROC for individual Size Discriminating Features for reduced pixel count.

Size	$v_{mass}$	$v_{dia}$	$v_{rot}$	$\Delta x$	$\Delta y$
0.98	0.98	0.62	0.95	1	1
0.96	0.96	0.61	0.85	2	1
0.95	0.96	0.59	0.74	4	1
0.89	0.88	0.53	0.59	8	1
0.96	0.97	0.50	0.92	1	2
0.94	0.94	0.54	0.88	2	2
0.94	0.94	0.50	0.91	4	2
0.88	0.88	0.49	0.65	8	2
0.93	0.9420	0.4968	0.8417	1	4
0.91	0.9031	0.5208	0.7995	2	4
0.88	0.8595	0.4961	0.7366	4	4
0.80	0.7864	0.5078	0.6979	8	4
0.90	0.91	0.50	0.81	1	8
0.88	0.88	0.50	0.75	2	8
0.82	0.77	0.50	0.60	4	8
0.72	0.71	0.52	0.54	8	8



Table A.4: AUROC for individual Size Discriminating Features for image degradation by filtering.

Size	$v_{mass}$	$v_{dia}$	$v_{rot}$	$\Delta x$	$\Delta y$
0.98	0.98	0.62	0.95	1	1
0.86	0.84	0.50	0.60	2	1
0.66	0.65	0.51	0.50	4	1
0.63	0.62	0.51	0.57	8	1
0.86	0.86	0.49	0.63	1	2
0.77	0.69	0.51	0.50	2	2
0.59	0.52	0.53	0.56	4	2
0.69	0.64	0.57	0.62	8	2
0.71	0.68	0.51	0.50	1	4
0.68	0.51	0.54	0.58	2	4
0.69	0.63	0.55	0.65	4	4
0.66	0.64	0.56	0.62	8	4
0.56	0.53	0.50	0.56	1	8
0.67	0.59	0.56	0.61	2	8
0.72	0.64	0.57	0.60	4	8
0.66	0.64	0.56	0.63	8	8

Table A.5: AUROC for individual Contrast Discriminating Features for reduced pixel count.

Contrast	$v_{peak}$	$v_{mean}$	$v_{per}$	$\Delta x$	$\Delta y$
0.86	0.59	0.51	0.78	1	1
0.94	0.62	0.55	0.83	2	1
0.93	0.60	0.54	0.82	4	1
0.94	0.63	0.53	0.81	8	1
0.93	0.64	0.52	0.81	1	2
0.99	0.68	0.58	0.93	2	2
0.93	0.59	0.60	0.84	4	2
0.94	0.68	0.54	0.82	8	2
0.90	0.61	0.51	0.80	1	4
0.98	0.66	0.53	0.91	2	4
0.92	0.62	0.55	0.81	4	4
0.91	0.67	0.51	0.74	8	4
0.90	0.61	0.52	0.81	1	8
0.96	0.64	0.53	0.88	2	8
0.86	0.58	0.55	0.78	4	8
0.82	0.62	0.56	0.70	8	8

Table A.6: AUROC for individual Contrast Discriminating Features for image degradation by filtering.

Contrast	$v_{peak}$	$v_{mean}$	$v_{per}$	$\Delta x$	$\Delta y$
0.86	0.59	0.51	0.78	1	1
0.98	0.69	0.61	0.87	2	1
0.89	0.70	0.63	0.70	4	1
0.68	0.67	0.59	0.51	8	1
0.98	0.72	0.58	0.86	1	2
0.91	0.82	0.65	0.74	2	2
0.82	0.79	0.67	0.51	4	2
0.83	0.79	0.63	0.53	8	2
0.93	0.72	0.59	0.73	1	4
0.84	0.79	0.62	0.61	2	4
0.83	0.81	0.64	0.53	4	4
0.81	0.78	0.60	0.52	8	4
0.72	0.70	0.58	0.56	1	8
0.64	0.63	0.58	0.52	2	8
0.76	0.74	0.59	0.56	4	8
0.75	0.75	0.62	0.55	8	8

Table A.7: AUROC for individual Texture Discriminating Features for reduced pixel count.

Texture	$v_{std}$	$v_{rank}$	$v_{dim}$	$\Delta x$	$\Delta y$
1.0	0.77	0.99	0.67	1	1
1.0	0.80	0.99	0.76	2	1
1.0	0.80	0.99	0.78	4	1
1.0	0.79	0.99	0.64	8	1
1.0	0.80	0.99	0.67	1	2
1.0	0.80	0.99	0.72	2	2
1.0	0.80	0.98	0.75	4	2
1.0	0.80	0.99	0.67	8	2
1.0	0.80	1.0	0.70	1	4
1.0	0.80	0.99	0.75	2	4
1.0	0.80	0.98	0.71	4	4
1.0	0.79	0.98	0.63	8	4
1.0	0.80	0.99	0.66	1	8
1.0	0.80	0.98	0.64	2	8
1.0	0.80	0.99	0.64	4	8
1.0	0.80	0.99	0.58	8	8

Table A.8: AUROC for individual Texture Discriminating Features for image degradation by filtering.

Texture	$v_{std}$	$v_{rank}$	$v_{dim}$	$\Delta x$	$\Delta y$
1.0	0.78	0.99	0.67	1	1
1.0	0.78	0.97	0.63	2	1
0.99	0.75	0.96	0.51	4	1
0.99	0.72	0.95	0.64	8	1
1.0	0.78	0.97	0.51	1	2
0.98	0.71	0.95	0.54	2	2
0.96	0.68	0.93	0.51	4	2
0.95	0.65	0.91	0.59	8	2
1.0	0.75	0.97	0.53	1	4
0.96	0.68	0.95	0.55	2	4
0.95	0.66	0.94	0.57	4	4
0.94	0.62	0.91	0.62	8	4
1.0	0.73	0.96	0.64	1	8
0.95	0.66	0.92	0.50	2	8
0.92	0.64	0.92	0.51	4	8
0.92	0.62	0.91	0.60	8	8

## Appendix B. App 2

This section presents the code used for this research. All scripts were written and tested using MATLAB 2006b.

### B.1 Image Reduction

Listing B.1: ATRToolbox/lowResPix.m

```
1 function [AA] = lowResPix(A,xa,yb, sinc_filter)
    %=====
    % xa is the factor x dim is reduced
    % yb is the factor y dim is reduced
    % sinc_filter turns filter on, 1, and off, 0,
    6 %=====
    [aa bb] = size(A);
    %scale factor fix
    if xa == 1
        rF = 0;
    11 else
        rF = 1;
    end
    if yb == 1
        cF = 0;
    16 else
        cF = 1;
    end
    %=====
    %filter with sinc fliter
    21 if sinc_filter == 1
        a = (ifft2(A));
        [P,Q] = size(a);
        p = 0:(P-1);
        q = 0:(Q-1);
    26     N = 128;
        m = log2(xa);
        n = log2(yb);
```

```

        Hp = 0.54 + 0.46*cos((2*pi*p)/(2^-m*N));
        Hq = 0.54 + 0.46*cos((2*pi*q)/(2^-n*N));
31    H = Hp'*Hq;
        a = a.*H;
        A = abs(fft2(a));

    end

%-----
36 x = floor(aa/xa);
    y = floor(bb/yb);
    AA = zeros(x,y);
    [a b] = size(AA);
    rowFactor = floor(aa/a);
41 colFactor = floor(bb/b);

    for ii = 1:a
        for jj = 1:b

46            AA(ii,jj) =sum(sum(A((round(ii*rowFactor)-rF):round(ii*...
                rowFactor),...
                round(jj*colFactor-cF):round(jj*colFactor))))./(xa*yb)...
                ;

        end
    end
    AA = abs(AA);
51 %-----

```

## B.2 Two-Paramter CFAR

Listing B.2: ATRToolbox/prescreener.m

```

function [H, ratio] = prescreener(M, N, gamma,image, pixSize)
%John McGowan
%Prescreener--this pulls in an entire scene image and screen for ...
    clusters of bright
4 %pixel that could be considered a target.
%
%M and N are the test location of a possible TGT

```

```

%gamma is the Threshold level
%H is the return if 1 (true) then that location is a possible TGT;...
    if 0
9  %(false) then no TGT
    %First generation test where the image chip is feed and not an ...
        entire
    %scene.
    test_on = 0;

14 if nargin == 0
    [ImageCellT72]= loadT72();
    [ImageCellClutter]= loadClutter();

19 image = ImageCellT72(:,:,1);
    %image = ImageCellClutter(:,:,1);
    %imshow(uint8(image))
    image = image./max(max(image));
    image = image-mean2(image);
24 gamma = 0;
    pixSize = 0; %defines the size test area make even
    %-----
    [m n] = size(image);
    M = floor(m/2):floor(m/2); %pixel under test
29 N = floor(n/2):floor(n/2); %pixel under test
    % [a b] = find(image == max(max(image)));
    % M = ceil(mean(a));
    % N = ceil(mean(b));
    end
34 %-----
    [m n] = size(image); %size of entire scene

    r = pixSize;% round(20/pixSize); %this number of surrounding pixels...
        that will be used to find clutter mean/sd

```

```

39 %=====
    %goes around edge to estimate clutter
    leftCol = (image(:,1:r));
    rightCol = (image(:,(n-r):n));
    topRow = (image((m-r):m,:));
44 bottomRow = (image(1:r,:));

    meanC = mean([mean(leftCol) mean(rightCol) mean(topRow,2)' mean(...
        bottomRow,2)']);
    stdC = std([std(leftCol) std(rightCol) std(topRow') std(bottomRow...
        ')]);
    %=====
49 %threshold test
    MeanTgt = mean2(image(M,N));
    ratio = (MeanTgt - meanC)/stdC;
    H = ratio > gamma; %this will give a 1 or 0
    %=====

```

### B.3 Feature Code

Listing B.3: ATRToolbox/SizeMass.m

```
function [massIm] = SizeMass(im, threshold,s,t)
2 %=====
%counts the number of bright scatters that exceed a
%set threshold
m = pIm(im, s, t, threshold);
massIm = sum(sum(m)).*s.*t;
```

Listing B.4: ATRToolbox/SizeDia.m

```
function [diaIm] = SizeDia(im, threshold,s,t)
%-----
m = pIm(im, s, t, threshold);
4 %-----
%cal diameter
[a b] = find(m == max(max(m))); %use mean pixel of all scatters
[alast v] = size(a);
[blast v] = size(b);
9 a = sort(a);
b = sort(b);
xx1 = a(1);
yy1 = b(1);
xx4 = a(alast);
14 yy4 = b(blast);
%find first and last x,y construct box
%-----
%%find smallest length
d1 = sqrt((xx4-xx1)^2+(yy4-yy1)^2);
19 d2 = (xx4-xx1);
d3 = (yy4-yy1);
if d2 == 0
    d2 = d3;
end
24 if d3 == 0
```



```

        d3 = d2;
    end
    dd = [d1 d2 d3];
    diaIm = max(dd);
29 %-----

```

Listing B.5: ATRToolbox/SizeRot.m

```

1 function [rotIm] = SizeRot(im, threshold,s,t)
    %=====
    m = pIm(im, s, t, threshold);
    [row col] = size(m);
    %=====
6 [a b] = find(m == max(max(m)));
    aa = mean(a);
    bb = mean(b);
    r = 0;
    for ii = 1:row
11     for jj = 1:col
        r = r + m(ii,jj)*((ii-aa)^2+(jj-bb)^2);
    end
    end
    rotIm = r./(aa*bb); %normalize by total pixel size
16 %=====

```

Listing B.6: ATRToolbox/peakCFAR.m

```
function [PeakCFAR] = peakCFAR(im, pixSizeS, pixSizeT, threshold)
%
%
4 %=====
%calcululates the maximum value from a CFAR image
imC = cfarIM(im, pixSizeS, pixSizeT, threshold);

PeakCFAR = max(max(imC));
```

Listing B.7: ATRToolbox/perbCFAR.m

```
function [PerBright] = perbCFAR(im, pixSizeS, pixSizeT, threshold)
2 %
%=====
%calcululates the maximum value from a CFAR image
imC = cfarIM(im, pixSizeS, pixSizeT, threshold);
[row col] = size(imC);
7 imCb = binIm(imC,threshold);
PerBright = sum(sum(imCb))./(row*col)*100;
```

Listing B.8: ATRToolbox/meanCFAR.m

```
function [MeanCFAR] = meanCFAR(im, pixSizeS, pixSizeT, threshold)
2 %
%=====
%calcululates the maximum value from a CFAR image
imC = cfarIM(im, pixSizeS, pixSizeT, threshold);

7 MeanCFAR = mean2(imC);
```

Listing B.9: ATRToolbox/disSTD.m

```
function [vFeature] = disSTD(Im)

3  %-----
    vFeature = std2(Im);
    %-----
```

Listing B.10: ATRToolbox/fracDim.m

```
function [dim] = fracDim(im, thresP)
%-----
%control panel
plot_on = 0;
5  dType = 0; %0 for threshold; 1 for %
    [r c]=size(im);
    aIm = min(min(im));
    bIm = max(max(im));
    %-----
10 %binary image
    if dType == 0
        threshold =(bIm-aIm)*thresP;
        %amplitude threshold
        Aim = im;
15 A = (Aim);
        ind= find(A < threshold);
        Aim(ind) = 0;

        %A = (Aim);
20 ind= find(A >= threshold);
        Aim(ind) = 1;
        fracim = Aim;
        %
        else
25 %-----
        %brightess Pixel
        numP = 50;
```

```

    numPixel = round(r*c*.05); %N brightest pixel
    q=im(:);
30 q = sort(q,'descend');
    if numP < size(q)
        numP = size(q);
    end
    threshold = q(numP);
35
    Bim = 0.*im;
    A = (im);
    ind= find(A >= threshold);
    Aind = size(ind);
40 if Aind < numPixel
        numPixel = Aind;
    end
    %ind(1)
    if numPixel > 0
45 Bim(ind(1:numPixel)) = 1;
    end
    fracim = Bim;
    end
    %-----
50 %calculate fractal dim

    M1 = sum(sum(fracim)); % number of points in 1 pixel boxes

    %increase image size to guard edges with zeros
55 fracIm = zeros(r+20,c+20);

    fracIm(10:r+9,10:c+9) = fracIm(10:r+9,10:c+9) + fracim;
    [aa bb] = find(fracIm == 1);
    M2 = 0; %intialize 2 pixel box count
60
    for ii = 1:length(aa)
        for jj = 1:length(bb)

```

```

        if fracIm(aa(ii),bb(jj)) == 1
            f1 = sum(sum(fracIm(aa(ii):aa(ii)+1,bb(jj):bb(jj)+1)))...
                ;
65         f2 = sum(sum(fracIm(aa(ii)-1:aa(ii),bb(jj)-1:bb(jj))))...
                ;
            f3 = sum(sum(fracIm(aa(ii):aa(ii)+1,bb(jj)-1:bb(jj))))...
                ;
            f4 = sum(sum(fracIm(aa(ii)-1:aa(ii),bb(jj):bb(jj)+1)))...
                ;

            %finds box that contains highest number of pixels
            f = [f1 f2 f3 f4];
70         b = find(f == max(f));
            if b(1) == 1
                fracIm(aa(ii):aa(ii)+1,bb(jj):bb(jj)+1) = 0;
            elseif b(1) == 2
                fracIm(aa(ii)-1:aa(ii),bb(jj)-1:bb(jj)) = 0;
75         elseif b(1) == 3
                fracIm(aa(ii):aa(ii)+1,bb(jj)-1:bb(jj)) = 0;
            else
                fracIm(aa(ii)-1:aa(ii),bb(jj):bb(jj)+1) = 0;
            end
80
            M2 = M2+1; %count boxes
        end
    end

85 end

dim = (log(M1)-log(M2))/log(2);
%-----
%plot
if plot_on == 1
90     if dType == 0
        figure(1)
        imagesc(Aim)
        colormap('gray')
    end
end

```

```

    title('Amplitude Thresholding')
95     else
    figure(2)
    imagesc(Bim)
    colormap('gray')
    title('Brightness Thresholding')
100    end
    end
end

```

Listing B.11: ATRToolbox/disINT.m

```

function [wRank] = disINT(Im)
%-----
[aa bb] = size(Im);
4 It = Im(:);

It = sort(It,'descend');
p = sum(It(1:ceil(.05*aa*bb)));
wRank = p/sum(sum(Im));
9 %-----

```

## B.4 Sub-Image

Listing B.12: ATRToolbox/binIm.m

```
1 function [im] = binIm(im, threshold)

    %create a binary image form SAR images
    %define dynamic range and apply threshold
    Bmax = max(max(im));
    6 Bmin = min(min(im));
    t = threshold*(Bmax-Bmin);
    if t == 0
        error('bad image')
    end
    11 [ r c] = size(im);
    %intialize image
    Aim = zeros(r,c);
    %
    ind= find(im >= t);
    16 Aim(ind) = 1;
    im = Aim;
    %-----
```

Listing B.13: ATRToolbox/pIm.m

```
function [p] = pIm(im,s,t,threshold);
    2 %from a binay image finds mean and gets rid of anything in a ...
        radius n.
    [aa bb] = size(im);
    %
    %create binary image with closely spaced points
    m = binIm(im,threshold);
    7 %find mean and std x,y
    [a b] = find(m == max(max(m))); %use mean pixel of all scatters
    mM = ceil(mean(a));
    nM = ceil(mean(b));
    mS = ceil(12/s);
```

```

12 nS = ceil(12/t);
   r = ceil(sqrt(mS^2+nS^2));
   for ii = 1:aa
       for jj = 1:bb
           if m(ii,jj) == 1
17             px = [ii jj; mM nM];
               dx = pdist(px);
               if dx > r
                   m(ii,jj) = 0;
               end
22         end
       end
   end
p = m;
%-----

```

Listing B.14: ATRToolbox/cfarIm.m

```

function [ratio] = cfarIM(image, pixSizeS, pixSizeT, threshold);
%=====
%CFAR image
4 %-----
[m n] = size(image); %size of entire scene

rS = pixSizeS; %this number of surrounding pixels that will be used...
    to find clutter mean/sd
rT = pixSizeT;
9 %=====
%goes around edge to estimate clutter
leftCol = (image(:,1:rT));
rightCol = (image(:,ceil(n-rT):n));
topRow = (image(ceil(m-rS):m,:));
14 bottomRow = (image(1:rS,:));

meanC = mean([mean(leftCol) mean(rightCol) mean(topRow,2)' mean(...
    bottomRow,2)']);

```



```

stdC  = std([std(leftCol) std(rightCol) std(topRow') std(bottomRow...
            ')]);
%=====
19 %threshold test
ratio = (image- meanC)/stdC;
%-----

```

## B.5 Fisher Line

Listing B.15: ATRToolbox/Fisher.m

```
function [fisher_pv, fisher_uv, Sigma, c, norm_plot, x, Asum, roc]...
    = Fisher(vector, plot_on, numClass, class1, class2, class3);

%-----
%variables
4 [r,c] = size(vector);
    totalsize = class1+class2+class3;
%-----
%program
%Use least square to find Fisher ine
9 mf1 = mean2(vector(1:class1,:));
    mf2 = mean2(vector((1+class1):totalsize));
    m1 = totalsize/class1.*ones(1,class1);
    m2 = -totalsize/class2.*ones(1,class2);
    m = [m1 m2]';
14
    one_v = ones(r,1);
    v = [one_v vector];
    v_tran = v';

19 V = v_tran*v;
    M= v_tran*m;
    c = inv(V)*M;
    y = v*c;

24 fisher_pv = y(1:class1,1);
    fisher_uv = y((1+class1):totalsize,1);
    [pv_row,pv_col] = size(fisher_pv);
    [uv_row, uv_col] = size(fisher_uv);

29 if plot_on == 1
    figure (8)
    z = y(1:30,1).*0;
```

```

plot(y(1:30,1),z,'+')
hold on
34
z = y(31:60,1).*0;
plot(y(31:60,1),z,'o')
% title('Fisher')
%h = legend('PV','UV',1);
39 %set(h,'Interpreter','none');
hold off
end

%-----

44
%Add a Gaussian disturbance over each target then vary the ...
variance until
%the sum of the Gaussian distribution of each class is smooth. The...
new
%Gaussian is then normalized, so it is a true pdf.
class_type = 1; % this is used to select b/w the 2 classes 1=pv; ...
2=uv
49 x = -10:.01:10;

for class_type = 1:2;
    if class_type == 1
        dis = fisher_pv;
54        class_size = pv_row;
    else
        dis = fisher_uv;
        class_size = uv_row;
    end
59 smooth = 0; %this is an indicator that there is one peak

sigma = .1; %this is the start value of the variance
step_size = .001; %controls the resolution of the sigma increases
while smooth == 0

```

```

64     count = 0; %Used to count number of peaks
[a b] = size(dis); %a is number of points

    for a_count = 1:a %creates gaussian distro over each point...
        in class
69     %each row holds 1 point of a single class' distro
        point = dis(a_count,1);
        gauss_plot(a_count,:,class_type) = gaussmf(x,[sigma point...
            ]);

        end
74     sum_plot(:,:,class_type) = sum(gauss_plot(:,:,class_type));
        a_max = max(max(sum_plot(:,:,class_type)));
        norm_plot(:,:,class_type) = sum_plot(:,:,class_type)./...
            class_size;%a_max;%
        %count peaks to determine unimotel (one peak)
        [A,B,C] = size (norm_plot);
79     a = 1;
        for B_count = 2:B
            pos = a*(norm_plot(A,(B_count),class_type)-norm_plot(A,...
                B_count-1),class_type));
            if pos > 0
            else
84             a = -1*a;
                count = count + 1; %When this is one then unimotel
            end

        end

    end
89     if count == 1
        smooth = 1;
    else
        sigma = sigma + step_size;
    end
94

```

```

        end
        Sigma(1,class_type) = sigma;
    end

99 %-----
    %Create a ROC curve of the two classes

    [roc, Asum] = ROC(norm_plot, plot_on);

104 %-----
    %plots
    if plot_on == 1
        figure(111)
        plot(x, gauss_plot(:, :, 1))
109    % hold on

        figure(112)
        plot(x, gauss_plot(:, :, 2))
114    %hold on
        figure(8)
        plot(x, norm_plot(:, :, 1))
        hold on
        plot(x, norm_plot(:, :, 2))
119    %h = legend('PV', 'UV', 1);
        %set(h, 'Interpreter', 'none');
        axis([-5.5 5 -.25 1])
    end
    %-----
124 %return

```

## B.6 ROC

Listing B.16: ATRToolbox/ROC.m

```
1 function [area, Asum] = ROC(norm_plot, plot_on);
   %-----
   %variables
   [a, b, c] =size(norm_plot);

6 %-----
   %program

   for class_type = 1:c
       class = norm_plot(:, :, class_type);
11
       %sum up the amount of area as going form left to right
       for a_sum = 1:a
           for b_sum = 1:b
               if b_sum == 1
16                   area(a_sum, b_sum ,class_type) = class(a_sum,b_sum)...
                       ;
               else
                   area(a_sum, b_sum ,class_type) = class(a_sum,b_sum)...
                       + area(a_sum, b_sum -1 ,class_type);
               end
           end
       end
21
       end

       a_max(1,class_type) = max(max(area(:, :, class_type)));
       area(:, :, class_type) = area(:, :, class_type)./a_max(1,...
           class_type);

26
       end

       Asum = area(:, 1:(length(area(:, :, 1))-1), 2)*diff(area(:, :, 1))';
   %-----
   %plots
```

```

    if plot_on == 1
31 figure (211)
    h211 = plot(area(:,:,1), area(:,:,2));
    xlabel('P_f')
    ylabel('P_d')
    axis equal
36 axis([-0.1 1.1 -0.1 1.1])
    %set(gca,'XTickLabel',{})
    %set(gca,'YTickLabel',{})
    hold on
    end
41 %-----
    return

```

## Bibliography

1. Carrara, Walter G., Ron S. Goodman, and Ronald M. Majewski. *Spotlight Synthetic Aperture Radar: Signal Processing Algorithms*. Artech House INC, Norwood, MA, first edition, 1995.
2. Irving, William W., Leslie M. Novak, and Alan S. Willsky. "A Multiresolution Approach to Discrimination in SAR Imagery". *IEEE Transactions on Aerospace and Electronic Systems*, 33(4):1157–1168, October 1997.
3. Kreithen, Daniel E., Shawn D. Halversen, and Gregory J. Owirka. "Discriminating Targets from Clutter". *The Lincoln Laboratory Journal*, 6:25–51, 1993.
4. Massonnet, Didier and Jean-Claude Souyris. *Imaging with Synthetic Aperture Radar*. EPFL Press, Lausanne, Switzerland, first edition, 2008.
5. Novak, Leslie M., Shawn D. Halversen, Gregory J. Owirka, and Margarita Hiett. "Effects of Polarization and Resolution on the Performance of a SAR Automatic Target Recognition System". *The Lincoln Laboratory Journal*, 8:49–68, 1995.
6. Novak, Leslie M., Gregory J. Owirka, and Christine M. Netishen. "Performance of a High-Resolution Polarimetric SAR Automatic Target Recognition System". *The Lincoln Laboratory Journal*, 6:11–24, 1993.
7. Oliver, Chris and Shaun Quegan. *Understanding Synthetic Aperture Radar Images*. SciTech Publishing, Raleigh, NC 27613, 2004.
8. Ross, Timothy, Stephen Worrell, Vincent Velten, John Mossing, and Michael Bryant. "Standard SAR ATR Evaluation Experiments using the MSTAR Public Release Data Set". *Proceedings of Algorithms for Synthetic Aperture Radar Imagery V*, volume 3370. The International Society for Optical Engineering (SPIE), Orlando, Florida, April 1998.
9. Scharf, Louis L. *Statistical Signal Processing*. Addison-Wesley Publishing Company, New York, 1991.
10. Skolnik. *Radar Systems*. McGraw-Hill Companies, Inc., New York, NY, 2001.
11. Skolnik. *Radar Handbook*. McGraw-Hill Companies, Inc., New York, NY, third edition, 2008.
12. Sullivan, Roger J. *Radar Foundations for Imaging and Advance Concepts*. SciTech Publishing INC, Raleigh, NC, 2000.
13. Theodoridis, Sergios and Konstantinos Koutroumbas. *Pattern Recognition*. Academic Press, San Diego, CA, third edition, 2006.
14. Ulaby, Fawwaz T., Richard K. Moore, and Adrian K. Fung. *Microwave Remote Sensing Active and Passive Volume 1*. Artech House, Norwood, MA, 1981.



15. Ulaby, Fawwaz T., Richard K. Moore, and Adrian K. Fung. *Microwave Remote Sensing Active and Passive Volume 2*. Artech House, Norwood, MA, 1981.

REPORT DOCUMENTATION PAGE				Form Approved OMB No. 074-0188	
<p>The public reporting burden for this collection of information is estimated to average 1 hour per response, including the time for reviewing instructions, searching existing data sources, gathering and maintaining the data needed, and completing and reviewing the collection of information. Send comments regarding this burden estimate or any other aspect of the collection of information, including suggestions for reducing this burden to Department of Defense, Washington Headquarters Services, Directorate for Information Operations and Reports (0704-0188), 1215 Jefferson Davis Highway, Suite 1204, Arlington, VA 22202-4302. Respondents should be aware that notwithstanding any other provision of law, no person shall be subject to a penalty for failing to comply with a collection of information if it does not display a currently valid OMB control number.</p> <p><b>PLEASE DO NOT RETURN YOUR FORM TO THE ABOVE ADDRESS.</b></p>					
1. REPORT DATE (DD-MM-YYYY) 25-03-2010		2. REPORT TYPE Thesis		3. DATES COVERED (From – To) Sep 2008-Mar 2010	
4. TITLE AND SUBTITLE  The Effect of Synthetic Aperture Radar Image Resolution on Target Discrimination			5a. CONTRACT NUMBER		
			5b. GRANT NUMBER		
			5c. PROGRAM ELEMENT NUMBER		
6. AUTHOR(S)  McGowan, John E., 2d Lt, USAF			5d. PROJECT NUMBER JONs 261 & 314		
			5e. TASK NUMBER		
			5f. WORK UNIT NUMBER		
7. PERFORMING ORGANIZATION NAMES(S) AND ADDRESS(S) Air Force Institute of technology Graduate School of engineering and Management 2950 Hobson Way WPAFB OH 45433-7765				8. PERFORMING ORGANIZATION REPORT NUMBER AFIT/GE/ENG/10-18	
9. SPONSORING/MONITORING AGENCY NAME(S) AND ADDRESS(ES) Dr Michael Talbert; AFRL/RYZT; 2241 Avionics Circle; Wright-Patterson AFB OH 45433, 937-255-1108, Michael.Talbert@WPAFB.AF.MIL; Dr. Daniel Atkins & LtCol Brannen Cohee NASIC/DA; 4180 Watson Way; Wright-Patterson AFB OH 45433, 937-257-4323; Daniel.Atkins@WPAFB.AF.MIL, Brannen.Cohee@WPAFB.AF.MIL				10. SPONSOR/MONITOR'S ACRONYM(S) AFRL/RYZT & NASIC/DA	
				11. SPONSOR/MONITOR'S REPORT NUMBER(S)	
12. DISTRIBUTION/AVAILABILITY STATEMENT  Approval for public release; distribution is unlimited					
13. SUPPLEMENTARY NOTES					
14. ABSTRACT This research details the effect of spatial resolution on target discrimination in Synthetic Aperture Radar (SAR) images. Multiple SAR image chips containing targets and non-targets are used to test a baseline Automatic Target Recognition (ATR) system with reduced spatial resolution obtained by lowering the pixel count or synthesizing a degraded image. The pixel count is lowered by averaging groups of adjoining pixels to form a new single value. The degraded image is synthesized by low-pass filtering the image frequency space and then lowering the pixel count. A two parameter Constant False Alarm Rate (CFAR) detector is tested, and three different types of feature spaces; size, contrast, and texture; are used to train a linear classifier. The results are scored using the Area Under the Receiver Operator Characteristic (AUROC) curve. The CFAR detector is shown to perform better at lower resolution. All three feature sets together performed well with the degradation of resolution; separately the sets had different performances. The texture features performed best because they do not rely on the number of pixels on the target, while the size features performed worst for the same reason. The contrast features yielded improved performance when the resolution was slightly reduced.					
15. SUBJECT TERMS Synthetic aperture radar, automatic target recognition, low resolution					
16. SECURITY CLASSIFICATION OF:			17. LIMITATION OF ABSTRACT UU	18. NUMBER OF PAGES 129	19a. NAME OF RESPONSIBLE PERSON Pr. Andrew J. Terzuoli; Jr., terzuoli@afit.edu
REPORT U	ABSTRACT U	c. THIS PAGE U			19b. TELEPHONE NUMBER (Include area code) (937)-255-6565, ext. 4717

Standard Form 298 (Rev: 8-98)  
Prescribed by ANSI Std. Z39-18